T H E U N I V E R S I T Y O F M I C H I G A N

COLLEGE OF ENGINEERING
Department of Electrical Engineering
Space Physics Research Laboratory

Final Report

A FEASIBLE SATELLITE EXPERIMENT FOR GAS MOLECULE-SOLID SURFACE INTERACTION STUDIES

Jens C. Zorn
John C. Pearl

ORA Project 08700

under contract with:

NATIONAL AERONAUTICS AND SPACE ADMINISTRATION
GEORGE C. MARSHALL SPACE FLIGHT CENTER
CONTRACT NO. NAS 8-21096
HUNTSVILLE, ALABAMA

administered through:

OFFICE OF RESEARCH ADMINISTRATION ANN ARBOR

October 1967

ERRATA

Page vii, line 11: "exected" should read "executed."

Page 1, line 1: "Contract NASA 8-2196" should read "Contract NAS 8-21096."

Page 24, second line from bottom: "$\frac{L+W}{v} + \tau\ t$"

should read "$\frac{L+W}{v} + \tau - t$"

Page 25, fourth line from bottom: "$\frac{L}{v} \leq t \leq \frac{L}{v}$"

should read "$\frac{L}{v} \leq t \leq \tau + \frac{L}{v}$"

Page 25, second line from bottom: "$L + \frac{W}{v} \leq t \leq \tau + \frac{L+W}{v}$

should read "$\frac{L+W}{v} \leq t \leq \tau + \frac{L+W}{v}$"

Page 31, fourth line from bottom:

$$\frac{c^4 t}{2} G_m\left(\frac{L}{ct}, s \cos\alpha\right) - G_m\left(\frac{L+W}{ct}, s \cos\alpha\right)$$

should read

$$\frac{c^4 t}{2}\left\{G_m\left(\frac{L}{ct}, s \cos\alpha\right) - G_m\left(\frac{L+W}{ct}, s \cos\alpha\right)\right\}$$

Page 32, second line from bottom: "$l = t\Delta v$" should read "$\Delta l = t\Delta v$"

Page 33, Figure 3.3: "W=0.1cm" should be included among the parameters

Page 39, Figure 3.6: "W=20cm" should read "W=0.1cm"

Page 42, line 5: "Figure 1" should read "Figure 3.7"

Page 43, caption of Figure 3.8: "incoming molecular velocities $\bar{v}$" should read "incoming molecular velocities $\bar{v}_o$"

TABLE OF CONTENTS

TABLE OF CONTENTS (Continued)

TABLE OF CONTENTS (Concluded)

ACKNOWLEDGEMENTS

The writers wish to express their gratitude to all of the persons whose efforts contributed both tangibly and intangibly to the material in this report. In particular

to George R. Carignan, Director of the Space Physics Research Laboratory of the University of Michigan who constantly made available his skill and knowledge to provide major contributions to all phases of the work;

to Neil B. Johnson and David Kaslow who performed the experiments on metastable detectors;

to William D. Hall who exected and analyzed the gas scattering measurements;

to David A. Crosby who did the research on the formation of surfaces by vapor decomposition;

to Hasso Niemann who provided the tables of expected flux and has given generously of his time to many other parts of the work;

to Robert F. Hoeberling for the derivation of the flux relation presented in the appendix;

to Andrew F. Nagy for many stimulating ideas and discussions;

to Mrs. Reynolds Denning for her considerable assistance in preparing the final report.

PROJECT PERSONNEL

Bechtel, James H.	Assistant Research Physicist
Carignan, George R.	Director, Space Physics Research Laboratory
Carter, Michael F.	Assistant Research Mathematician
Cederberg, James	Research Physicist
Crosby, David A.	Assistant Research Physicist
Denning, Helen G.	Research Associate
Gamble, Thomas D.	Assistant Research Physicist
Hoeberling, Robert F.	Assistant Research Physicist
Johnson, Neil B.	Assistant Research Physicist
Kaslow, David E.	Assistant Research Physicist
Niemann, Hasso B.	Associate Research Engineer
Pearl, John C.	Assistant Research Physicist
Rhee, Chong K.	Assistant Research Engineer
Shumate, William E.	Draftsman
Stephenson, Frances H.	Programmer
Zorn, Jens C.	Associate Professor of Physics

LIST OF ILLUSTRATIONS

LIST OF ILLUSTRATIONS (Continued)

LIST OF ILLUSTRATIONS (Concluded)

1. INTRODUCTION

1.1 OUTLINE OF STUDY

The objective of the study made under Contract NASA 8-2196 is to define an experiment for meaningful, quantitative measurements on gas-surface interactions as they occur in an earth satellite environment. Such an experiment would lead to a better understanding of satellite drag phenomena by providing information on gas-surface momentum and energy transfer. The relevant data would be obtained through a detailed study of the velocity distributions in incident and reflected gas beams. The original proposal defined an experimental concept based on the experience and current efforts of the Space Physics Laboratory and the Molecular Beam Laboratory of the University of Michigan. The experiment proposed was to provide a flux of reflected particles and an analysis of the composition, velocity distribution, and angular distribution of the reflected stream. The proposal emphasized the possibility of using a metastable detector for measurements of velocity distributions and a mass spectrometer for the measurement of flux composition.

The study has proceeded very nearly along the lines proposed. The importance of the velocity distribution determination has dictated a further shift of emphasis toward the study of metastable time-of-flight (MTOF) analyzers which show great promise in this application. In addition, the experimental geometry originally proposed has been changed to a configuration which appears able to provide more meaningful measurements.

The present report is mainly concerned with techniques and problems associated with measurements involving molecular nitrogen. The general features of the proposed experimental configuration and of the metastable time-of-flight analyzer are considered in Section 1. The fluxes of N_2, O_2, and O expected along the ODYSSEY orbit are presented in Section 2. Section 3 contains the interpretation of a time-of-flight- spectrum in terms of a molecular velocity distribution function. The collision-induced modifications of the veloctiy distribution of a collimated molecular beam have been measured; the analysis of this experiment and its implications for the proposed gas-surface interaction studies are given in Section 4. Properties of molecular nitrogen relevant to the MTOF analysis are presented in Section 5. In Section 6 the operation of metastable detectors is shown to be stable and reliable under adverse operating conditions. Section 7 describes experimental sutdies of novel methods for preparing clean target surfaces which can feasibly be done in orbit. In the concluding section, the work performed under the contract is summarized, and the construction of a satellite-borne MTOF analyzer for analysis of N_2 scattered from various target surfaces is recommended.

1.2 PROPOSED EXPERIMENTAL CONFIGURATION

1.2.1 General Description

The main objective of the proposed experiment is to explore the interactions of nitrogen molecules with engineering and scientific surfaces under conditions of relative velocity and general environment found on an earth satellite. The nitrogen molecules which strike the satellite are scattered in all directions; the angular distribution of the molecules which scatter from a target surface is to be measured. The velocity of the N_2 molecules relative to the satellite before impact is relatively uniform and is on the order of 10^6 cm/sec; their velocity distribution after scattering is to be measured. An additional objective is the measurement of the composition of the total molecular flux incident on the satellite.

The experiments as currently conceived are operable between 100 and 350 km altitude: the upper altitude limit is reached when the reflected flux of N_2 is too weak to be measured, while the lowest operating altitude is that at which the mean free path of fast molecules in the detectors is appreciably less that the characteristic dimensions of the detector.

The general features of the experiment are shown in Figure 1.1. A quadrupole mass spectrometer to measure the composition of the incoming flux is shown on one side. An instrument for measuring the flux of N_2 alone is on the other side. Centered between these two instruments is an enclosed analyzer which is used for the measurement of the angular distribution and velocity

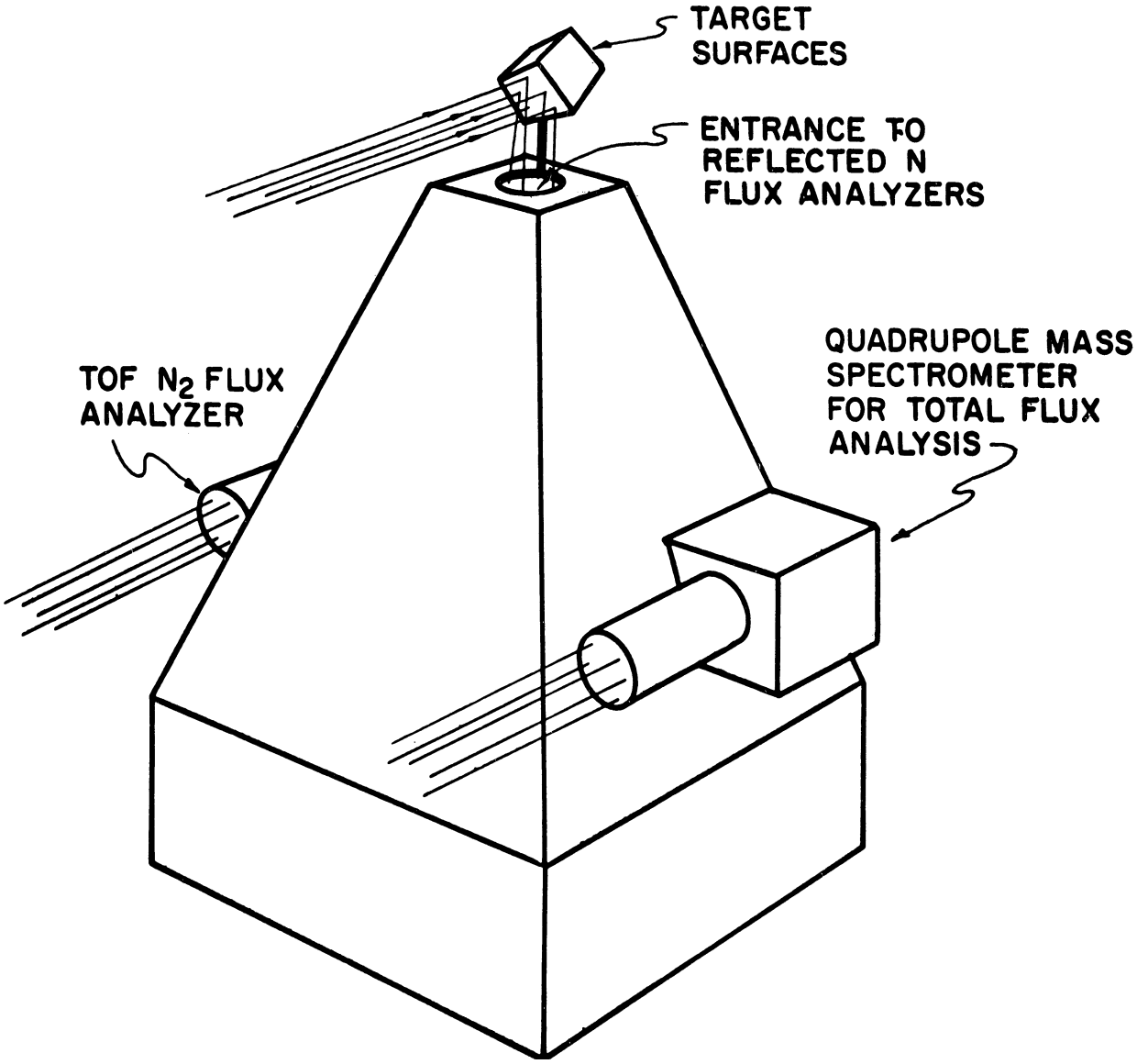

Figure 1.1 General View of Proposed Experiment

distribution of the nitrogen flux which is reflected from a target surface. Molecules strike the target surface at an angle determined by the attitude of the satellite with respect to its velocity vector. Although rigorous attitude stabilization is not required for the proposed experiment, not all attitudes of the spacecraft will give a useful flux into the TOF analyzer. The effective angular aperture of the instrument will depend on the final design, but should be about 1 steradian. If this large aperture is to be useful, care must be taken to place the experiment so that its attitude relative to the velocity vector of the satellite will be about as shown in Figure 1.1 during at least part of each tumbling cycle. Noteworthy features of the proposed experiment include:

1. No moving parts are employed other than the target surface indexer.
2. Attitude stabilization is not required for the satellite; in fact the tumbling of the vehicle provides a variety of incidence angles for the molecules on the target.
3. Target surfaces are directly exposed to the space environment.

1.2.2 Measurements of Velocity Distribution in Reflected Flux

The velocity distribution of a beam of ions inside an apparatus is governed more by electric fields within the enclosure than by the velocities of the incoming neutral molecules, indicating that the velocity analysis on the reflected flux should be

done on the molecules while they are electrically neutral. The velocity analysis of a neutral molecular beam can be done with a mechanical velocity filter (Miller and Kusch, 1955; see also Section 4.2.3) or by observing the time of flight (TOF) of groups of molecules in a chopped molecular beam. However, rotating velocity filters are manifestly unsuited for satellite experiments and mechanical beam choppers do not seem practical (Grumman report on this study for the month of July, 1967, contract NAS 8-21096) for the velocities of interest in this work.

To avoid difficulties inherent in mechanical systems, it is proposed that a pulsed electron gun be used to create a spatially concentrated group of neutral, metastable N_2 molecules. The time of flight of these metastables over a 20 cm path in the apparatus would be observed. Since the metastable molecules are neutral, the detector output will be an accurate measure of the velocity distribution of the reflected neutral flux. The MTOF method has been employed to measure the velocity distribution in metastable helium (French, 1967) and in $2^2S_{1/2}$ atomic hydrogen (Leventhal, et al, 1967). No moving mechanical parts are involved and electron guns can give short pulses with ease, so the system is well suited for analysis of very fast molecular beams. Moreover, the present study shows that metastable detectors are efficient, stable, and very rugged. On these grounds, therefore, it appears that metastable TOF analysis is by far the most practical method for the measurement of velocity distributions in the cases relevant to the study of satellite drag.

1.2.3 General Description of TOF Analyzer Operation

The operation of the proposed N_2 TOF analyzer is most easily discussed with reference to Figure 1.2. The molecules enter the analyzer either directly, as for flux measurements, or after reflection from a target as shown in the figure. The molecules pass into a pulsed electron gun where some of them are excited to their metastable state. If a metastable molecule passes through the collimator (an array of parallel tubes) without collision, it will arrive in its excited state at the metal detector surface; here the metastable molecule undergoes a radiationless decay (a so-called "Auger Process") and ejects an electron from the metal. These electrons are accelerated into a multiplier, the output of which is a series of pulses at a rate proportional to the flux of metastable molecules through the analyzer.

At an altitude of 300 km, there will be a flux of about 10^{14} N_2 molecules $sec^{-1}cm^{-2}$ incident on the target (see Section 2). Suppose that 1% of these are reflected into the analyzer and bombarded with 1μsec pulses from an electron gun whose duty cycle is 10^{-3}. Then, if the probability for metastable excitation is accounted for, about one in every 10^8 N_2 molecules entering the analyzer will be excited to its metastable state. The Auger detector is about 10% efficient, so a counting rate of 10^3/sec is expected. This is ample for time-of-flight analysis by well proven methods.

The use of a cluster of TOF analyzers to measure reflected N_2 at five different angles is shown in Figure 1.3. Note that one electron gun serves for all five units.

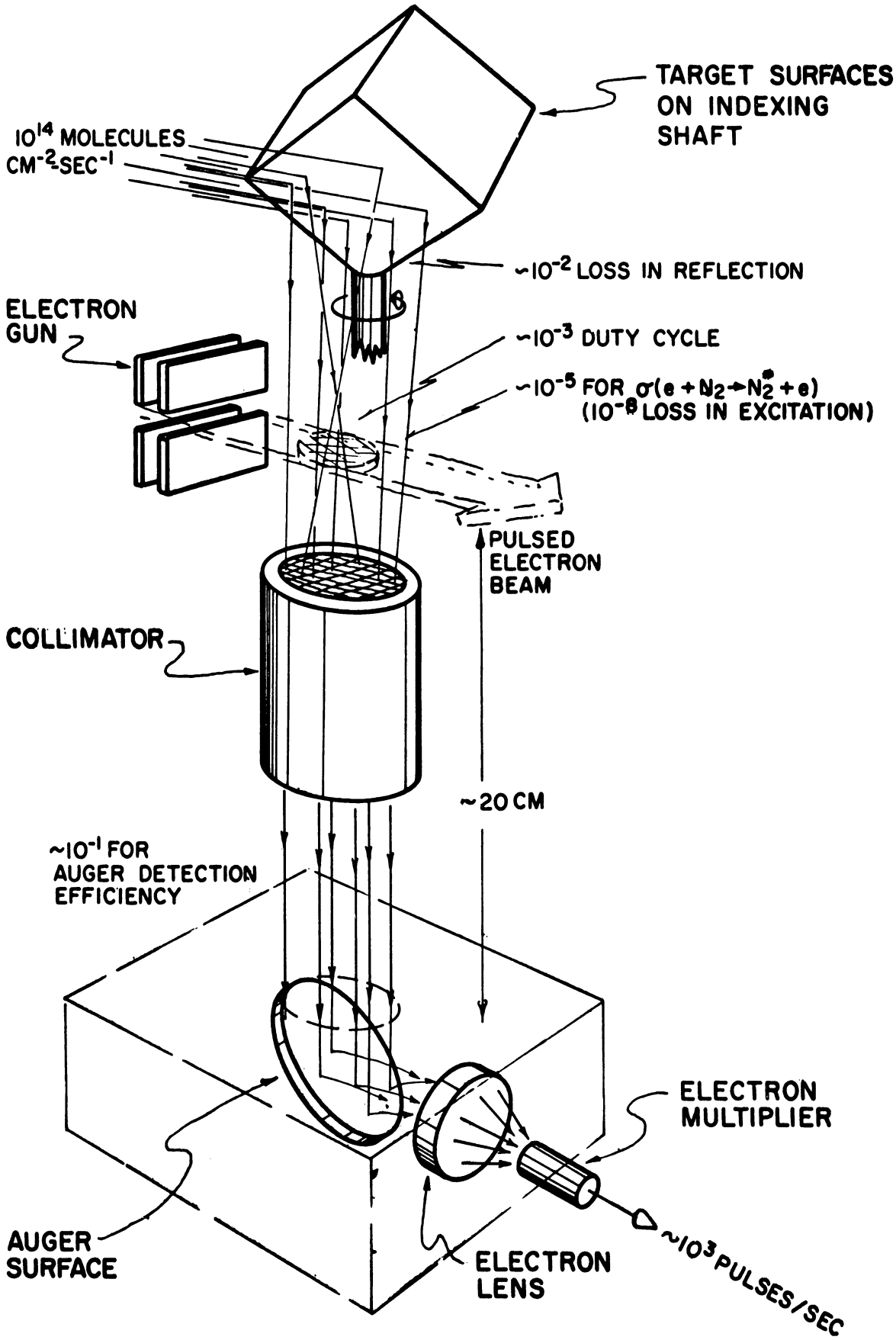

Figure 1.2 N_2 TOF Analyser Operation

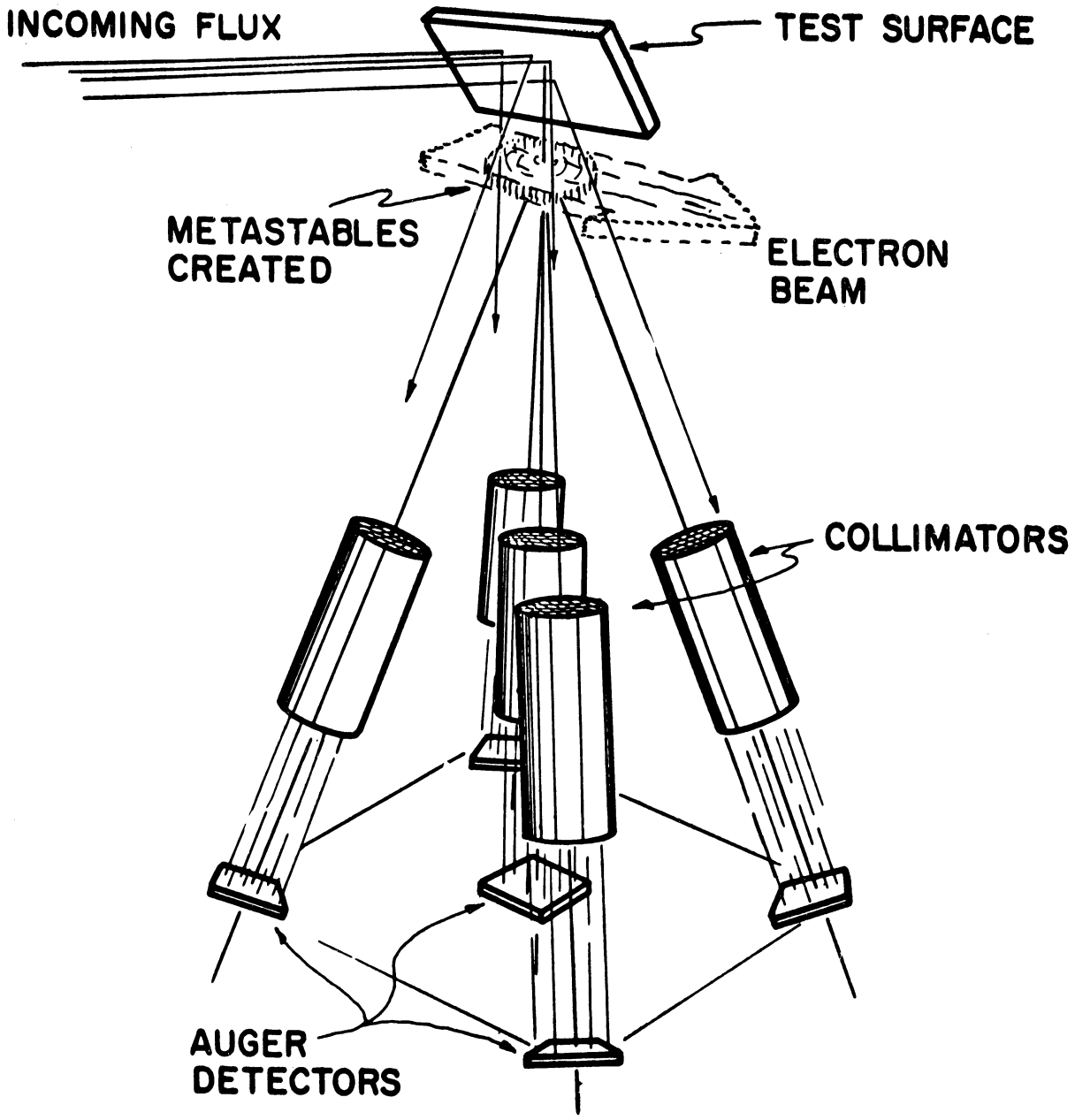

Figure 1.3 Measurement of Angular Distribution of Reflected Flux

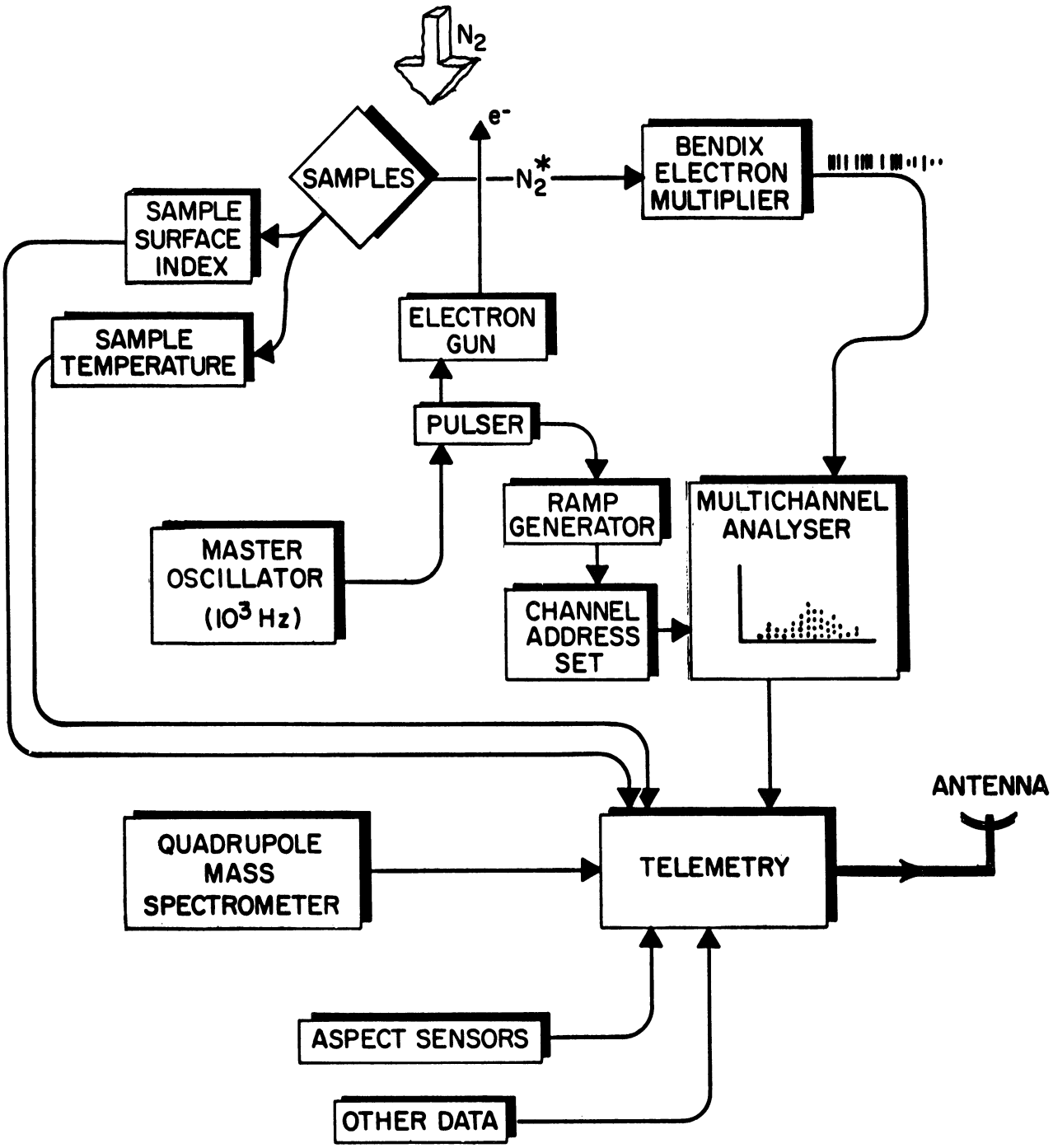

Figure 1.4 Functional Block Diagram

A system functional block diagram is shown in Figure 1.4.

1.2.4 Problems from Background

The following sources of background noise signals have been considered:

IONS

The ions and free electrons which wander into the TOF analyzer or which are created by the electron gun are to be kept away from the Auger detectors by DC electromagnetic ion traps. These traps will have a negligible effect on the neutral, metastable N_2.

PHOTONS

With the exception of infrequent occurrences when solar radiation is reflected into the instrument from the sample surface, the Auger detectors are not directly exposed to radiation from space, so photon background from this source will not be troublesome. The pulse of electrons which excites the metastable N_2 will also excite optical levels of the molecules which happen to be in the bombardment region at the time; these photons will arrive at the Auger surface within nanoseconds of the electron pulse time, and the detector signal which comes from these photons can be used to calibrate the zero-time of the TOF analyzer.

BACKGROUND MOLECULES

The metastable time-of-flight analyzer is well adapted to discriminating against background molecules because it measures

both the direction and the speed of the incoming particles.[#] By collimating the metastable beam, the instrument selects only molecules which enter the electron bombardment region with their momenta in a specified direction (parallel to the collimator axis). Consequently, by orienting the collimator to face the target surface under investigation, essentially all metastable molecules which strike the Auger detector will have come from that surface.

Because the electron excitation process produces practically no change in the velocity of the incoming molecules, the TOF analysis accurately measures the distribution of speeds of the particles arriving from the target surface. As a result, the high speed ($> 5 \times 10^4$ cm/sec) component of the reflected flux should be relatively free of background because the molecules which strike the target after previous collisions with the instrument will be very nearly thermalized and therfore contribute only to the low speed portion of the data.

This contrasts sharply with the abilities of the time-of-flight mass spectrometer, in which ions, formed by electron bombardment of a heterogeneous sample of molecules, are accelerated through a potential difference φ. The resulting speed of a singly charged ion, $v=\sqrt{\frac{2q}{m}\varphi}$, is in no way related to the speed at which the original molecule entered the ionizing region. In addition, particles entering this region from all directions are ionized and become part of the same ion beam, so that the instrument lacks directional resolution as well. Thus, while the TOF mass spectrometer is well adapted to making composition measurements, it is unable to provide information on the velocity distribution of the incoming particles.

In order to obtain meaningful measurements on the low speed portion of the reflected flux, the component arising from multiply reflected particles must be eliminated, regardless of the method used for the velocity analysis. One way to accomplish this background reduction might be to place the target samples and the analyzer inside a cryogenically cooled enclosure, such as the molecular sink developed by the Celestial Research Company. While such a configuration may remove most of the background gas, the samples would no longer be exposed to the actual space environment, and the experimental lifetime would be limited by the storage capacity for the cryogenic coolants.

2. ATMOSPHERIC ENVIRONMENT

In order to provide convenient numerical data on conditions encountered during the experiment, tables of particle densities and fluxes have been prepared from a standard atmosphere (Tables 2.I and 2.II). The low altitude portions of these tables are shown graphically in Figures 2.1 and 2.2.

The densities and fluxes of N_2, O_2, O and the totals are tabulated for each minute of a half orbit; the proposed ODYSSEY orbit with an apogee of 2,000 km and a perigee of 200 km has been used. Satellite altitude and velocity are also indicated. All atmospheric parameters have been taken from the CIRA 1965 reference atmosphere, Model 4.

Table 2.I and Figure 2.1 have been made from parameters for 0400 hours. Table 2.II and Figure 2.2 have been made from parameters for 1400 hours. Consequently, the two sets of data provide results for the extreme diurnal exospheric temperatures encountered during one equatorial orbit.

Table 2.I Densities and fluxes of major atmospheric constituents as seen by a satellite in proposed ODYSSEY orbit for 0400 hours local time.

0400 HOURS

TIME (sec)	ALTITUDE (Km)	VELOCITY (m/sec)	N_2 DENSITY (part/cm^3)	N_2 FLUX (part/cm^{2}sec)	O_2 DENSITY (part/cm^3)	O_2 FLUX (part/cm^{2}sec)	O DENSITY (part/cm^3)	O FLUX (part/cm^{2}sec)	TOTAL DENSITY (part/cm^3)	TOTAL FLUX (part/cm^{2}sec)
0	200	7825.0	2.821×10^{9}	2.207×10^{15}	2.920×10^{8}	2.285×10^{14}	3.223×10^{9}	2.522×10^{15}	6.330×10^{9}	4.953×10^{15}
60	202	7822.6	2.627	2.055	2.698	2.111	3.081	2.410	5.978	4.677
120	208	7815.6	2.046	1.599	2.034	1.590×10^{14}	2.653	2.073	4.902	3.831
180	218	7804.1	1.356×10^{9}	1.058×10^{15}	1.274×10^{8}	9.942×10^{13}	2.081	1.624	3.564	2.781
240	231	7788.0	8.012×10^{8}	6.240×10^{14}	6.997×10^{7}	5.449	1.531	1.192×10^{15}	2.402	1.871
300	249	7767.6	4.013	3.117	3.187	2.476	1.022×10^{9}	7.939×10^{14}	1.455×10^{9}	1.130×10^{15}
360	270	7743.0	1.822×10^{8}	1.411×10^{14}	1.295×10^{7}	1.003×10^{13}	6.477×10^{8}	5.015	8.428×10^{8}	6.526×10^{14}
420	294	7714.5	7.762×10^{7}	5.988×10^{13}	4.908×10^{6}	3.787×10^{12}	3.943	3.042	4.773	3.682
480	322	7682.2	2.898	2.226×10^{13}	1.596×10^{6}	1.226×10^{12}	2.187	1.680×10^{14}	2.493	1.915
540	353	7646.4	1.032×10^{7}	7.891×10^{12}	4.944×10^{5}	3.780×10^{11}	1.223×10^{8}	9.389×10^{13}	1.331×10^{8}	1.018×10^{14}
600	388	7607.3	3.128×10^{6}	2.379×10^{11}	1.264×10^{5}	9.623×10^{10}	6.189×10^{7}	4.708	6.514×10^{7}	4.955×10^{13}
660	424	7565.2	9.585×10^{5}	7.251×10^{11}	3.265×10^{4}	2.470×10^{9}	3.156×10^{7}	2.388	3.255	2.462
720	464	7520.5	2.578×10^{5}	1.939×10^{10}	7.291×10^{3}	5.484×10^{9}	1.490×10^{7}	1.121×10^{13}	1.517×10^{7}	1.141×10^{13}
780	506	7473.3	6.693×10^{4}	5.002×10^{10}	1.565×10^{3}	1.170×10^{8}	7.114×10^{6}	5.316×10^{12}	7.182×10^{6}	5.367×10^{12}
840	550	7424.0	1.662×10^{4}	1.234×10^{9}	3.196×10^{2}	2.373×10^{8}	3.095	2.298×10^{12}	3.112	2.310×10^{12}
900	596	7373.0	3.852×10^{3}	2.840×10^{9}	6.014×10^{1}	4.434×10^{7}	1.346×10^{6}	9.924×10^{11}	1.350×10^{6}	9.954×10^{11}
960	643	7320.4	8.833×10^{2}	6.466×10^{8}	1.115×10^{1}	8.162×10^{6}	5.835×10^{5}	4.271	5.844×10^{5}	4.278
1020	693	7266.5	1.959×10^{2}	1.423×10^{8}	2.005×10^{0}	1.457×10^{6}	2.452	1.782×10^{11}	2.454	1.783×10^{11}
1080	743	7211.7	4.234×10^{1}	3.054×10^{7}	3.470×10^{-1}	2.503×10^{5}	1.029×10^{5}	7.421×10^{10}	1.029×10^{5}	7.421×10^{10}
1140	794	7156.1	9.482×10^{0}	6.785×10^{6}	6.311×10^{-2}	4.516×10^{4}	4.357×10^{4}	3.118	4.357×10^{4}	3.118
1200	846	7100.1	2.054×10^{0}	1.458×10^{6}	1.096×10^{-2}	7.782×10^{3}	1.822×10^{4}	1.294×10^{10}	1.822×10^{4}	1.294×10^{10}
1260	899	7043.8	4.182×10^{-1}	2.946×10^{5}	1.770×10^{-3}	1.247×10^{3}	7.394×10^{3}	5.208×10^{9}	7.394×10^{3}	5.208×10^{9}
1320	952	6987.4	9.518×10^{-2}	6.650×10^{4}	3.260×10^{-4}	2.278×10^{2}	3.174	2.218×10^{9}	3.174	2.218×10^{9}
1380	1005	6931.3	2.153×10^{-2}	1.492×10^{4}	5.964×10^{-5}	4.134×10^{1}	1.357×10^{3}	9.405×10^{8}	1.357×10^{3}	9.405×10^{8}
1440	1058	6875.5	4.975×10^{-3}	3.421×10^{3}	1.118×10^{-5}	7.687×10^{0}	5.876×10^{2}	4.400	5.876×10^{2}	4.400
1500	1112	6820.3	1.142×10^{-3}	7.788×10^{2}	2.080×10^{-6}	1.419×10^{-1}	2.535	1.729×10^{8}	2.535	1.729×10^{8}
1560	1164	6765.9	2.825×10^{-4}	1.912×10^{2}	4.214×10^{-7}	2.851×10^{-1}	1.141×10^{2}	7.720×10^{7}	1.141×10^{2}	7.720×10^{7}
1620	1216	6712.3	7.123×10^{-5}	4.781×10^{1}	8.727×10^{-8}	5.858×10^{-2}	5.192×10^{1}	3.485	5.192×10^{1}	3.485
1680	1267	6659.7	1.878×10^{-5}	1.251×10^{1}	1.902×10^{-8}	1.267×10^{-2}	2.424×10^{1}	1.614×10^{7}	2.424×10^{1}	1.614×10^{7}
1740	1318	6608.4	5.040×10^{-6}	3.330×10^{0}	4.230×10^{-9}	2.795×10^{-3}	1.143×10^{1}	7.553×10^{6}	1.143×10^{1}	7.553×10^{6}
1800	1367	6558.3	1.448×10^{-6}	9.496×10^{-1}	1.017×10^{-9}	6.669×10^{-4}	5.604×10^{0}	3.675	5.604×10^{0}	3.675
1860	1415	6509.6	4.331×10^{-7}	2.819×10^{-2}	2.560×10^{-10}	1.667×10^{-4}	2.812	1.831×10^{6}	2.812	1.831×10^{6}
1920	1463	6462.4	1.315×10^{-7}	8.498×10^{-2}	6.555×10^{-11}	4.236×10^{-5}	1.423×10^{0}	9.195×10^{5}	1.423×10^{0}	9.195×10^{5}
1980	1508	6416.8	4.358×10^{-8}	2.797×10^{-3}	1.855×10^{-11}	1.190×10^{-5}	7.571×10^{-1}	4.858	7.571×10^{-1}	4.858
2040	1552	6373.0	1.498×10^{-8}	9.547×10^{-3}	5.477×10^{-12}	3.490×10^{-6}	4.113	2.621	4.113	2.621
2100	1595	6330.8	5.339×10^{-9}	3.380×10^{-3}	1.684×10^{-12}	1.066×10^{-6}	2.281×10^{-1}	1.444×10^{5}	2.281×10^{-1}	1.444×10^{5}

Table 2.I (Concluded)

0400 HOURS

TIME (sec)	ALTITUDE (Km)	VELOCITY (m/sec)	N_2 DENSITY ($part/cm^3$)	N_2 FLUX ($part/cm^2 sec$)	O_2 DENSITY ($part/cm^3$)	O_2 FLUX ($part/cm^2 sec$)	O DENSITY ($part/cm^3$)	O FLUX ($part/cm^2 sec$)	TOTAL DENSITY ($part/cm^3$)	TOTAL FLUX ($part/cm^2 sec$)
2160	1635	6290.5	2.065×10^{-9}	1.299×10^{-3}	5.686×10^{-13}	3.576×10^{-7}	1.325×10^{-1}	8.334×10^{4}	1.325×10^{-1}	8.334×10^{4}
2220	1674	6252.2	8.251×10^{-10}	5.159×10^{-4}	1.993×10^{-13}	1.246×10^{-7}	7.847×10^{-2}	4.906	7.847×10^{-2}	4.906
2280	1711	6215.8	3.485	2.166×10^{-4}	7.442×10^{-14}	4.626×10^{-8}	4.795	2.981	4.795	2.981
2340	1746	6181.5	1.553×10^{-10}	9.601×10^{-5}	2.955	1.827×10^{-8}	3.021	1.868	3.021	1.868
2400	1780	6149.2	7.131×10^{-11}	4.385	1.214×10^{-14}	7.465×10^{-9}	1.937	1.191×10^{4}	1.937	1.191×10^{4}
2460	1810	6119.0	3.607	2.207	5.572×10^{-15}	3.410	1.312×10^{-2}	8.028×10^{3}	1.312×10^{-2}	8.028×10^{3}
2520	1840	6091.0	1.834	1.117×10^{-5}	2.572	1.567×10^{-9}	8.914×10^{-3}	5.430	8.914×10^{-3}	5.430
2580	1865	6065.1	1.048×10^{-11}	6.356×10^{-6}	1.356×10^{-15}	8.224×10^{-10}	6.473	3.926	6.473	3.926
2640	1890	6041.5	6.005×10^{-12}	3.628	7.179×10^{-16}	4.338	4.709	2.845	4.709	2.845
2700	1912	6020.2	3.690	2.221	4.115	2.477	3.565	2.146	3.565	2.146
2760	1932	6001.2	2.375	1.425×10^{-6}	2.487	1.492×10^{-10}	2.772	1.663	2.772	1.663
2820	1950	5984.4	1.601	9.580×10^{-7}	1.584	9.479×10^{-11}	2.212	1.324	2.212	1.324
2880	1964	5970.0	1.179×10^{-12}	7.039	1.117×10^{-16}	6.668	1.858	1.109×10^{3}	1.858	1.109×10^{3}
2940	1977	5958.0	8.884×10^{-13}	5.293	8.084×10^{-17}	4.816	1.580	9.414×10^{2}	1.580	9.414×10^{2}
3000	1987	5948.2	7.150	4.253	6.308	3.752	1.396	8.303	1.396	8.303
3060	1995	5941.0	6.013	3.572	5.175	3.074	1.264	7.509	1.264	7.509
3120	2000	5936.0	5.396	3.203	4.573	2.715	1.189	7.058	1.189	7.058
3180	2002	5933.4	5.168	3.066	4.353	2.583	1.160	6.882	1.160	6.882
3240	2002	5933.2	5.168×10^{-13}	3.066×10^{-7}	4.353×10^{-17}	2.583×10^{-11}	1.160×10^{-3}	6.882×10^{2}	1.160×10^{-3}	6.882×10^{2}

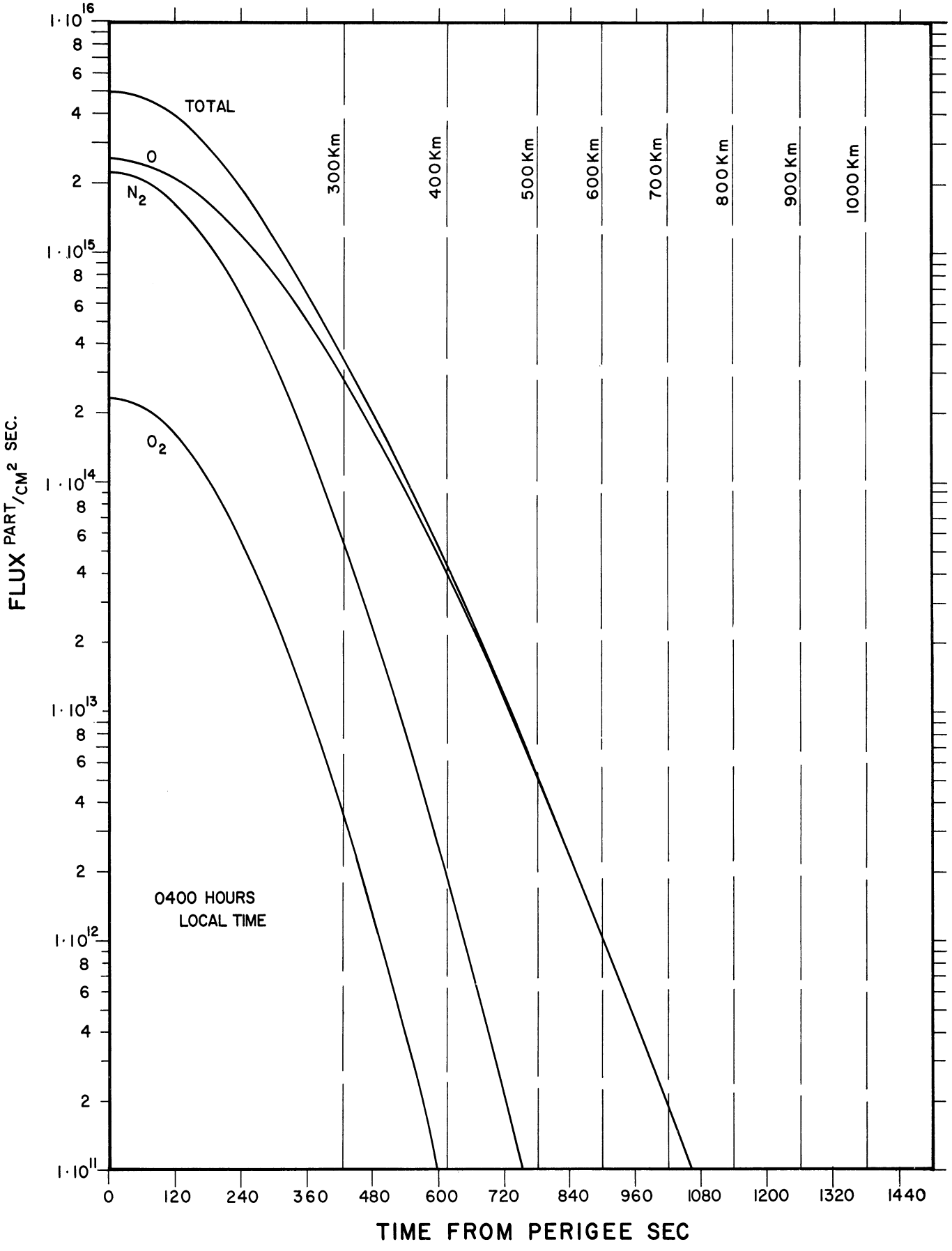

Figure 2.1 Fluxes of major atmospheric constituents to a satellite in proposed ODYSSEY orbit for 0400 hours local time.

Table 2.II Densities and fluxes of major atmospheric constituents as seen by a satellite in proposed ODYSSEY orbit for 1400 hours local time.

1400 HOURS

TIME (sec)	ALTITUDE (Km)	VELOCITY (m/sec)	N_2 DENSITY (part/cm^3)	N_2 FLUX (part/cm^{2}sec)	O_2 DENSITY (part/cm^3)	O_2 FLUX (part/cm^{2}sec)	O DENSITY (part/cm^3)	O FLUX (part/cm^{2}sec)	TOTAL DENSITY (part/cm^3)	TOTAL FLUX (part/cm^{2}sec)
0	200	7825.0	3.665×10^{9}	2.868×10^{15}	4.115×10^{8}	3.220×10^{14}	3.276×10^{9}	2.563×10^{15}	7.352×10^{9}	5.753×10^{15}
60	202	7822.6	3.460	2.707	3.860	3.020	3.155	2.468	7.001	5.477
120	208	7815.6	2.844	2.223	3.098	2.421	2.793	2.183	5.947	4.648
180	218	7804.1	2.076	1.620	2.172	1.695	2.301	1.796	4.594	3.585
240	231	7788.0	1.885×10^{9}	1.468×10^{15}	1.947×10^{8}	1.516×10^{14}	2.172	1.692	4.252	3.311
300	249	7767.6	8.482×10^{8}	6.589×10^{14}	7.885×10^{7}	6.125×10^{13}	1.342×10^{9}	1.042×10^{15}	2.269	1.763
360	270	7743.0	4.846	3.752	4.175	3.233	9.638×10^{8}	7.463×10^{14}	1.490×10^{9}	1.154×10^{15}
420	294	7714.5	2.663	2.055	2.117×10^{7}	1.633×10^{13}	6.775	5.227	9.650×10^{8}	7.445×10^{14}
480	322	7682.2	1.351×10^{8}	1.038×10^{14}	9.774×10^{6}	7.508×10^{12}	4.565	3.507	6.014	4.620
540	353	7646.4	6.619×10^{7}	5.061×10^{13}	4.346	3.323	3.010	2.301	3.715	2.840
600	388	7607.3	2.954	2.247×10^{13}	1.730×10^{6}	1.316×10^{12}	1.894	1.441×10^{14}	2.207	1.679
660	424	7565.2	1.313×10^{7}	9.933×10^{12}	6.852×10^{5}	5.184×10^{11}	1.192×10^{8}	9.017×10^{13}	1.330×10^{8}	1.006×10^{14}
720	464	7520.5	5.417×10^{6}	4.074	2.493×10^{5}	1.875×10^{11}	7.182×10^{7}	5.400	7.749×10^{7}	5.827×10^{13}
780	506	7473.3	2.179×10^{6}	1.628×10^{12}	8.822×10^{4}	6.593×10^{10}	4.262	3.185	4.489	3.355
840	550	7424.0	8.512×10^{5}	6.319×10^{11}	3.017×10^{4}	2.240×10^{10}	2.487	1.846	2.575	1.912
900	596	7373.0	3.192	2.353×10^{11}	9.838×10^{3}	7.254×10^{9}	1.422×10^{7}	1.048×10^{13}	1.455×10^{7}	1.073×10^{13}
960	643	7320.4	1.191×10^{5}	8.718×10^{10}	3.187×10^{3}	2.333×10^{9}	8.113×10^{6}	5.939×10^{12}	8.235×10^{6}	6.028×10^{12}
1020	693	7266.5	4.304×10^{4}	3.127	9.984×10^{2}	7.254×10^{8}	4.524	3.287	4.568	3.319
1080	743	7211.7	1.547×10^{4}	1.116×10^{10}	3.098×10^{2}	2.234×10^{8}	2.529	1.824	2.544	1.835
1140	794	7156.1	5.633×10^{3}	4.031×10^{9}	9.791×10^{1}	7.006×10^{7}	1.417×10^{6}	1.014×10^{12}	1.423×10^{6}	1.018×10^{12}
1200	846	7100.1	2.021×10^{3}	1.435×10^{9}	3.031×10^{1}	2.152×10^{7}	7.892×10^{5}	5.603×10^{11}	7.913×10^{5}	5.618×10^{11}
1260	899	7043.8	6.988×10^{2}	4.922×10^{8}	8.986×10^{0}	6.330×10^{6}	4.317	3.041	4.324	3.046
1320	952	6987.4	2.586×10^{2}	1.807×10^{8}	2.886×10^{0}	2.016×10^{6}	2.446	1.709×10^{11}	2.448	1.710×10^{11}
1380	1005	6931.3	9.534×10^{1}	6.608×10^{7}	9.223×10^{-1}	6.393×10^{5}	1.383×10^{5}	9.586×10^{10}	1.384×10^{5}	9.592×10^{10}
1440	1058	6875.5	3.565	2.451×10^{7}	2.996×10^{-1}	2.060×10^{5}	7.883×10^{4}	5.420	7.886×10^{4}	5.422
1500	1112	6810.3	1.327×10^{1}	9.050×10^{6}	9.688×10^{-2}	6.607×10^{4}	4.482	3.057	4.483	3.057
1560	1164	6765.9	5.195×10^{0}	3.515	3.316×10^{-2}	2.244×10^{4}	2.623	1.775	2.624	1.775
1620	1216	6712.3	2.060×10^{0}	1.383×10^{6}	1.152×10^{-2}	7.732×10^{3}	1.546×10^{4}	1.038×10^{10}	1.546×10^{4}	1.038×10^{10}
1680	1267	6659.7	8.415×10^{-1}	5.604×10^{5}	4.142×10^{-3}	2.759×10^{3}	9.268×10^{3}	6.172×10^{9}	9.268×10^{3}	6.172×10^{9}
1740	1318	6608.4	3.479	2.299×10^{5}	1.509×10^{-3}	9.971×10^{2}	5.595	3.697	5.595	3.697
1800	1367	6558.3	1.505×10^{-1}	9.870×10^{4}	5.795×10^{-4}	3.800	3.467	2.339	3.467	2.339
1860	1415	6509.6	6.695×10^{-2}	4.358	2.295×10^{-4}	1.494×10^{2}	2.182	1.420×10^{9}	2.182	1.420×10^{9}
1920	1463	6462.4	3.007	1.943×10^{4}	9.195×10^{-5}	5.942×10^{1}	1.381×10^{3}	8.924×10^{8}	1.381×10^{3}	8.924×10^{8}
1980	1508	6416.8	1.432×10^{-2}	9.189×10^{3}	3.940	2.528	9.040×10^{2}	5.800	9.040×10^{2}	5.800
2040	1552	6373.0	6.994×10^{-3}	4.457	1.737×10^{-5}	1.107×10^{1}	6.001	3.824	6.001	3.824
2100	1595	6330.8	3.498×10^{-3}	2.215×10^{3}	7.866×10^{-6}	4.980×10^{0}	4.039×10^{2}	2.557×10^{8}	4.039×10^{2}	2.557×10^{8}

Table 2.II (Concluded)

1400 HOURS

TIME (sec)	ALTITUDE (Km)	VELOCITY (m/sec)	N_2 DENSITY (part/cm^3)	N_2 FLUX (part/cm^{2}sec)	O_2DENSITY (part/cm^3)	O_2 FLUX (part/cm^{2}sec)	O DENSITY (part/cm^3)	O FLUX (part/cm^{2}sec)	TOTAL DENSITY (part/cm^3)	TOTAL FLUX (part/cm^{2}sec)
2160	1635	6290.5	1.848×10^{-3}	1.162×10^{3}	3.794×10^{-6}	2.386×10^{0}	2.805×10^{2}	1.764×10^{8}	2.805×10^{2}	1.764×10^{8}
2220	1674	6252.2	9.984×10^{-4}	6.242×10^{2}	1.877×10^{-6}	1.174×10^{0}	1.973	1.234×10^{8}	1.973	1.234×10^{8}
2280	1711	6215.8	5.597	3.479	9.687×10^{-7}	6.021×10^{-1}	1.417	8.808×10^{7}	1.417	8.808×10^{7}
2340	1746	6181.5	3.253	2.011	5.210	3.221	1.039×10^{2}	6.423	1.039×10^{2}	6.423
2400	1780	6149.2	1.929	1.186×10^{2}	2.867	1.763	7.711×10^{1}	4.741	7.711×10^{1}	4.741
2460	1810	6119.0	1.221×10^{-4}	7.471×10^{1}	1.700	1.040×10^{-1}	5.937	3.633	5.937	3.633
2520	1840	6091.0	7.749×10^{-5}	4.720	1.011×10^{-7}	6.158×10^{-2}	4.580	2.790	4.580	2.790
2580	1865	6065.1	5.321	3.227	6.580×10^{-8}	3.990	3.694	2.240	3.494	2.240
2640	1890	6041.5	3.662	2.213	4.293	2.594	2.984	1.803	2.984	1.803
2700	1912	6020.2	2.640	1.589	2.954	1.778	2.475	1.490	2.475	1.490
2760	1932	6001.2	1.964	1.179×10^{1}	2.107	1.264×10^{-2}	2.090	1.254	2.090	1.254
2820	1950	5984.4	1.507	9.018×10^{0}	1.558	9.323×10^{-3}	1.797	1.075×10^{7}	1.797	1.075×10^{7}
2880	1964	5970.0	1.227	7.325	1.231×10^{-8}	7.349	1.598	9.540×10^{6}	1.598	9.540×10^{6}
2940	1977	5958.0	1.022×10^{-5}	6.089	9.906×10^{-9}	5.902	1.433	8.538	1.433	8.538
3000	1987	5948.2	8.772×10^{-6}	5.218	8.386	4.988	1.319	7.845	1.319	7.845
3060	1995	5941.0	7.809	4.639	7.342	4.362	1.234	7.331	1.234	7.331
3120	2000	5936.0	7.262	4.527	6.757	4.014	1.184	7.034	1.184	7.034
3180	2002	5933.4	7.054	4.185	6.537	3.878	1.164	6.906	1.164	6.906
3240	2002	5933.2	7.054×10^{-6}	4.185×10^{0}	6.537×10^{-9}	3.878×10^{-3}	1.164×10^{1}	6.906×10^{6}	1.164×10^{1}	6.906×10^{6}

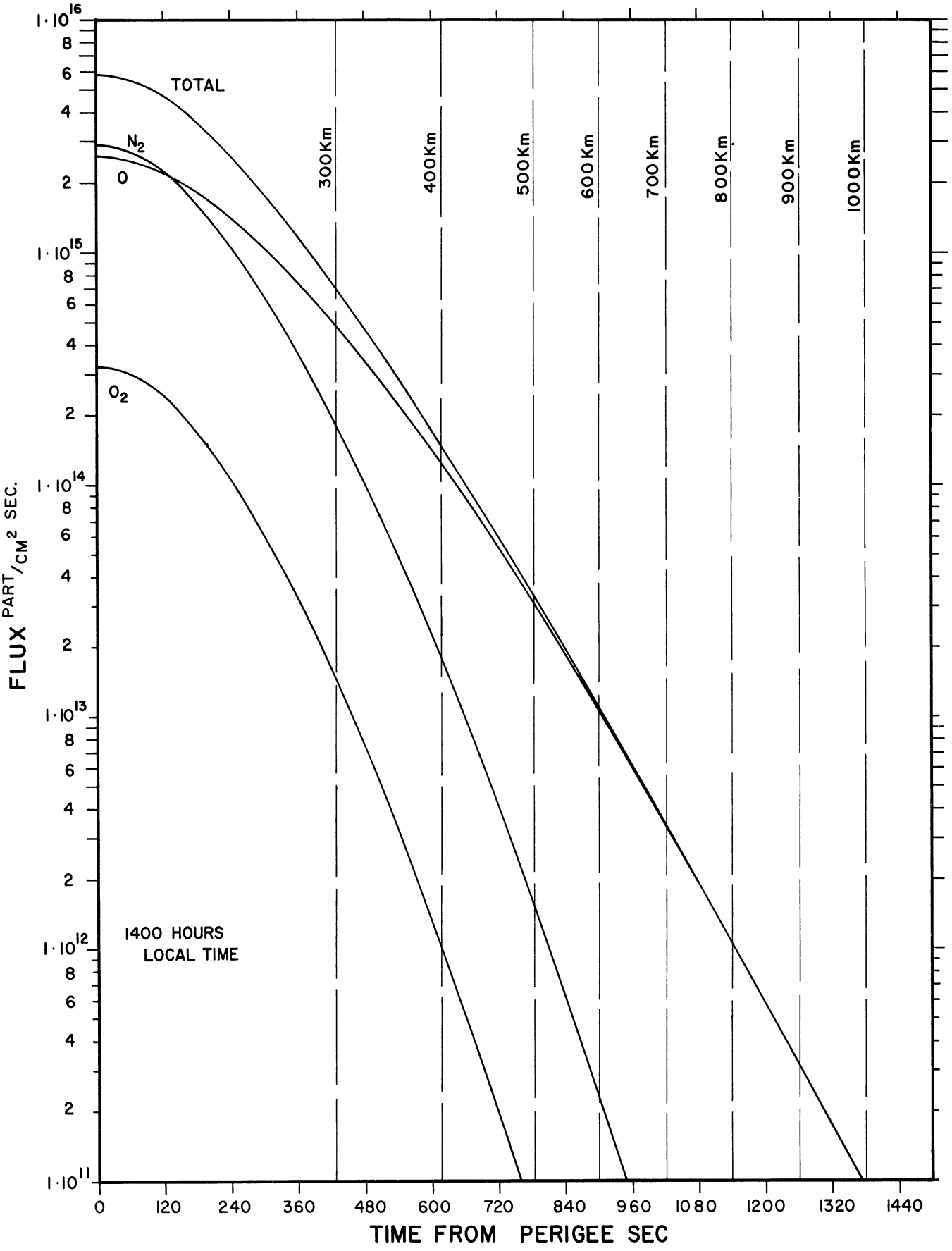

Figure 2.2 Fluxes of major atmospheric constituents to a satellite in proposed ODYSSEY orbit for 1400 hours local time.

3. TIME-OF-FLIGHT (TOF) ANALYSIS OF VELOCITY DISTRIBUTION

3.1 INTRODUCTION AND ASSUMPTIONS

Given a beam of neutral particles with arbitrary velocity distribution and a burst of electrons for excitation, the problem at hand is to determine the metastable particle flux at a downstream detector as a function of time. Once this has been done, the experimental problem of determining the velocity distribution from the metastable particle flux can be discussed.

The geometry to be considered is shown in Figure 3.1.

The analysis is based on the following assumptions:

(1) The metastable lifetime is infinite (no metastable decay occurs over relevant time intervals);

(2) The fraction of the neutral beam which is metastabilized is negligible (the neutral particle density is constant over the region of excitation);

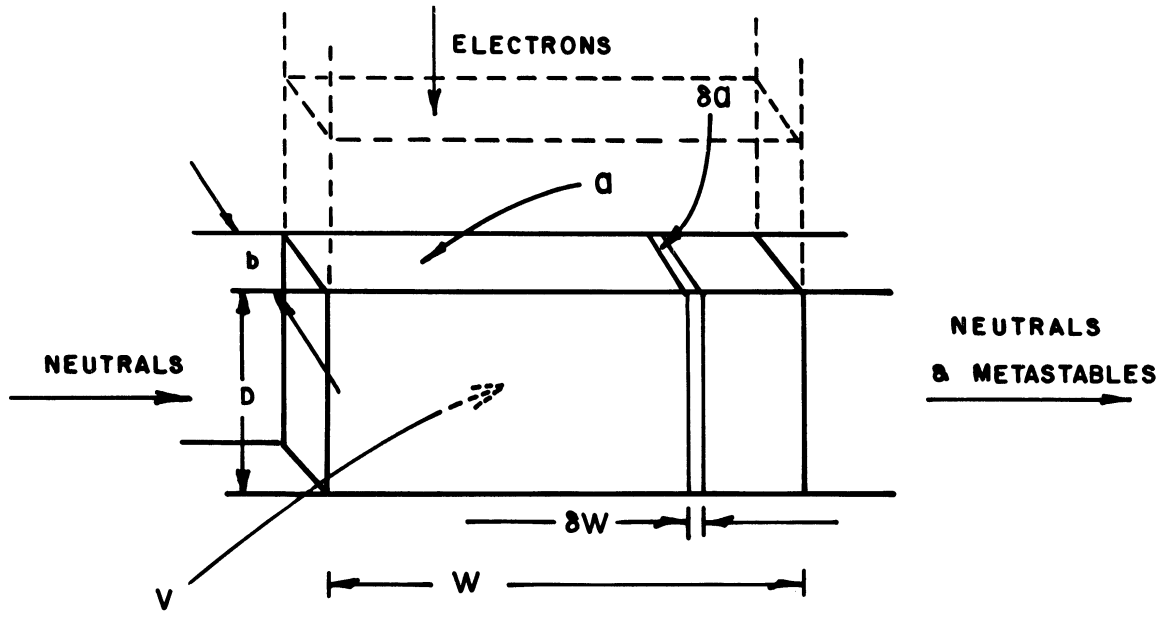

Figure 3.1 Geometry of neutral stream and electron beam.

(3) The electron density is uniform over the cross-section of the electron beam;

(4) The electron pulse is rectangular in time (zero rise and fall times; constant over an interval τ).

(5) The metastable particles are undeflected by the electron bombardment (no recoil occurs).

As will be seen, these assumptions, along with certain reasonable physical requirements, lead to an extremely simple interpretation of the detected metastable flux. The effects of deviations from these simple assumptions on this interpretation are discussed in Sections 3.5 and 3.6.

3.2 RESPONSE TO A MONOENERGETIC NEUTRAL BEAM

As a foundation for the development, consideration is first given to an elemental volume δV of the neutral beam (see Figure 3.1)

$$\delta V = D\delta a$$

$$= Db\ \delta W$$

as it drifts with its particles (assumed to have speed v) across the electron beam.

If one electron per second crosses δa, and if one neutral particle with excitation cross-section δ^* resides in δV, then the probability of excitation per unit time will be $\sigma^*/\ \delta a$, or, stated another way, $\sigma^*/\delta a$ metastables will be produced per second. If there are N_n neutral particles in δV, and $\mathcal{N}_e$ electrons cross δa per second, then the total number of metastables produced during a time increment dt will be

$$dN^* = N_n \mathcal{N}_e \frac{\sigma^*}{\delta a} dt$$

By utilizing the facts that

$$N_n = n_o \delta V$$

$$\mathcal{N}_e = \frac{i^-}{e} \cdot \frac{\delta a}{a}$$

where n_o is the neutral particle density, i^- the electron current, and e the electronic charge, the above becomes

$$dN^* = n_o \delta V \frac{i^-}{e} \frac{\delta a}{a} \frac{\sigma^*}{\delta a} dt.$$

Dividing by δV yields the increment in the metastable density

$$dn^* = \frac{i^-}{e} \frac{\sigma^*}{a} n_o dt.$$

By integrating over the time that the volume element in question remains in the electron beam, the resulting metastable density is found to be

$$n^* = \beta t$$

where

$$\beta = \frac{i^-}{e} \frac{\sigma^*}{a} n_o$$

and t represents the time that δV has been exposed to the electron beam. With this result it is now possible to determine the temporal behavior of the metastable particle density at any position along the emerging stream.

An important parameter for the following discussion is the transit time, T, of a neutral particle across the electron beam:

$$T = \frac{W}{v}$$

The description of the emerging metastable density depends on whether this quantity is greater than or less than the time interval, τ, over which the electron beam is fired. The first case ($T > \tau$) corresponds to "slow" particles. Here, some particles

remain in the electron beam over its full firing interval; for these, the maximum possible metastable density, $\beta\tau$, is achieved. In the second case, no particles linger in the electron beam for its full duration, so the greatest metastable density possible is only βt $(t < \tau)$. By utilizing the definition of T, and adopting the convention that all times are measured from the instant at which the electron beam is turned on, the metastable density at a collector located a distance L from the edge of the electron beam may be expressed in the following way:

$$v < \frac{W}{\tau} \qquad \text{(slow neutrals)}$$

$$n^*(t) = \beta \begin{cases} 0 & 0 \leq t \leq \frac{L}{v} \\ t - \frac{L}{v} & \frac{L}{v} \leq t \leq \tau + \frac{L}{v} \\ \tau & \tau + \frac{L}{v} \leq t \leq \frac{L+W}{v} \\ \frac{L+W}{v} + \tau - t & \frac{L+W}{v} \leq t \leq \tau + \frac{L+W}{v} \\ 0 & \tau + \frac{L+W}{v} \leq t < \infty \end{cases}$$

$$v > \frac{W}{\tau} \qquad \text{(fast neutrals)}$$

$$n^*(t) = \beta \begin{cases} 0 & 0 \leq t \leq \frac{L}{v} \\ t - \frac{L}{v} & \frac{L}{v} \leq t \leq \frac{L+W}{v} \\ \frac{W}{v} & \frac{L+W}{v} \leq t \leq \tau + \frac{L}{v} \\ \frac{L+W}{v} + \tau - t & \tau + \frac{L}{v} \leq t \leq \tau + \frac{L+W}{v} \\ 0 & \tau + \frac{L+W}{v} \leq t < \infty \end{cases}$$

In these expressions the term $\frac{L}{v}$ accounts for the time the particles take to drift from the electron beam to the collector. Multiplying these relations by v yields at once the metastable flux density at the collector as a function of time:

$$F^*(t) = n^*(t)\, v$$

The total number of metastables striking unit area of the collector is obtained by integrating this expression over all time:

$$N^* = \int_0^\infty dt\, F^*(t)$$
$$= \beta W \tau$$

The absence of some measure of the particle speed in this result may at first seem surprising. It arises from the fact that the <u>total</u> number of metastables produced in a given time increment depends only on the neutral density, not on the speed at which these particles pass through the electron beam.

By using the above result, a normalized metastable flux density can be conveniently defined by

$$f^*(t) = \frac{F^*(t)}{N^*}$$

More explicitly:

$$v < \frac{W}{\tau} \quad \text{(slow neutrals)}$$

$$f^*(t) = \frac{1}{W\tau} \begin{cases} 0 & 0 \leq t \leq \frac{L}{v} \\ vt - L & \frac{L}{v} < t < \frac{L}{v} \\ v\tau & \tau + \frac{L}{v} \leq t \leq \frac{L+W}{v} \\ L+W+v\tau-vt & L + \frac{W}{v} \leq t \leq \tau + \frac{L+W}{v} \\ 0 & \tau + \frac{L+W}{v} \leq t < \infty \end{cases}$$

$$v > \frac{W}{\tau} \qquad \text{(fast neutrals)}$$

$$f^*(t) = \frac{1}{W\tau} \begin{cases} 0 & 0 \leq t \leq \frac{L}{v} \\ vt - L & \frac{L}{v} \leq t \leq \frac{L+W}{v} \\ W & \frac{L+W}{v} \leq t \leq \tau + \frac{L}{v} \\ L+W+v\tau-vt & \tau + \frac{L}{v} \leq t \leq \tau + \frac{L+W}{v} \\ 0 & \tau + \frac{L+W}{v} \leq t < \infty \end{cases}$$

The significance of such a normalized flux is that it provides the "flux" distribution associated with a single metastable particle. Consequently, actual counting rates can be obtained simply by scaling to the total number of metastables in the beam.

3.3 RESPONSE TO A NEUTRAL BEAM WITH ARBITRARY DISTRIBUTION OF PARTICLE SPEEDS

In the following discussion it will be useful to consider the electron beam as the superposition of two hypothetical beams. At time t=0 an "exciting" beam is turned on, to be left running indefinitely. At time $t=\tau$, a "deexciting" beam, assumed to produce "anti-metastable" particles with the same efficiency as the previous beam produces metastables, is turned on, also to be left running indefinitely. The superposition of these beams is then equivalent to no beam at all after $t=\tau$. The utility of this approach is that only the response to the first case (which is relatively simple) need be determined, since the total response is then obtained by subtracting from this the same result shifted in time by τ.

Suppose that the fraction of the neutral particles having speeds within dv of v is given by g(v) dv. Then g(v) satisfies the relation

$$\int_0^\infty dv\ g(v) = 1.$$

Momentarily paralleling the development of Section 3.2, consideration is given to a small volume element δV, weighted by the factor g(v)dv, for each small increment dv of particle speeds.

If only the exciting beam, which is left on indefinitely, is considered, all neutral particles will be "fast", and the metastable density at the collector for particles within dv of v can be written at once:

$$dn^*(v,t) = \beta\ g(v)\ T\ (v,t)\ dv$$

where

$$T(v,t) = \begin{cases} 0 & 0 \le t < \frac{L}{v} \\ t - \frac{L}{v} & \frac{L}{v} \le t < \frac{L+W}{v} \\ \frac{W}{v} & \frac{L+W}{v} \le t < \infty \end{cases}$$

Multiplying by v and integrating over all possible speeds provides the metastable flux at the collector due to the exciting beam:

$$F_e^*(t) = \beta\int_0^\infty dv\ g(v)\ v\ T\ (v,t)$$
$$= \beta\ H(t;L,W)$$

where

$$H(t;L,W) = \int_{\frac{L}{t}}^{\frac{L+W}{t}} du\ g(u)\ (ut-L) + W\int_{\frac{L+W}{t}}^{\infty} du\ g(u)$$

By using the superposition principle, the metastable flux due to the actual electron beam is

$$F^*(t,\tau;L,W) = \beta\Big\{H(t;L,W) - \theta(t-\tau)\, H(t-\tau;L,W)\Big\}$$

where θ is the unit step function

$$\theta(x) = \begin{cases} 0 & x < 0 \\ 1 & x > 0 \end{cases}$$

Integrating this result over all time yields

$$N^* = \beta W\tau \int_0^\infty dv\; g(v)$$
$$= \beta W\tau$$

as before. Thus, the normalized metastable flux density is given by

$$f^*(t,\tau;L,W) = \frac{1}{N^*} F^*(t,\tau;L,W)$$
$$= \frac{1}{W\tau} \{H(t;L,W) - \theta(t-\tau)H(t-\tau;L,W)\}$$

3.4 THE DRIFTING MAXWELLIAN GAS

A particular case which is of interest for the proposed experiment is the drifting Maxwellian gas. Here the velocities of the neutral gas particles obey the Maxwellian distribution law in a frame in which the gas is macroscopically at rest. The inclusion of a macroscopic drift term allows a description of the ambient gas flux to an instrument mounted on the satellite. Any totally thermalized portion of the gas reflected from a specimen target surface can be investigated by considering the limiting case of zero drift.

As a model for the following discussion, consider a right handed coordinate system with origin located at the orifice of the

instrument (Figure 3.2). The z-axis is directed into the instrument, along the orifice inner normal $\bar{n}$. The ambient Maxwellian gas moves toward the orifice with macroscopic drift velocity $\bar{V}$. which makes an angle ψ with $\bar{n}$. The vectors $\bar{n}$ and $\bar{V}$ define the xz-plane, which is also taken as the plane of zero azimuth for a spherical coordinate system. The azimuthal angle ϕ is measured from the x-axis, while the polar angle θ is measured from the z-axis.

A particle drifting through the orifice has velocity $\bar{w}$ in the rest frame of the gas, and velocity $\bar{v}$ in the frame of the orifice.

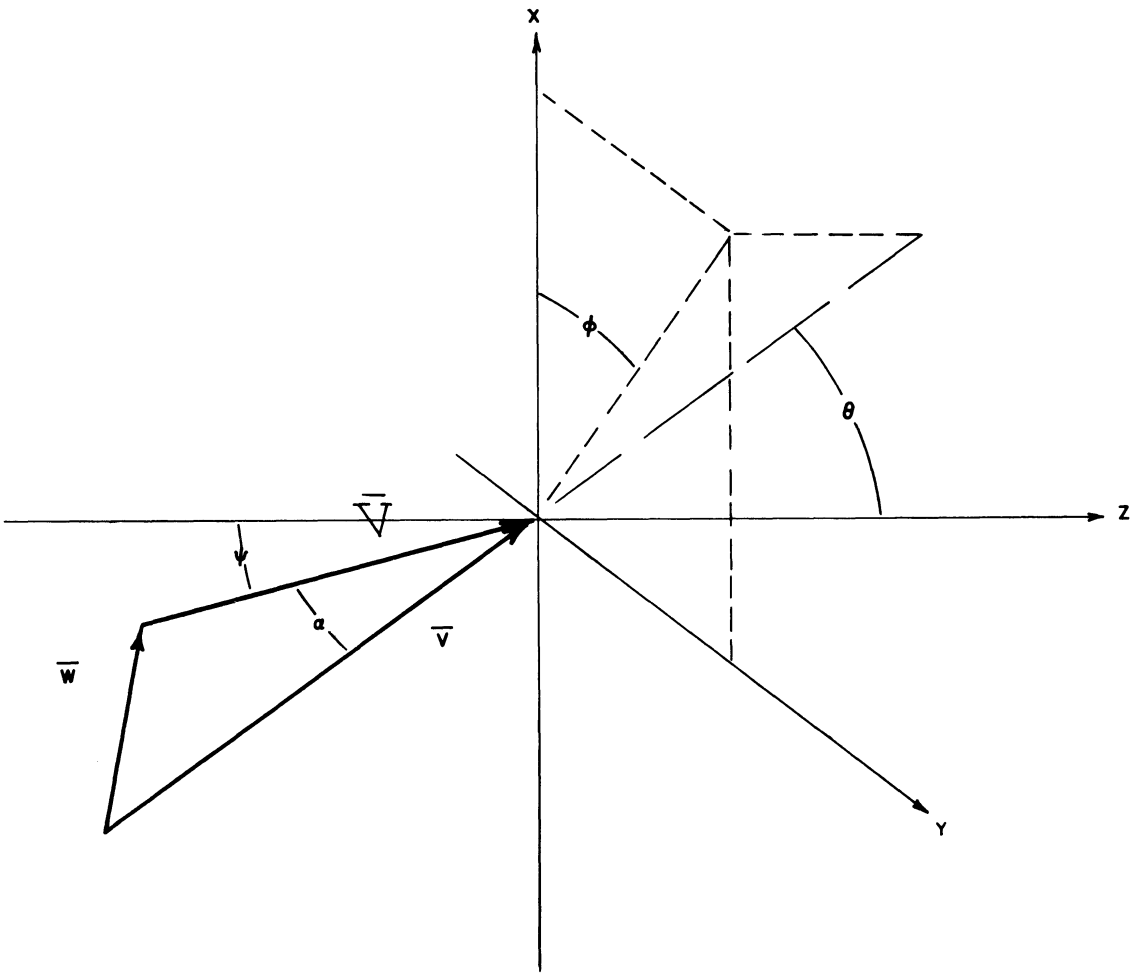

Figure 3.2 Velocity vectors and coordinate systems for discussion of drifting Maxwellian gas.

These quantities are related by

$$\bar{w} = \bar{v} - \bar{V}$$

from which it follows that

$$w^2 = v^2 - 2vV \cos\alpha + V^2$$
$$= (v - V\cos\alpha)^2 + V^2 \sin^2\alpha$$

where α is the angle between $\bar{v}$ and $\bar{V}$. Consequently, the exponential term in the Maxwellian distribution becomes

$$e^{-\frac{w^2}{c^2}} = e^{-(\frac{V \sin\alpha}{c})^2} e^{-(\frac{v - V\cos\alpha}{c})^2}$$

where c is the most probable thermal speed of the particles.

Suppose now that, seen from the orifice, the collector of the instrument subtends solid angle $d\omega$ in the direction indicated by polar and azimuthal angles θ and ϕ respectively. The unit vectors describing the orientations of $\bar{V}$ and $\bar{v}$ are then given by

$$\hat{V} = (\sin\psi, 0, \cos\psi)$$
$$\hat{v} = (\sin\theta\cos\phi, \sin\theta\sin\phi, \cos\theta)$$

so that

$$\cos\alpha \equiv \hat{V} \cdot \hat{v}$$
$$= \cos\psi\cos\theta + \sin\psi\sin\theta\cos\phi.$$

In the spherical coordinate system (v, θ, ϕ) the distribution of particles in $d\omega$ and within dv of v is proportional to

$$v^2 e^{-\frac{w^2}{c^2}} dv\, d\omega.$$

Accordingly, the normalized speed distribution function is

$$g(v) = \frac{2}{c^3 N(s \cos \alpha)} \; v^2 \; e^{-\left(\frac{v - V \cos \alpha}{c}\right)^2}$$

where, by direct integration, it is found that

$$N(x) = xe^{-x^2} + \sqrt{\frac{\pi}{2}} \; (1+2x^2)(1+\operatorname{erf} x)$$

and $s = \frac{V}{c}$ is the speed ratio.

Inserting these expressions in the relation for H and carrying out the integration gives

$$\frac{c^3}{2} N(s \cos \alpha) \; H(t;L,W) = \int_{\frac{L}{t}}^{\frac{L+W}{t}} dv \; v^2 e^{-\left(\frac{v - V \cos \alpha}{c}\right)^2} \qquad (vt-L)$$

$$+W \int_{\frac{L+W}{t}}^{\infty} dv \; v^2 \; e^{-\left(\frac{v - V \cos \alpha}{c}\right)^2}$$

$$= \frac{c^4 t}{2} \; G_m\left(\frac{L}{ct}, \; s \cos \alpha\right) - G_m \left(\frac{L+W}{ct}, \; s \cos \alpha\right)$$

where

$$G_m(x,y) = (1+y^2) \; e^{-(x-y)^2}$$

$$+\sqrt{\frac{\pi}{2}} \; [y(3+2y^2) - x(1+2y^2)] \; \operatorname{erfc} (x-y).$$

Consequently, the normalized metastable flux density is given by

$$f^*(t,\tau;L,W) = \frac{c}{W\tau N(s\cos\alpha)} \cdot \left\{ t\left[G_m\left(\frac{L}{ct}, s\cos\alpha\right) - G_m\left(\frac{L+W}{ct}, s\cos\alpha\right)\right] - (t-\tau)\,\theta\,(t-\tau)\left[G_m\left(\frac{L}{c(t-\tau)}, s\cos\alpha\right) - G_m\left(\frac{L+W}{c(t-\tau)}, s\cos\alpha\right)\right]\right\}.$$

Computer evaluation of this expression for values of the parameters in the range of interest yields the results shown in Figures 3.3 and 3.4.

An interesting phenomenon can be discussed upon referring to Figure 3.4. In a Maxwellian gas macroscopically at rest, the peak of the distribution function is known to occur at v=c. In the instrument under consideration, this peak corresponds to a time of flight $t=\frac{L}{c}$; for each curve of the figure, this time is indicated by a cross near the corresponding peak. It is observed that every flux curve peaks much earlier than this time (earlier, also, than the time of flight corresponding to the r.m.s. speed). That this "early peaking" is a normal occurence can be seen in the following way.

For simplicity, consider a flat distribution function, focusing attention on particles in two small intervals of identical width Δv about two different speeds (Figure 3.5). If the time for one such "packet" to travel to the collector is t, it will disperse spatially to a length $l=t\Delta v$. The time increment over which this extended packet actually strikes the collector will then be $\Delta t=\frac{\Delta l}{v}$.

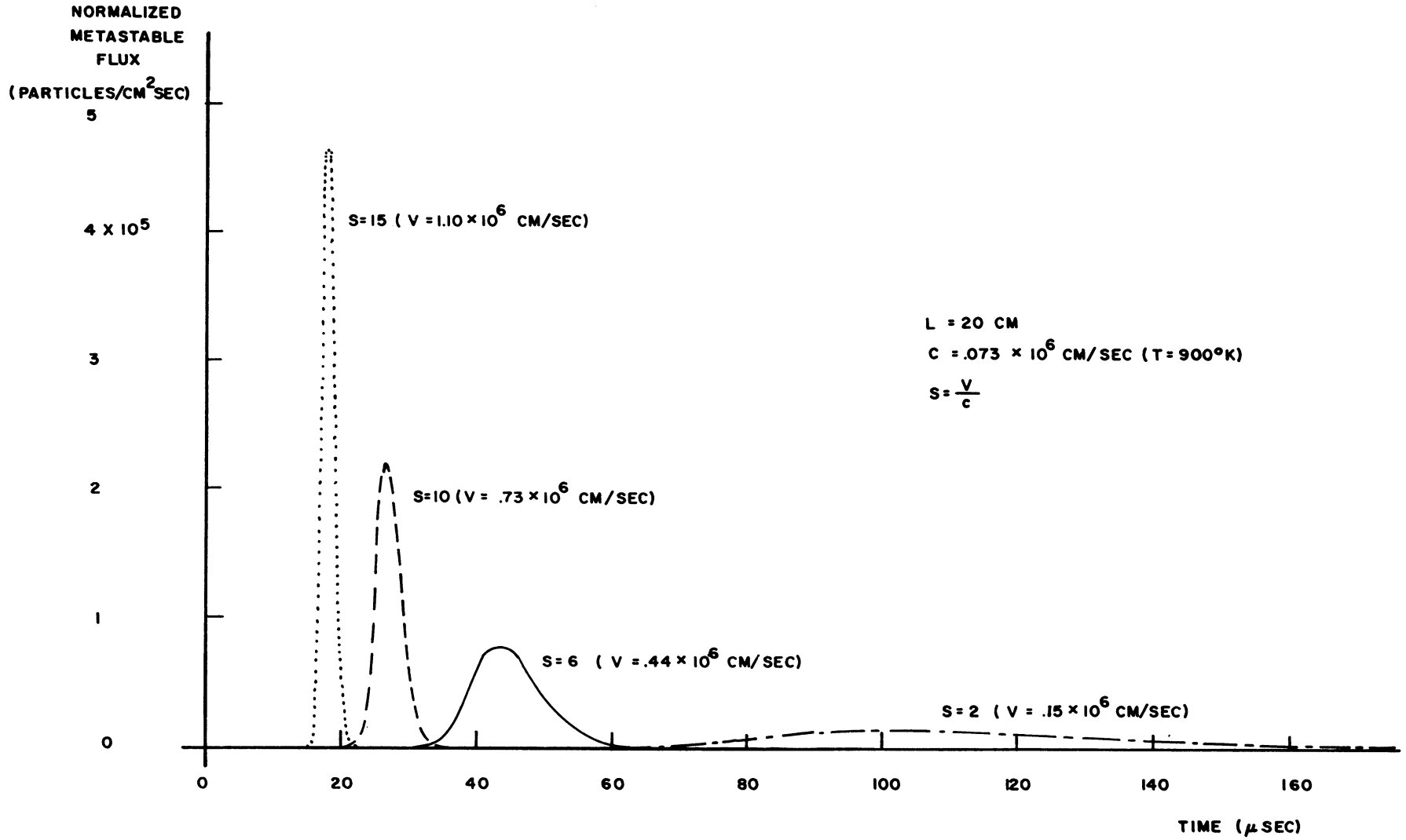

Figure 3.3 Expected flux distribution for 900°K gas normally incident on a TOF analyzer moving with speed V. Curves normalized to give flux per single mestable.

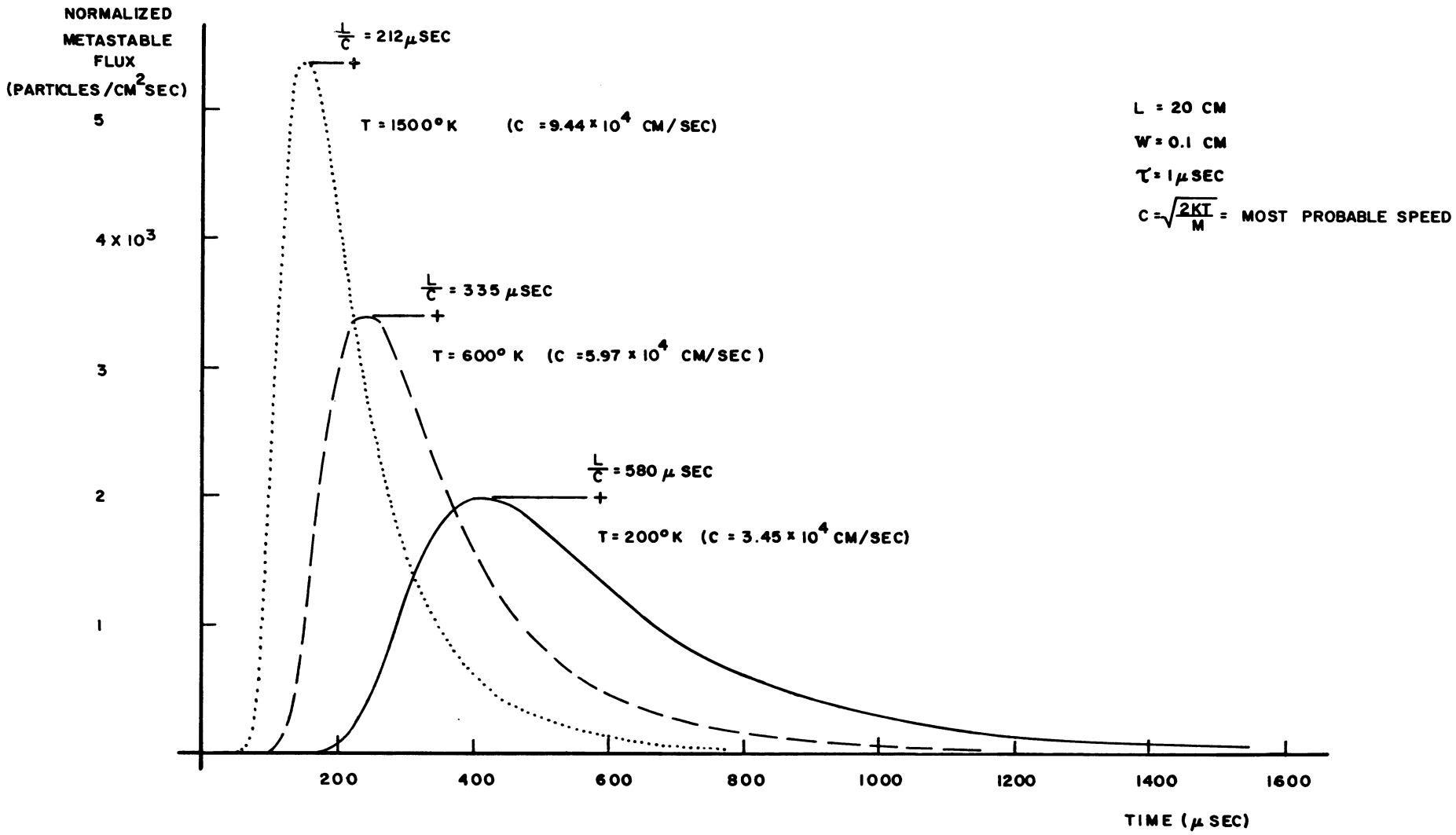

Figure 3.4 Expected flux distribution for gas accommodated to various surface temperatures. Curves normalized to give flux per single mestable. Crosses indicate flight times for particles having the appropriate most probable thermal speed.

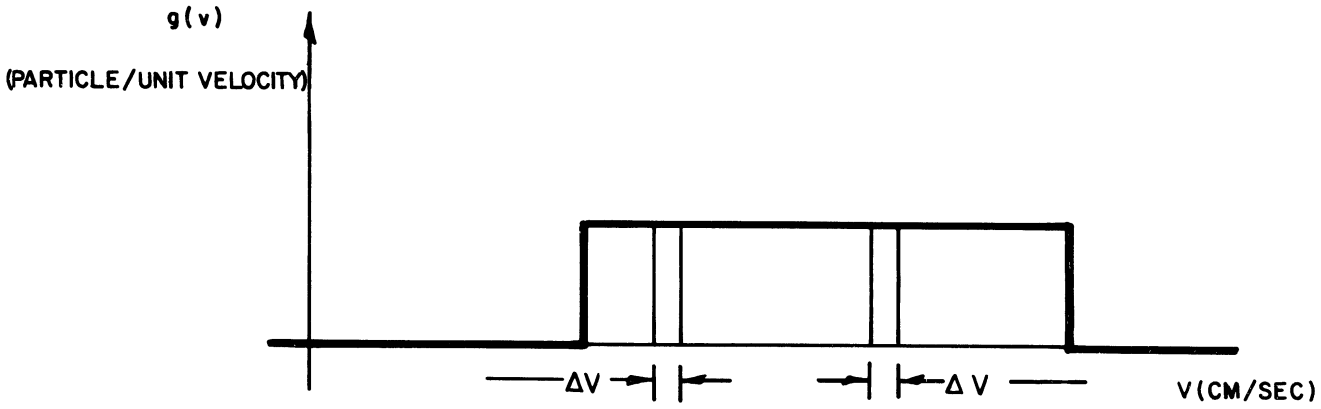

Figure 3.5 Simplified velocity distribution for discussion of shift in flux intensity peak relative to peak of velocity distribution.

Since the transit time to the collector is $t=L/v$, it follows that $\Delta t=\frac{L\Delta v}{v^2}$ from which it is seen that the particles in the faster packet will strike the collector over the shorter interval, i.e., the flux density is greater. It is noted that this condition will remain true even if one factor of $\frac{1}{v}$ is removed to account for the velocity dependent excitation process.

3.5 A USEFUL APPROXIMATION

Two factors strongly compel simplification of the previously obtained results. First, the complexity of the flux expression, even for the simple Maxwellian case, obscures the nature of the distribution function almost entirely. Second, and more important, the experimental problem is essentially the inverse of that so far considered: to infer the distribution function of the neutral gas from the temporal behavior of the metastable flux.

With available experimental techniques it is possible to design a system in which $\frac{W}{L} << 1$ and $\frac{\tau}{t} << 1$ for all meaningful times (for example: $W=0.1$ cm, $L=20$cm, $\tau=1$ μ sec give a transit time of 20 μ sec for a particle with speed $v=10^6$ cm/sec.) Consider, therefore, an expansion in which these ratios are treated as small quantities.

In section 3.3 the metastable flux density was found to be

$$F^*(t,\tau;L,W) = \beta\{H(t;L,W) - \theta\,(t-\tau)\,H(t-\tau;L,W)\}$$

where

$$H(t;L,W) = \int_{\frac{L}{t}}^{\frac{L+W}{t}} dv\; g(v)\;(vt-L) + W\int_{\frac{L+W}{t}}^{\infty} dv\; g(v).$$

By proceeding formally, $H(t-\tau,L,W)$ may be written as

$$H(t-\tau;L,W) = H(t;L,W) - \tau \frac{\partial H(t;L,W)}{\partial t}$$

$$+\frac{\tau^2}{2} \frac{\partial^2 H(t;L,W)}{\partial t^2} + R_H$$

where R_H is the remainder term. Similarly, expanding $F^*(t,\tau;L,W)$ about $W=0$ yields

$$F^*(t,\tau;L,W) = F^*(t,\tau;L,0) + W \frac{\partial F^*(t,\tau;L,0)}{\partial W}$$

$$+\frac{W^2}{2} \frac{\partial^2 F^*(t,\tau;L,0)}{\partial W^2} + R_F.$$

From the definition of H, $F^*(t,\tau;L,0)$ vanishes identically, and the above expressions may be combined to give

$$F^*(t,\tau;L,W) = \beta\left\{W\tau \frac{\partial^2 H(t;L,0)}{\partial W \partial t} + \frac{W^2\tau}{2} \frac{\partial^3 H(t;L,0)}{\partial W^2 \partial t}\right.$$

$$\left. -\frac{W\tau^2}{2} \frac{\partial^3 H(t;L,0)}{\partial W \partial t^2} + W\tau R_{FH}\right\}$$

Evaluating the indicated derivatives by using the definition of $H(t;L,W)$ and dividing by $\beta W\tau$ provides the normalized metastable flux density explicitly in terms of the distribution function:

$$f^*(t,\tau;L,W) = \frac{L}{t^2}\left\{\left[1+\frac{W}{2L} + \frac{\tau}{t}\right] g\left(\frac{L}{t}\right) + 1/2 \frac{L}{t}\left[\frac{W}{L} + \frac{\tau}{t}\right] g'\left(\frac{L}{t}\right) + R_{FH}\right\}$$

where the prime denotes differentiation with respect to the argument.

For purposes of data reduction it is extremely desirable to suppress the g' and higher order terms, since the leading term is a direct measure of the distribution function. Clearly, the most straightforward way to accomplish this suppression is by making L as large as possible. By doing so, not only is $\frac{W}{L}$ small, but for any given v, $\frac{\tau}{t}$ becomes small as well, since the transit time is $t=\frac{L}{v}$. In this limit, the flux density is given by the zeroth order term

$$f_o^*(t,\tau;L,W) = \frac{L}{t^2} g\left(\frac{L}{t}\right)$$

which corresponds to the flux resulting from an instantaneous excitation of particles in an infinitesimally thin slice of the neutral beam (it is noted that for the Maxwellian case, this result predicts a peak at $t=\frac{1}{\sqrt{2}}\frac{L}{c}$, in good agreement with the previously discussed curves of Figure 3.4. A more physical derivation of the limiting result is given in the appendix.

Comparison of the above approximation (the zeroth) with the next order approximation (up to terms of order $\frac{W}{L}$ and $\frac{\tau}{t}$), and points from the exact result for an extreme Maxwellian case ($c = 10^6$ cm/sec or $T= 11{,}600^{\circ}K$) is given in Figure 3.6. Even here, the zeroth order term is quite a good approximation to the actual curve.

Designing the experiment around this expression has the additional advantage of allowing significant relaxation of assumptions 1, 3, and 4 of section 3.1 (assumption 5 is discussed in section 3.6). In particular, as long as the firing time τ is small

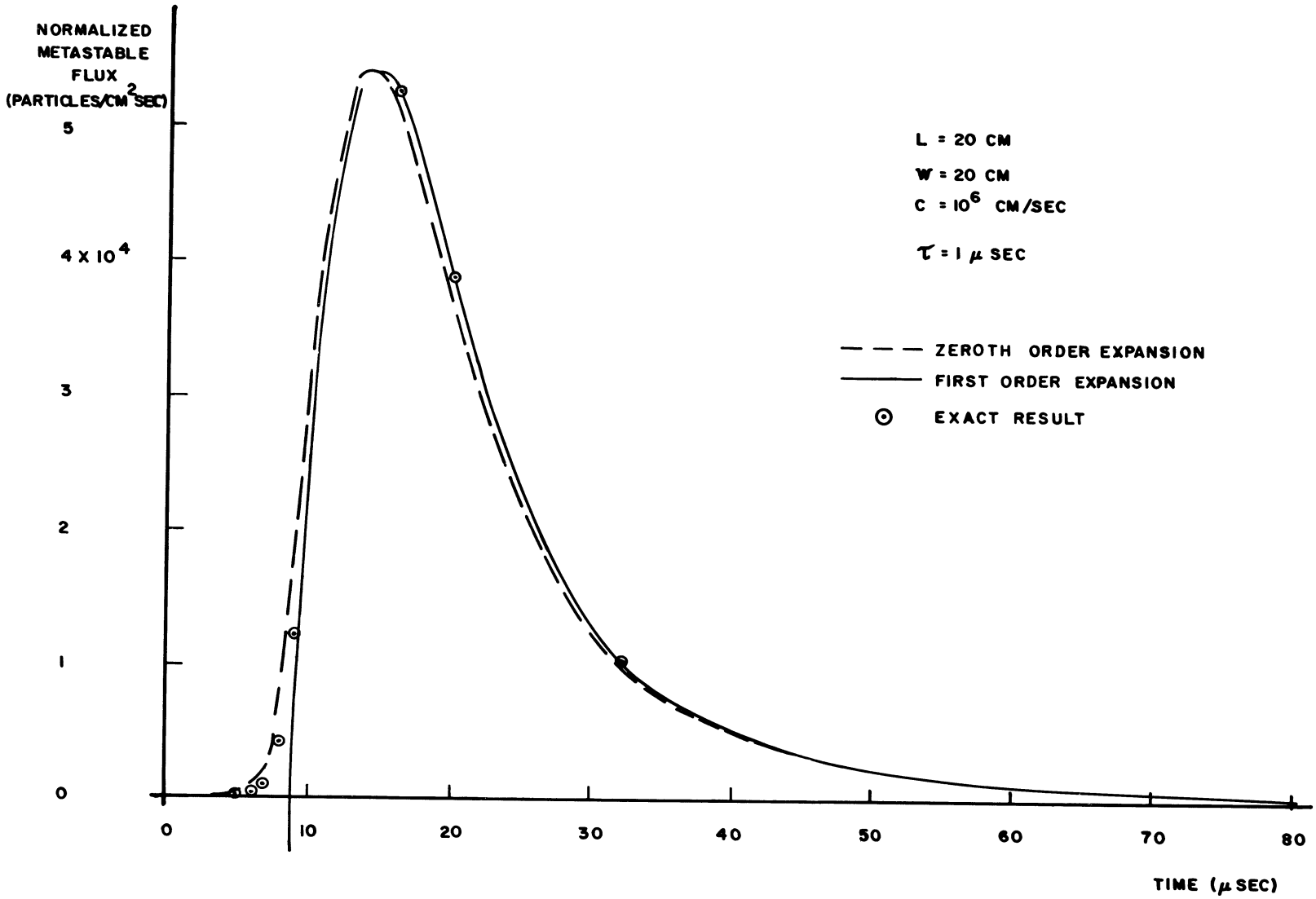

Figure 3.6 An extreme example. Comparison of exact flux distribution and first two approximations for gas accomodated to 11,600°K. Results based on distribution normalized to give flux per single metastable.

relative to the metastable lifetime τ_m, metastable decay can be accounted for by the simple factor e^{-t/τ_m}. Further, since the spatial extent of the exciting region does not enter the above result, the uniformity of electron density through this region is immaterial. Similarly, the exact pulse shape is also unimportant. These last two considerations justify the use of a relatively unsophisticated, and therefore simple, electron gun.

3.6 RECOIL EFFECTS

In Sections 3.1 through 3.5, the investigation of the metastable flux has been conducted on the assumption that the metastables are not deflected during the excitation process (assumption 5, Section 3.1). It will now be shown that this assumption may not always be justified, but that generally the resulting effects are small and can be accounted for by applying a velocity dependent correction to the time of flight data.

The behavior of a neutral molecule undergoing excitation by electron bombardment is governed by the conservation laws for momentum and energy, written respectively

$$M\bar{v}_o + m\bar{u}_o = M\bar{v} + m\bar{u}$$

$$\frac{Mv_o^2}{2} + \frac{mu_o^2}{2} = \frac{Mv^2}{2} + \frac{mu^2}{2} + h\nu^*$$

Here

M = molecular mass

$\bar{v}_o$ = initial molecular velocity

$\bar{v}$ = final metastable velocity

m = electron mass

$\bar{u}_o$ = initial electron velocity

$\bar{u}$ = final electron velocity

$h\nu^*$ = excitation energy of metastable state.

Under the conditions of the experiment the incoming electron velocity $\bar{u}_o$ may be considered given; metastable velocities $\bar{v}$ are measured by the time of flight analyzer. The present problem is to infer the initial neutral particle velocities $\bar{v}_o$ from the above quantities. To this end, it is useful to rewrite the conservation laws, isolating the knowns and unknowns:

$$\bar{v}_o - \mu\bar{u} = \bar{v} - \mu\bar{u}_o \triangleq \bar{B}$$

$$v_o^2 - \mu u^2 = v^2 - \mu u_o^2 + \frac{2h\nu^*}{M} \triangleq \alpha^2$$

where $\mu = \frac{m}{M} << 1$ is the electron-neutral mass ratio. As defined by these equations, the quantities $\bar{B}$ and α^2 are known. Note that α^2 can be negative.

The above rearrangement of the momentum law provides the vector triangle shown in Figure 3.7.

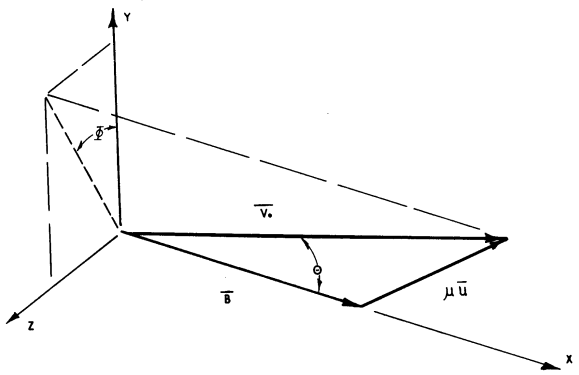

Figure 3.7 Vector representation of momentum conservation law showing imposed coordinate systems.

In the figure, θ is the angle between $\bar{v}_o$ and $\bar{B}$, and ϕ is the angle between the plane of the triangle and the xy plane of a right-handed coordinate system with origin at the tail of $\bar{B}$.

According to the cosine law for triangles, the quantities in Figure 1 obey the relation

$$\mu^2 u^2 = v_o^2 + B^2 - 2B\, v_o \cos\theta$$

Solving the energy equation for $\mu^2 u^2$ and defining normalized cartesian coordinates by the equations

$$X = \frac{x}{B} = \frac{v_o}{B} \cos\theta$$

$$Y = \frac{Y}{B} = \frac{v_o}{B} \sin\theta \cos\phi$$

$$Z = \frac{z}{B} = \frac{v_o}{B} \sin\theta \sin\phi$$

make it possible to reduce the above relation to

$$\left[X - \left(1 + \frac{\mu}{1-\mu}\right)\right]^2 + Y^2 + Z^2 = \left[\frac{\sqrt{\mu}}{1-\mu} \sqrt{1 - \frac{\alpha^2}{B^2}(1-\mu)}\right]^2$$

This equation describes a sphere centered on the line $\bar{B}$ but at a point a fractional distance $\frac{\mu}{1-\mu}$ beyond the tip of the vector. It can be shown that the complicated quantity in the radical is positive for all values of α^2 and B which correspond to metastable excitation.

The interpretation of this result is facilitated by reference to Figure 3.8.

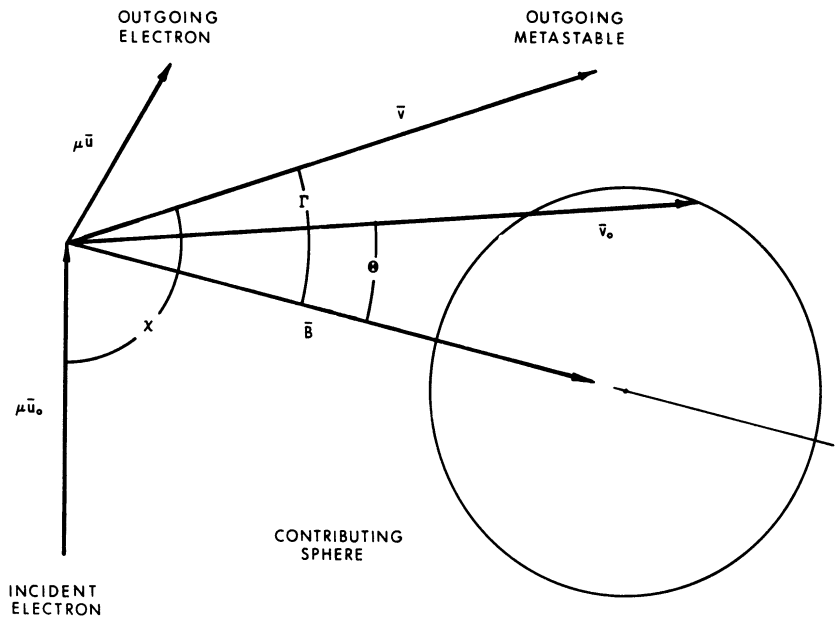

Figure 3.8 Vector diagram for incident and outgoing particles, showing range of incoming molecular velocities $\bar{v}$ (those terminating on the contributing sphere) which are deflected into a single outgoing velocity $\bar{v}$.

The following conclusions may be drawn:

(1) Metastables with velocity $\bar{v}$ arise from neutral particles with a range of velocities $\bar{v}_o$ terminating on the "contributing sphere" defined by the above equation;

(2) The contributing values of $\bar{v}_o$ can be characterized by a mean deflection angle Γ and by a mean speed $\frac{1}{1-\mu} B$;

(3) The contributing values of $\bar{v}_o$, as characterized above, are subject to fractional uncertainties in magnitude given by the normalized sphere radius, $\frac{r}{1+\frac{\mu}{1-\mu}}$ and to angular uncertainties up to the maximum angle Θ_{max} subtended by the sphere.

By algebraic manipulation of the above equations it can be shown that

$$\cos \Gamma \equiv \frac{\bar{B} \cdot \bar{v}}{Bv} = \frac{v - \mu \bar{u}_o \cdot \hat{v}}{v^2 + \mu^2 u_o^2 - 2\mu\, \bar{u}_o \cdot \bar{v}}$$

$$\sin \theta_{max} \equiv \frac{r}{1 + \frac{\mu}{1-\mu}} = \sqrt{\mu} \sqrt{1 - (1-\mu) \frac{\alpha^2}{B^2}}$$

In these expressions $\hat{v}$ is a unit vector along the direction of $\bar{v}$, and r is the radius of the contributing sphere.

For molecular nitrogen it is found that

$$\mu = 1.94 \times 10^{-5}$$

so that Γ and θ_{max} are usually small quantities. Figures 3.9, 3.10 and 3.11 present graphs of $\frac{B}{1-\mu}$, Γ, θ_{max} and $r\,(1-\mu)$ for an electron energy of 7.2 ev (the value corresponding to the maximum metastable excitation cross section of the $A^3\Sigma_u^+$ state of N_2 (see section 5.2)). The angle χ between the incident electron velocity and the final metastable velocity (taken as the direction to the detector) is the parameter. Figures 3.12, 3.13 and 3.14 present the same information for an electron energy of 20 ev.

For a flight path of 20 cm and transit times up to 1 millisecond, corresponding to measurement of speeds of 2×10^4 cm/sec and greater, it is seen that the 7.2 ev case provides a speed resolution of better than 5% and an angular resolution of 3^o or better.

The above development shows that the characteristic initial

speed $\frac{B}{1-\mu}$ and the deflection angle Γ must be used in data reduction to infer the representative contributing velocity $\bar{v}_o$. The measured flux intensity for a given $\bar{v}$ can then be interpreted as that due to particles in the small volume of velocity space (of order r^3B^3) contained in the contributing sphere, weighted by the distribution function $g(v_o)$ evaluated at the characteristic speed $v_o = \frac{B}{1-\mu}$.

The only factor neglected in the above analysis is the actual concentration of the scattered electron velocity vectors over the surface of the contributing sphere. This is determined by the inelastic differential scattering cross section for the excitation process (Lamb & Retherford, 1950; Rubin, et al., 1960; Stebbings, et al., 1960). For electron energies just above the metastable excitation energy, the scattered electron distribution is nearly spherically symmetric, but as the electron energy is increased, bunching of the scattered electrons in favor of the forward direction occurs. Thus, while the subtended angle of the scattering sphere, Θ_{max}, increases with electron energy, the concomitant favoring of forward scattering tends to select contributing values of $\bar{v}_o$ on a progressively smaller portion of the sphere. Under these conditions, Θ_{max} becomes progressively a less valid measure of the error in direction of contributing values of $\bar{v}_o$, Γ a poorer estimate of the average initial direction, and $\frac{B}{1-\mu}$ a less accurate indicator of the initial speed. Since the necessary differential cross-section information on the $A^3\Sigma_u^+$ state of N_2 is not available, nothing further will be said on this point other than to indicate that the curves of Figures 3.12, 3.13, and 3.14 will tend to overestimate Γ, Θ_{max}, and $r(1-\mu)$, while underestimating $\frac{B}{1-\mu}$

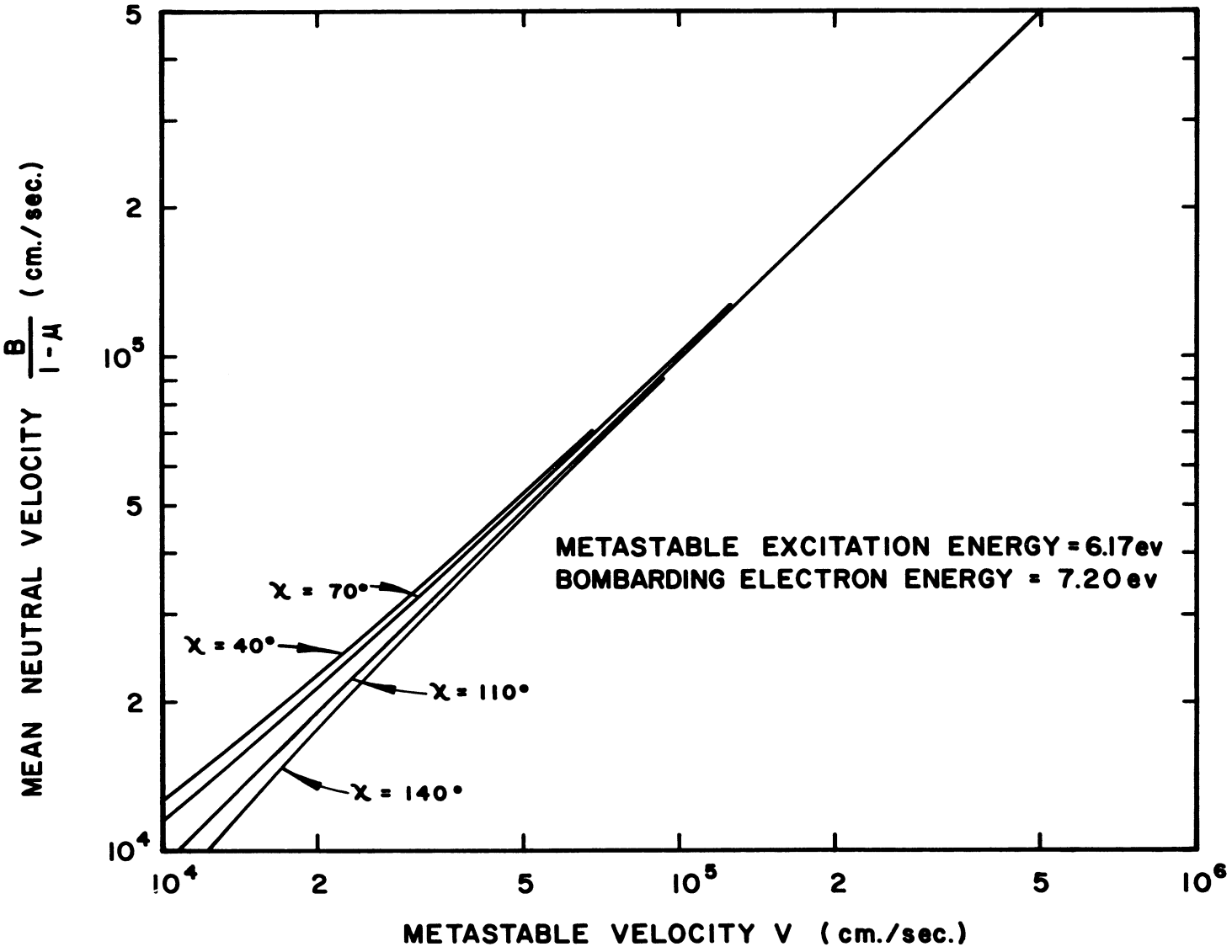

Figure 3.9 Incoming mean neutral velocity ($\frac{B}{1-\mu}$) associated with measured metastable velocity (v) for N_2 ($A\ ^3\Sigma_u^+$) produced by 7.2 ev electron bombardment.

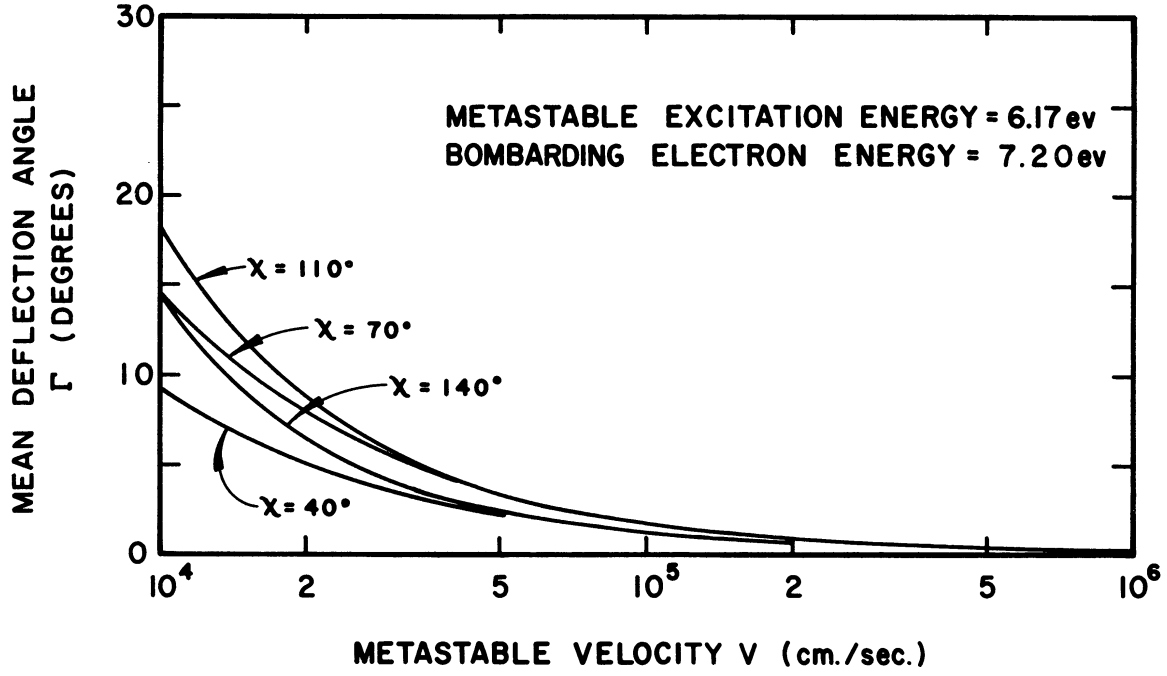

Figure 3.10 Mean deflection angle (Γ) of incoming neutrals associated with measured metastable velocity (v) for N_2 ($A\ ^3\Sigma_u^+$) produced by 7.2 ev electron bombardment.

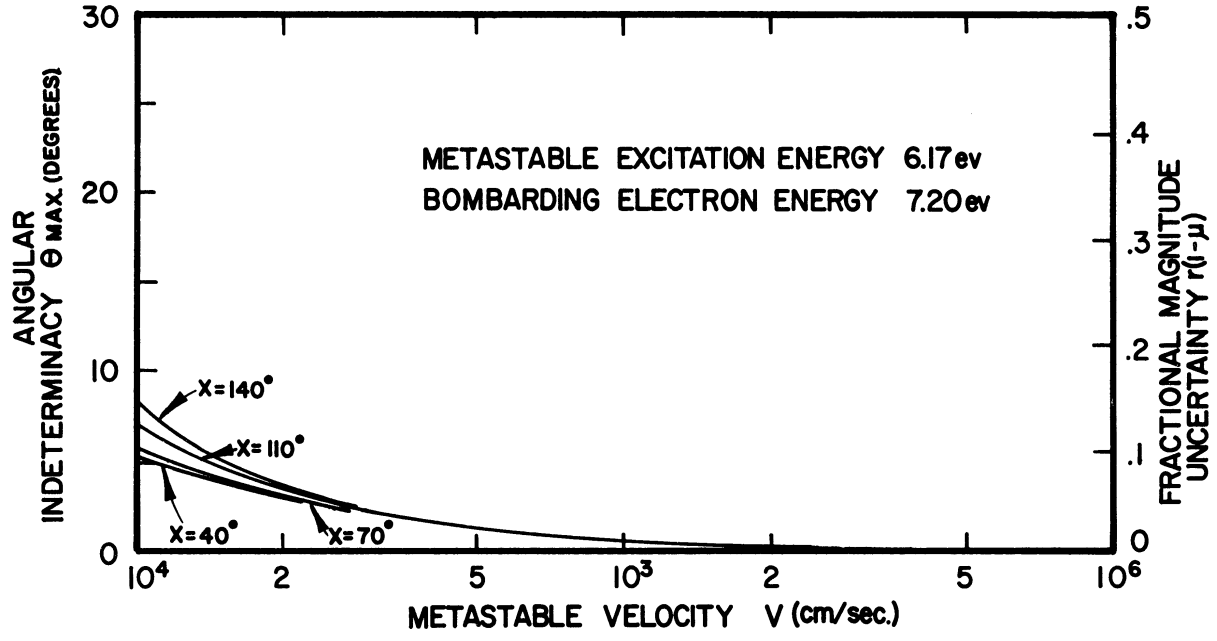

Figure 3.11 Angular (Θ_{max}) and magnitude [r(1-μ)] deviations from mean incoming neutral velocity vector associated with measured metastable velocity (v) for N_2 ($A\ ^3\Sigma_u^+$) produced by 7.2 ev electron bombardment.

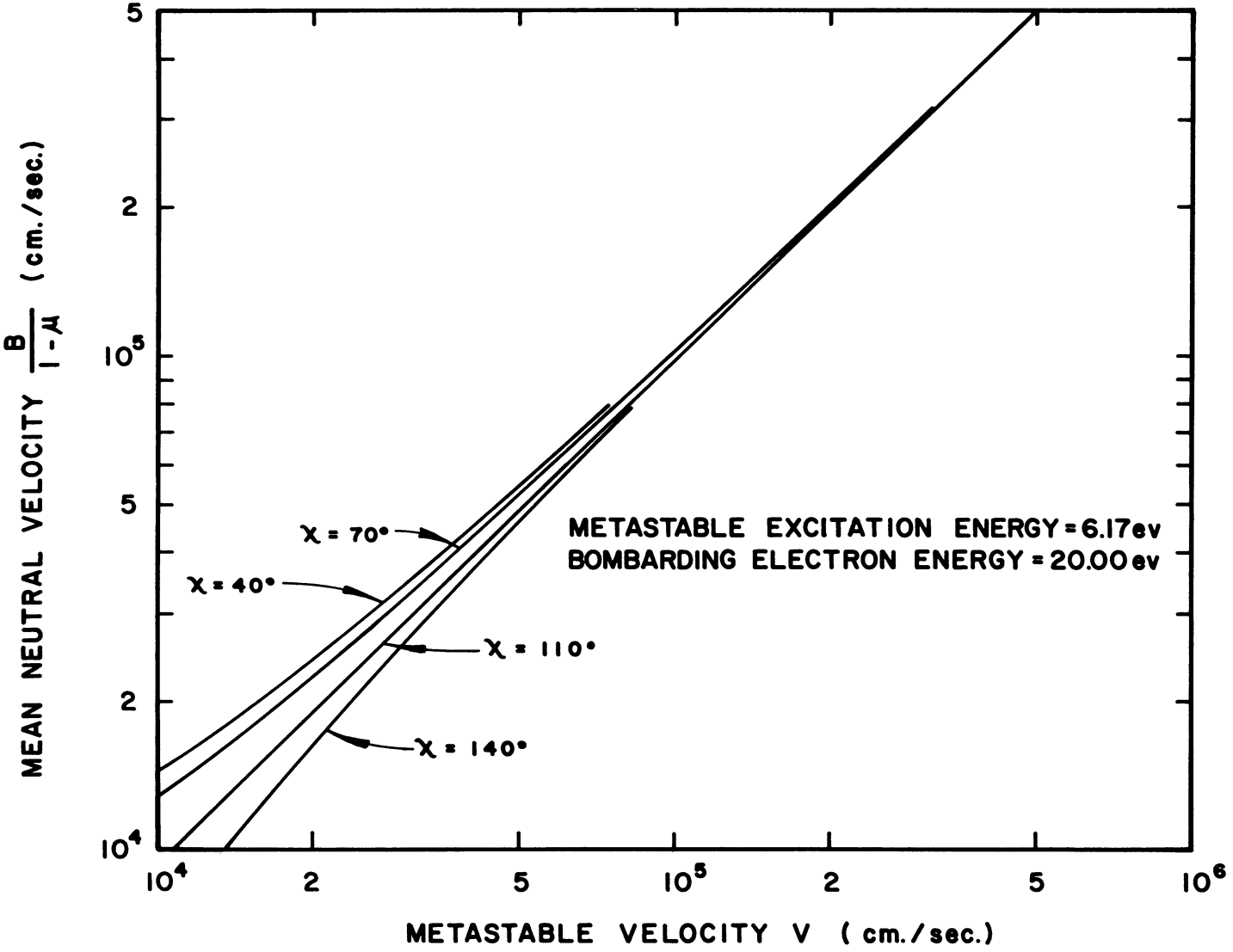

Figure 3.12 Incoming mean neutral velocity ($\frac{B}{1-\mu}$) associated with measured metastable velocity (v) for N_2 ($A\ ^3\Sigma_u^+$) produced by 20.0 ev electron bombardment.

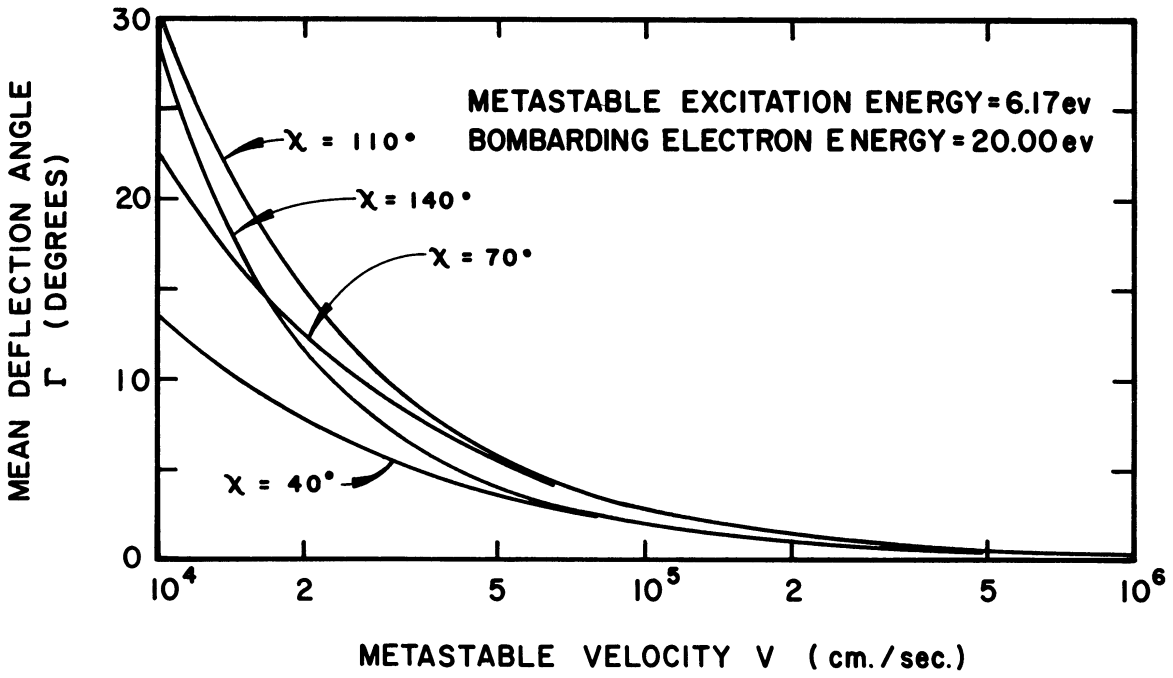

Figure 3.13 Mean deflection angle (Γ) of incoming neutrals associated with measured metastable velocity (v) for N_2 ($A\ ^3\Sigma_u^+$) produced by 20.0 ev electron bombardment.

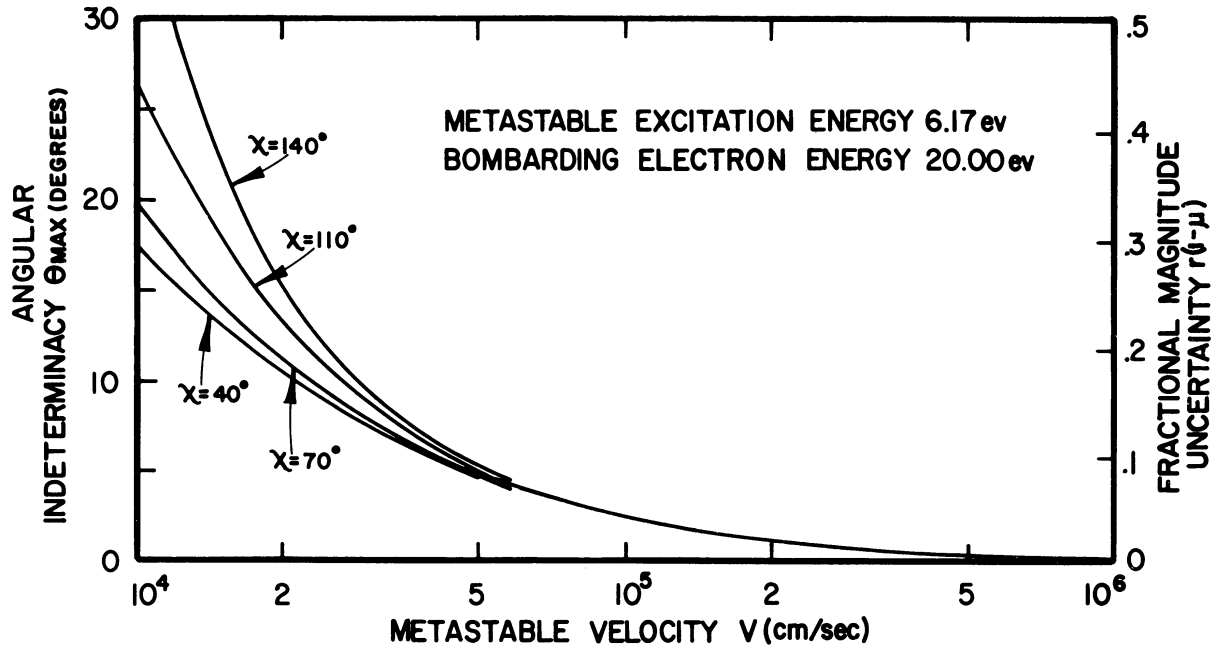

Figure 3.14 Angular (θ_{max}) and magnitude [r(1-μ)] deviations from mean incoming neutral velocity vector associated with measured metastable velocity (v) for N_2 ($A\ ^3\Sigma_u^+$) produced by 20.0 ev electron bombardment.

4. MODIFICATION OF MEASURED VELOCITY DISTRIBUTION BY RESIDUAL GAS SCATTERING

4.1 RELATION OF COLLISIONS TO VELOCITY DISTRIBUTION

4.1.1 Statement of Problem

Because the molecules in the reflected beam must pass through a background gas during the measurements, one must insure that collisions between molecules of the beam and those of the background gas do not introduce systematic errors into the results of the velocity distribution measurements. The probability for a beam molecule to undergo a collision with a molecule of the background gas is directly proportional to the length of time the beam molecule spends in its flight from entrance to the detector. Therefore, if sufficient background gas is present, the detected flux may be relatively deficient in slow molecules.

The mean free path of molecules at the pressures in question ($\lesssim 10^{-6}$ torr) is customarily quoted as many meters, well in excess of the dimensions of the apparatus proposed. Nevertheless, it is important to consider two points:

(1) When good angular resolution is wanted in the analysis of the reflected beam, even small angle collisions become important. The usual experimental verifications of mean free path calculations (Bates, 1962) are not sensitive to the occurrence of glancing encounters between molecules.

(2) Long range interactions between molecules may not involve enough momentum transfer to qualify as a

collision in the gas kinetic sense, but such an interaction may quench a metastable molecule and thus remove it completely from the detectable component of the reflected beam.

An alkali atom beam apparatus has been used to measure the velocity distribution of a directional atomic beam as modified by scattering from a background gas. The alkali beam has been chosen for the following reasons: (1) The atoms are particularly easy to produce and to detect; and (2) the collision cross sections for alkalis have been well studied. The results achieved are generally applicable to gas kinetic collisions of any non-polar species. The results can be extrapolated with reasonable confidence to collisions between metastable beam molecules and ground state background gas molecules.

4.1.2 Modification of Velocity Distribution by Collisions

Ideally, the flux of atoms (mass M) with velocities between v and v + dv in a beam emerging from a source at temperature T is given by

$$f(v)\, dv = \kappa\, v^3\, e^{-v^2/c^2}\, dv \qquad (4.1)$$

where

$$c = \sqrt{\frac{2kT}{M}}$$

and κ is a normalization constant reflecting the total number of particles in the beam. If the beam passes through a dilute scattering gas, then the flux decreases with distance because of

collisions, so that at distance ℓ from the source f(v) is changed to

$$\tilde{f}(v,\ell) = f(v)e^{-\ell/\lambda(v)} \tag{4.2}$$

where $\lambda(v)$ is the mean free path of the beam atoms in the gas. The mean free path is dependent on v because the probability of undergoing a collision increases with the time the beam atom spends in the region ℓ.

The number of collisions per second for beam atoms moving with velocity v through a background gas of number density n_G in which the most probable molecular speed is $c_G = \sqrt{\frac{2kT_G}{M_G}}$, is given by (Loeb, 1934)

$$Z(v) = \pi^{-1/2}\, n_G\, \sigma_{BG}\, \frac{c_G^2}{v}\, \chi\left(\frac{v}{c_G}\right) \tag{4.3}$$

where σ_{BG} is the total collision cross section between beam and gas atoms and $\chi(x)$ is given by

$$\chi(x) = xe^{-x^2} + (2x^2 + 1)\int_0^x dy\, e^{-y^2} \tag{4.4}$$

The mean free path is then

$$\lambda(v) = \frac{v}{Z(v)} = \frac{\pi^{1/2}\, v^2}{n_G \sigma_{BG}\, c_G^2\, \chi\left(\frac{v}{c_G}\right)} \tag{4.5}$$

Consequently,

$$\tilde{f}(v,\ell) = \kappa\, v^3\, e^{-\left[\frac{v^2}{c^2} + A\,\frac{\ell}{v^2}\,\chi\left(\frac{v}{c_G}\right)\right]} \tag{4.6}$$

where

$$A = \pi^{-1/2}\, n_G\, \sigma_{BG}\, c_G^2$$

In obtaining the above results, the following assumptions are made:

(1) The density of the scattering gas is constant in the scattering cell.

(2) The effective length of the scattering cell is taken to be the geometric length of the scattering chamber.

(3) Multiple scattering is neglected.

(4) Scattering of atoms into the detected beam is neglected.

(5) All scattering events are considered to originate in the scattering cell and are exclusively attributed to the scattering gas.

4.1.3 Evaluation of Modified Distribution

It is convenient to evaluate $\tilde{f}(v,\ell)$ on a computer. The density of scattering gas, n_G, is obtained from reading a calibrated ion gauge. The temperature of the apparatus ($\sim 300^{\circ}K$) is assumed to govern the characteristic velocity of the scattering gas, c_G. Comparison with the experiments is facilitated if κ is chosen to make the peak value of $\tilde{f}(v,\ell)$ equal to unity when n_G equals zero. The collision cross section σ_{BG} is then chosen to obtain the best fit between the theoretical and the experimental results for $\tilde{f}(v,\ell)$ at finite values of n_G.

If the description given by kinetic theory is adequate, there will be good agreement between the value of σ_{BG} as obtained above and the value for this cross section determined by other experiments. More important for the present study, however, will be the verication of the shape of the function $\tilde{f}(v,\ell)$ as a function of v.

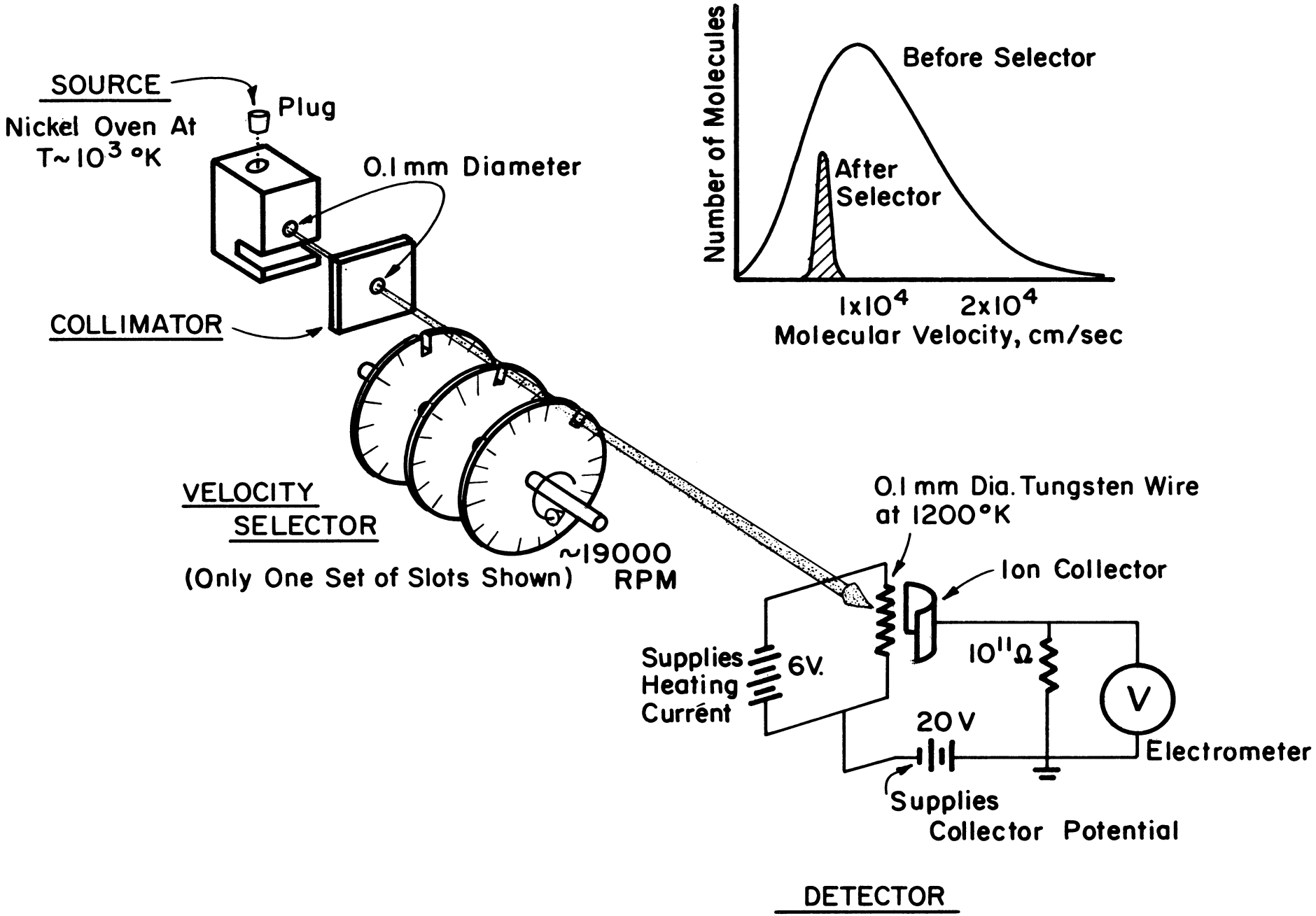

Figure 4.1 Apparatus for Measurement of Beam Velocity Distribution

4.2 DESCRIPTION OF APPARATUS AND PROCEDURE

Figure 4.1 shows the apparatus with its source, velocity selector, collimator, and detector. A description of these components follows.

4.2.1 Vacuum System

The vacuum envelope is composed of four interconnected brass chambers which comprise the oven, velocity selector, scattering cell, and detector units. A straight-through, vacuum valve separates the oven chamber from the rest of the apparatus and allows one to reload the oven without destroying the vacuum in the rest of the machine. Seals are provided by viton O-rings lightly coated with Apiezon "L" grease. Since brass is the primary construction material, no bake-out procedures are used. The vacuum is maintained by four 750 liters/sec oil diffusion pumps using DC 705 silicone pump fluid. In addition, three liquid nitrogen traps provide additional pumping for the system. Figure 4.2 shows a schematic diagram of the vacuum system used for the apparatus.

The pressure of each chamber is monitored by an ionization gauge. Typical pressures observed in each chamber with liquid nitrogen in the three traps and a beam in the machine are as follows:

Section	Pressure
Oven Chamber	1×10^{-6} torr
Velocity Selector Housing	2×10^{-7} torr
Scattering Chamber (no gas)	1×10^{-7} torr
Detector Chamber	1×10^{-7} torr

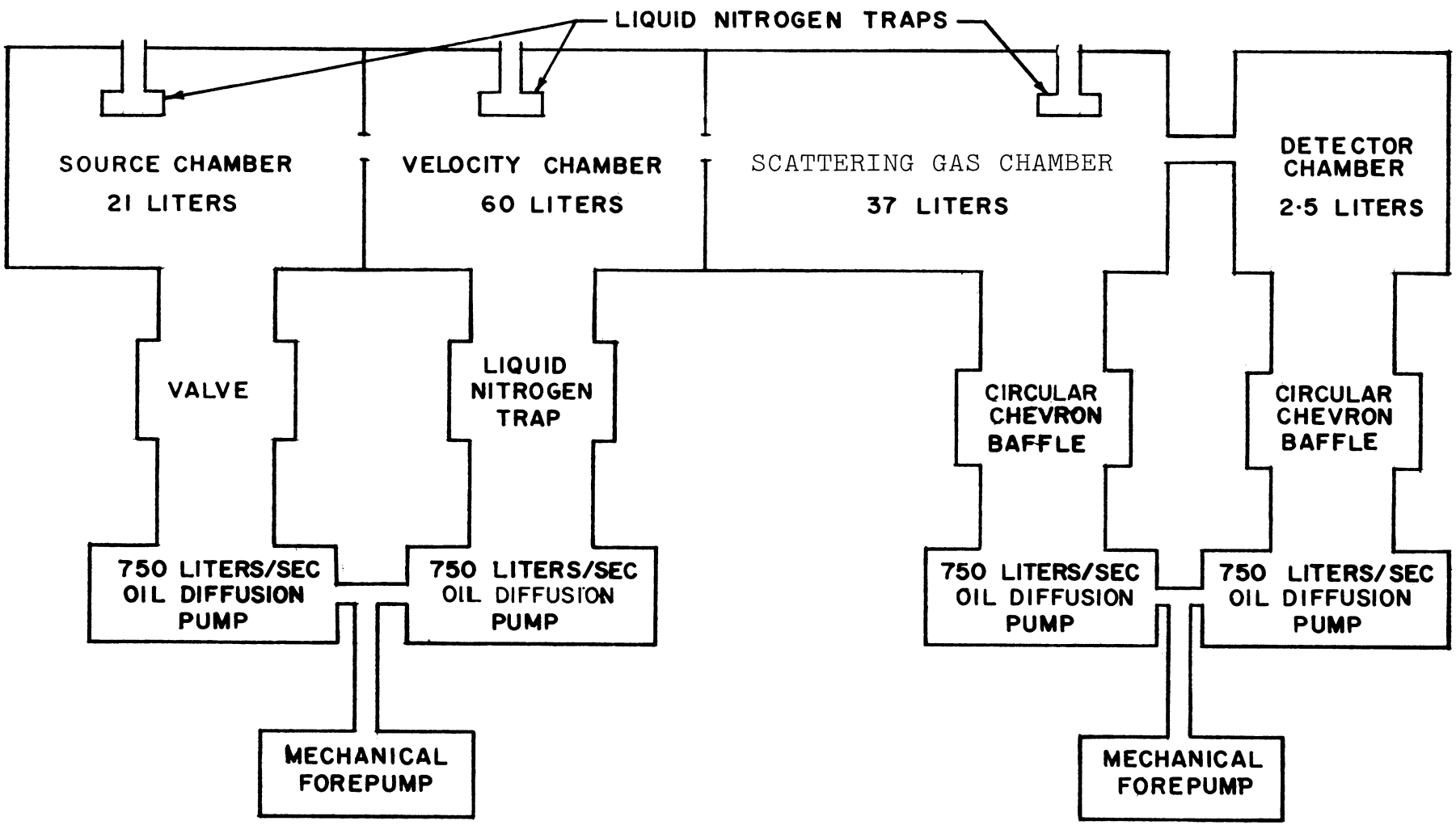

Figure 4.2 Schematic of Vacuum System for Velocity Distribution Measurements

Because most of the measurements of velocity profiles have been made with argon as the scattering gas, it is necessary to calibrate one of the Bayard-Alpert vacuum gauge tubes (Veeco RG-75) and its associated control unit for argon gas. The calibration has been accomplished by attaching the RG-75 gauge unit to an ultra-high vacuum system upon which three calibrated ionization gauges are mounted. (The three gauges have been calibrated previously for N_2 by using a McLeod gauge as the primary reference.) Readings between the four gauges have been compared over the pressure range of 10^{-10} torr up to 10^{-5} torr. Each individual run produces 60 data points from which pressure comparison curves have been constructed. An average correction factor for the gauge, obtained from five separate runs, has been calculated. The resulting gauge constant for the RG-75 gauge, when 10 ma electron current is used, is 1.26×10^{-1} amps/torr for nitrogen. The above calibration procedure is estimated to be accurate to $\pm$ 25%.

4.2.2 Alkali Oven

The oven source for the alkali beam is of the standard design (Kusch and Hughes, 1959) and is shown in Figure 4.3. The oven is made of nickel and has knife-edge slits gapped at 0.25 mm; the slit height is 1 cm. A coil of tungsten wire is used as the heater element.

The samples of the alkali metals used in the runs have a quoted purity greater than 99%. In order to check the purity, the emission spectra of the samples are examined with a double prism spectrograph. The results of this check indicated that the

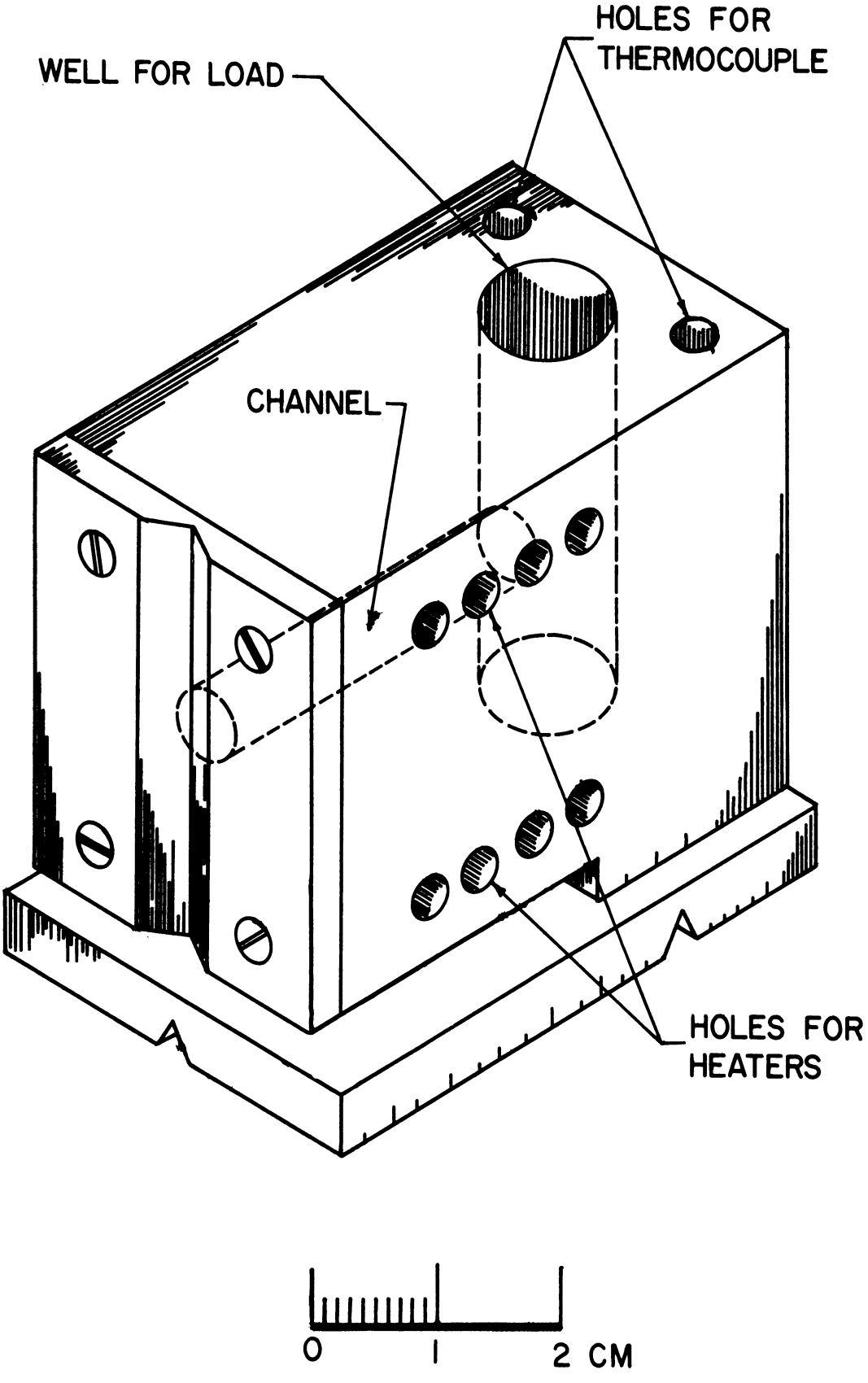

Figure 4.3 Alkali Oven

samples are free of any impurities to within 2%. Details of this check are contained in an internal laboratory report (Bechtel, 1967).

A Chromel-P Alumel thermocouple, mounted in the back of the oven as shown in Figure 4.3, is used to record the oven temperature. The reference junction temperature, governed by room temperature, is a fairly constant 25°C for all the runs. The emf of the thermocouple is measured by a potentiometer. The accuracy of the potentiometer and thermocouple circuit is checked by measuring the ice point and boiling point of water.

4.2.3 Collimator and Velocity Selector

The collimator is a slit constructed of stainless steel razor blade edges. The height of the slit is 1 cm and the width, 7.6×10^{-3} cm. The collimator is mounted about 30cm away from the velocity selector.

The velocity selector used in the velocity profile measurements consists of six rotating slotted disks, spaced so that the beam is completely free of sidebands (Hostettler and Bernstein, 1960). The dimensions and general details of the rotor assembly are shown in Figure 4.4. The disks are all mounted on a single shaft, and a Syntorque Corporation hysteresis motor (Type 17H71) provides the necessary torque to rotate the disks in the range from zero to 13,000 rpm.

The system used to supply two-phase power for the rotor motor needs a phase shifter between the two outputs because the reactance of the motor changes with rotor speed. A calibrated General Radio Model 1531-A stroboscope is used to check the rate rotation of the velocity selector rotor.

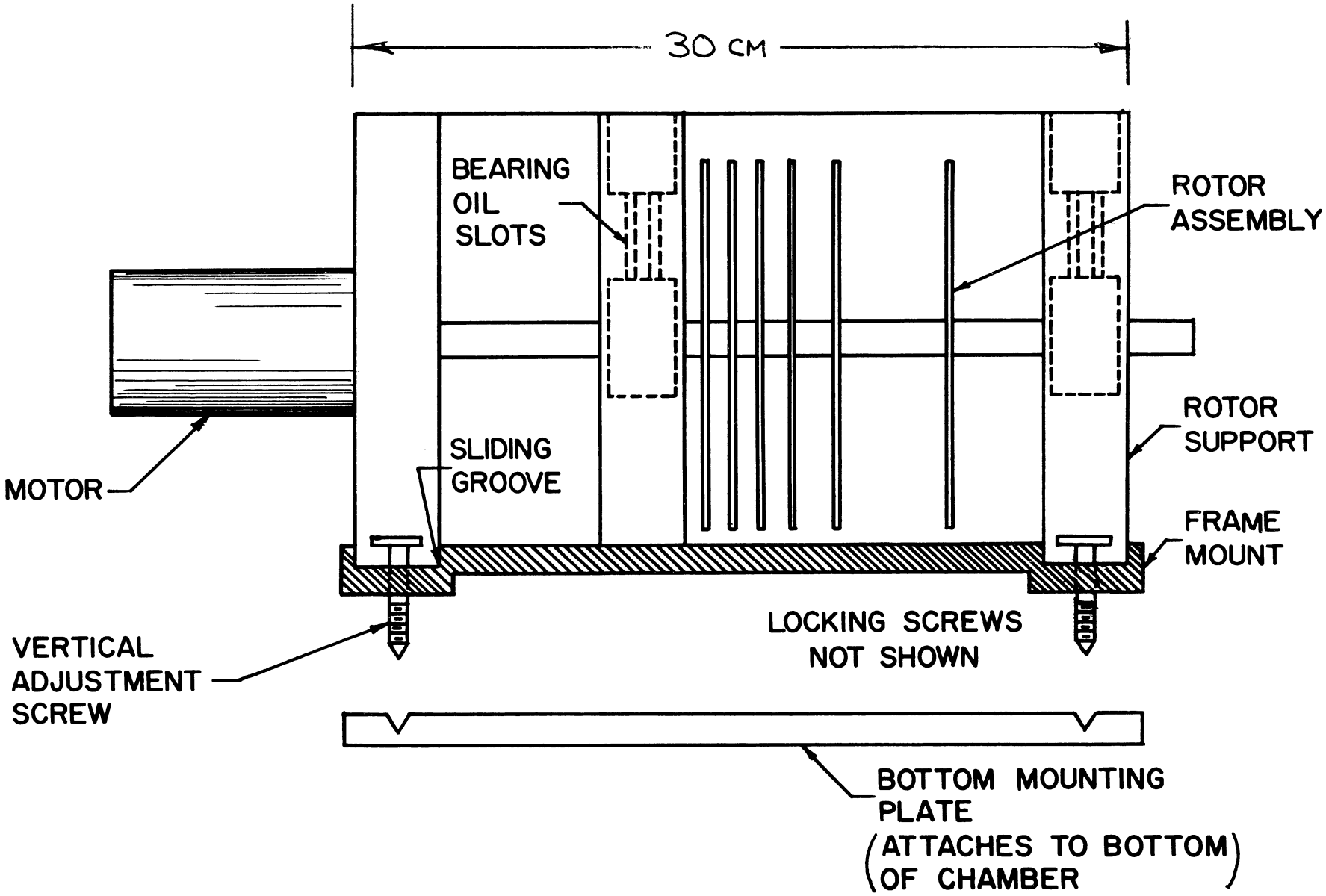

Figure 4.4 Velocity Selector and Its Mounting

4.2.4 Detector

The detector used in the experiments with the alkali metals is a standard surface ionization detector with a 7.6×10^{-3} cm diameter heated tungsten filament 3cm long. The positive ions which are formed at the surface of the wire are drawn off by a 20 volt potential difference and collected with a semi-cylindrical electrode in front of the wire. A Keithley Model 610BR Electrometer is used to monitor the positive ion current which is proportional to the total beam incident on the wire. The linearity of the electrometer through the ranges of application has been measured to be better than 0.1%. With the collimator and detector as described, the apparatus has an angular resolution (Kusch, 1964) of 5×10^{-5} radians.

4.2.5 Scattering Gas

The flow of gas to the scattering cell is regulated with a needle valve. Because extensive data are available from other experiments on argon-alkali interactions, argon is used for most of the scattering experiments. The argon is rated by the supplier as being 99.9% pure. A filter is used to remove water vapor and dust particles from the gas. Since scattering gas pressures in excess of 10^{-5} torr reduce the peak of detected beam intensities well below 10^{-13} amperes, measurements have not been continued into the region where the conventional mean free path is less than apparatus dimensions.

With no scattering gas admitted, the residual gas pressure in the system is about 10^{-7} torr. The composition of the residual gas has not been measured because no suitable mass spec-

trometer is available, but studies of similar diffusion pumped vacuum systems have shown that the principal constituents of such gas are probably CO, CO_2, H_2O, and CH_4.

4.2.6 Velocity Profile Measurements

Velocity profile measurements have been obtained by holding the detector position fixed while the angular speed of the velocity selector rotor is varied. Each point plotted has been obtained by averaging ten data points taken at a particular velocity. Typical intensities ranged from 1×10^{-13} amps to 3×10^{-12} amps. The statistical fluctuations associated with each point are on the order of 1×10^{-15} amps. The representative curves are plotted on graph paper and normalized to afford a comparison with the theoretical velocity profile. Velocity profiles for potassium, rubidium, and cesium are measured as a function of the argon scattering gas density.

The upper limit for the velocity measurements is set by the maximum allowable angular speed of the velocity selector rotor, about 13,000 rpm. The upper velocity limit is 67,000 cm/sec; thus, for potassium the data do not extend very far into the high velocity side of the peak.

4.3 RESULTS

4.3.1 Velocity Profiles and Scattering Cross Sections

The results of measurements with potassium, rubidium, and cesium are shown on Figures 4.5-4.10. The velocities are plotted in units of $c = \sqrt{\frac{2kT}{m}}$, the most probable velocity in an ideal,

Maxwellian beam. The uncertainty in data points is on the order of the width of the lines in the graphs.

POTASSIUM: Figure 4.5 shows that the velocity profile for potassium with no deliberate addition of scattering gas is in fairly good agreement with the Maxwellian prediction. The measurement does not extend beyond v = 1.2 because of mechanical limitations on the velocity selector. The slight deficiency of K atoms below v = 0.6 probably arises from scattering of the beam by residual gas in the apparatus at 10^{-7} torr. When argon scattering gas is introduced (Figure 4.6), a reduction in overall beam intensity and a shift of the maximum to higher velocities occur. Both the overall intensity reduction and the alteration of the flux distribution are well matched by the prediction of Equation 4.6, when a K-Ar cross section of 630 $\mathring{A}^2$ is used. This cross section may be compared to the value of (734 ± 100) $\mathring{A}^2$ found by Rothe and Bernstein (1959).

RUBIDIUM: In Figure 4.7 the deficiency of slow rubidium atoms due to residual gas scattering is evident. When argon is introduced, the results shown in Figure 4.8 are obtained. The theoretical curves have been calculated from Equation 4.6 by using 715 $\mathring{A}^2$ for the Rb-Ar cross section.

CESIUM: Figure 4.9 shows that the residual gas in a relatively good laboratory vacuum (10^{-7} torr) has a very pronounced effect on the velocity distribution of a long cesium beam. Figure 4.10 shows the agreement between experiment and theory when 750 $\mathring{A}^2$ is used for the Cs-Ar cross section. Rothe and Bernstein (1959)

measured this cross section to be (857 ± 120) $\mathring{A}^2$.

The present results confirm the applicability of the known collision cross sections to the problem of predicting velocity distributions in the presences of scattering gas.

4.3.2 Discussion

For gas-surface interaction measurements, the importance of residual gas scattering is that the measured velocity profiles are deficient in slow molecules. Since accommodation at a surface is judged by comparing the incoming velocity distribution (dominated by satellite velocity) with the distribution measured in the reflected beam, accommodation may be underestimated if the effects of residual gas scattering are ignored. The principal result of this section of the study is a verified, quantitative understanding of the way in which a scattering gas alters the velocity distribution of a collimated molecular beam.

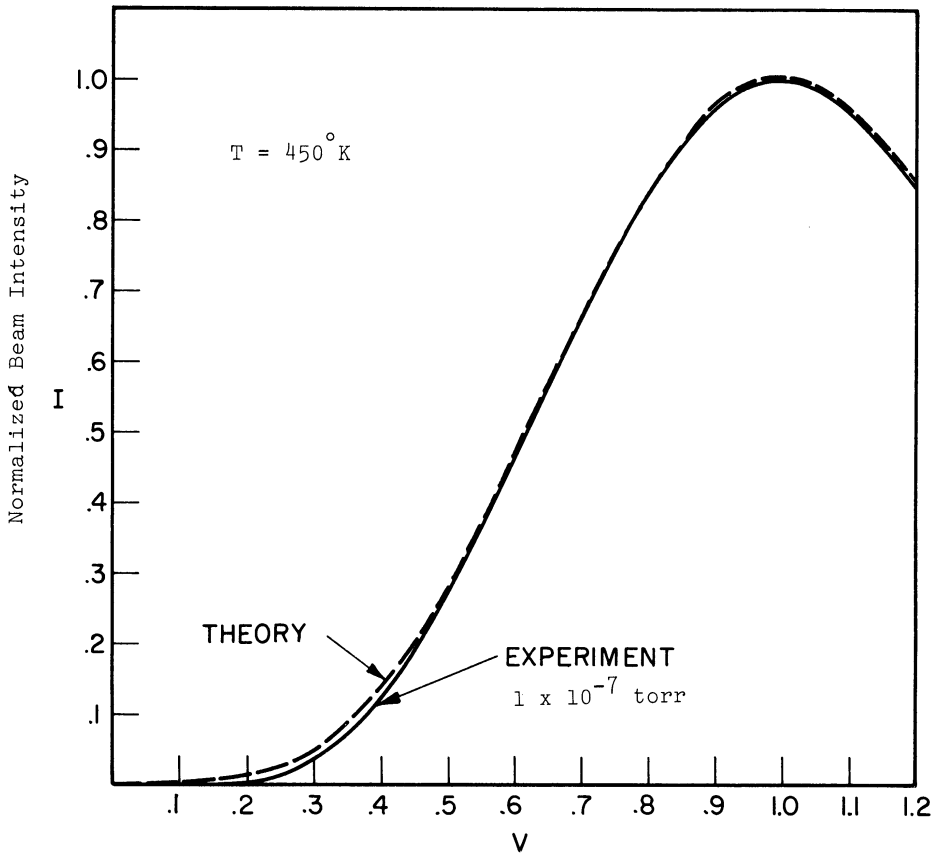

Figure 4.5 Potassium Velocity Profile with no Addition of Scattering Gas

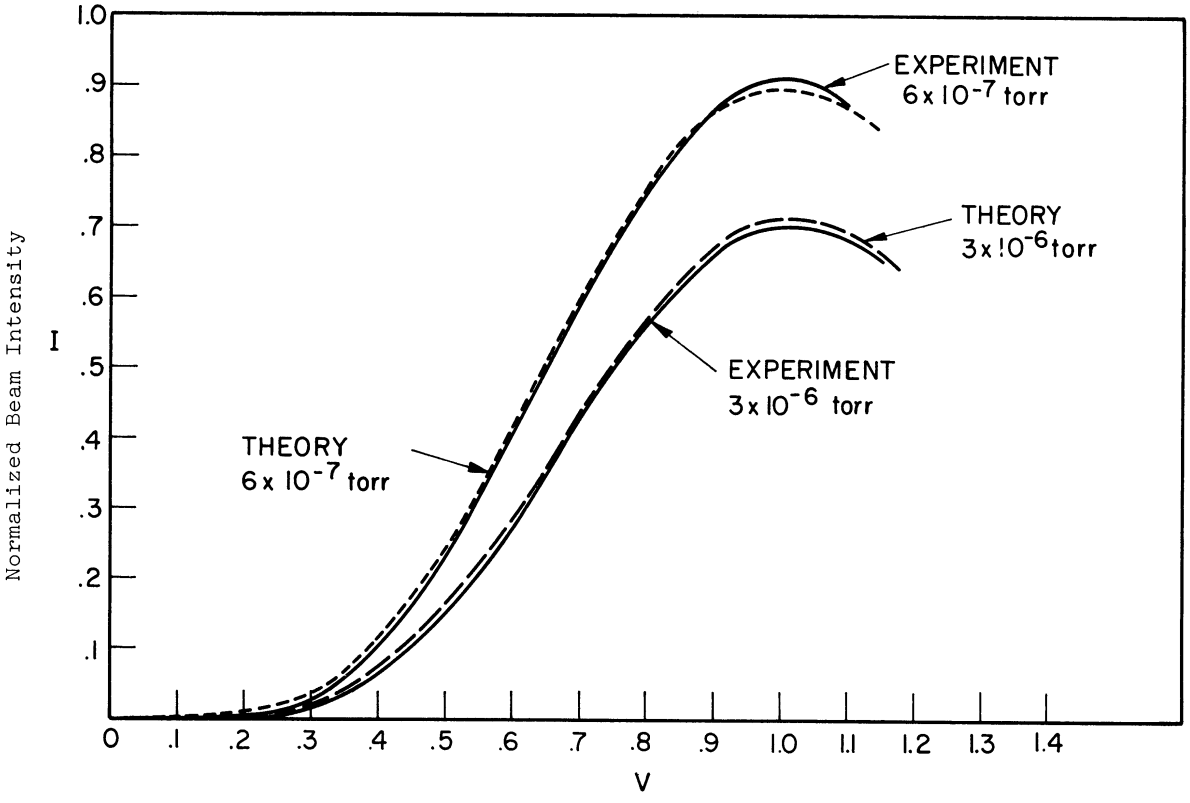

Figure 4.6 Potassium Velocity Profile in the Presence of Argon Scattering Gas

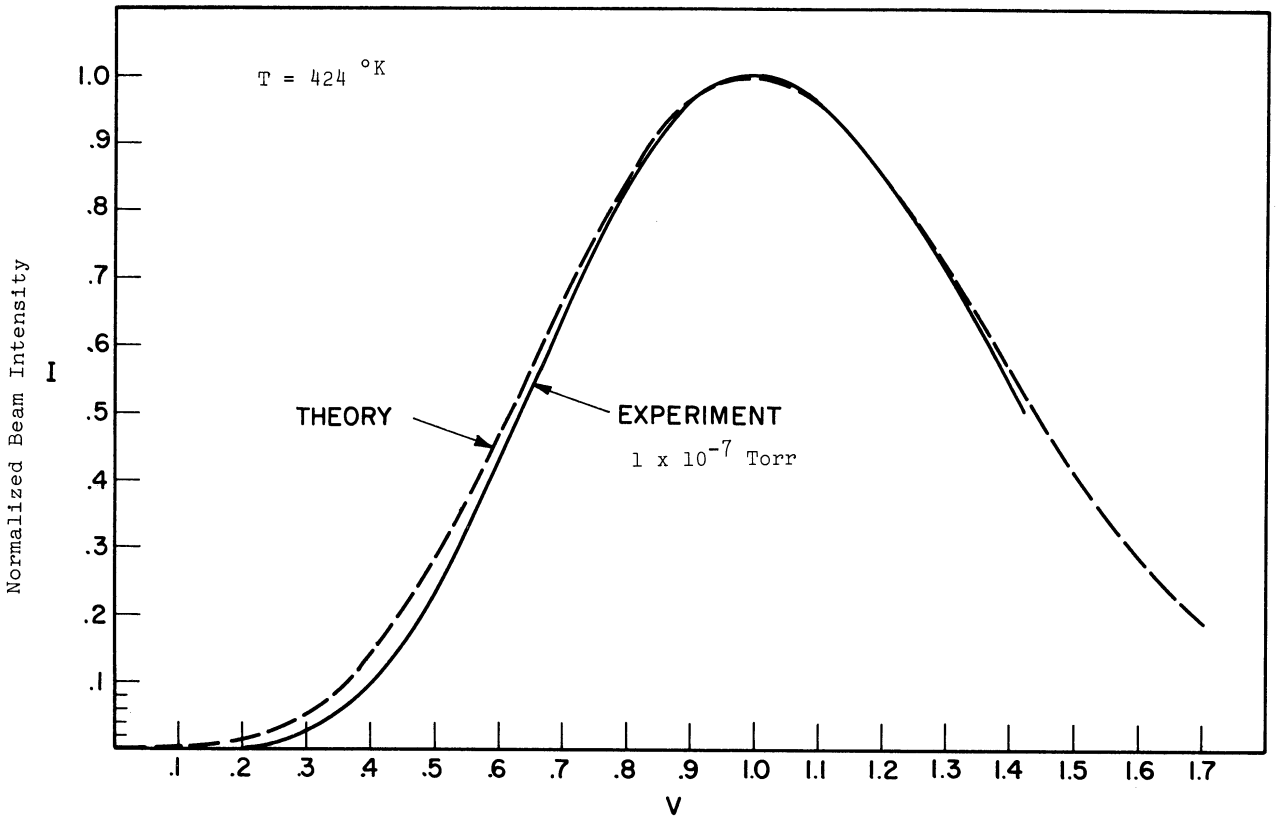

Figure 4.7 Rubidium Velocity Profile with no Addition of Scattering Gas

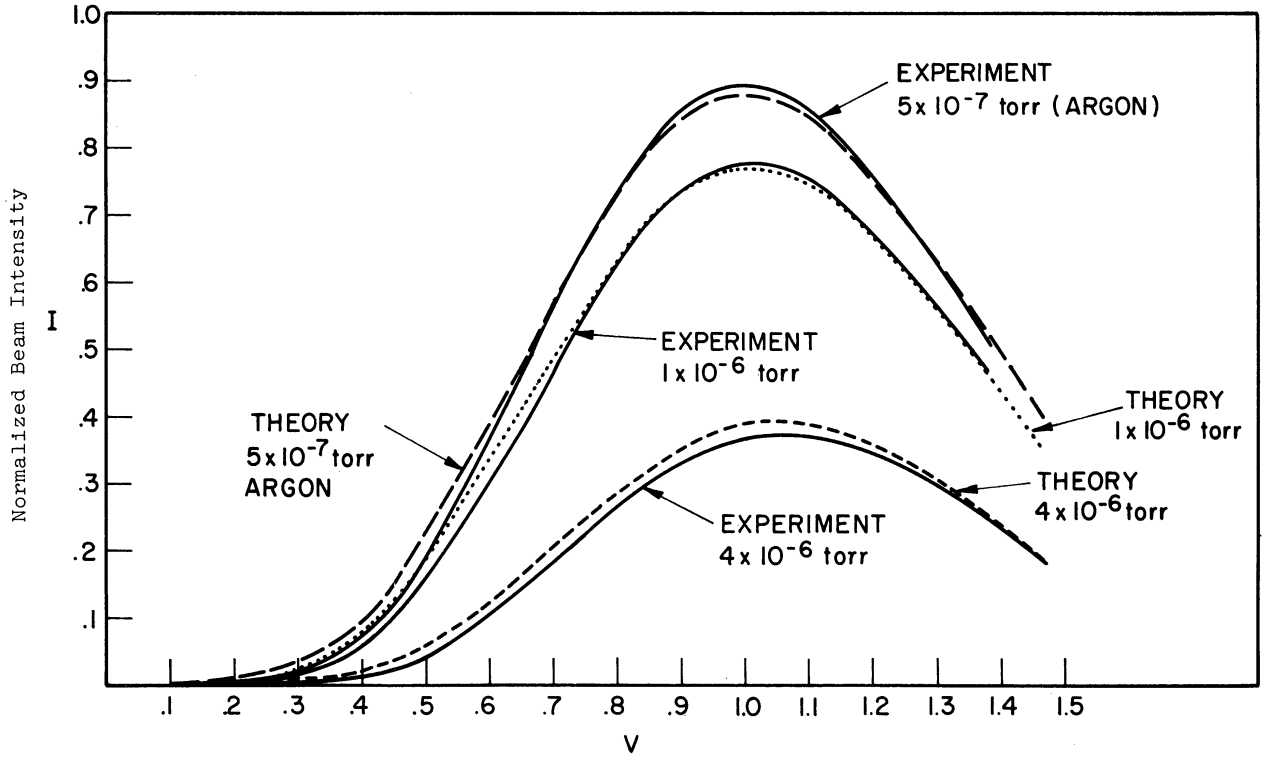

Figure 4.8 Rubidium Velocity Profile in the Presence of Argon Scattering Gas

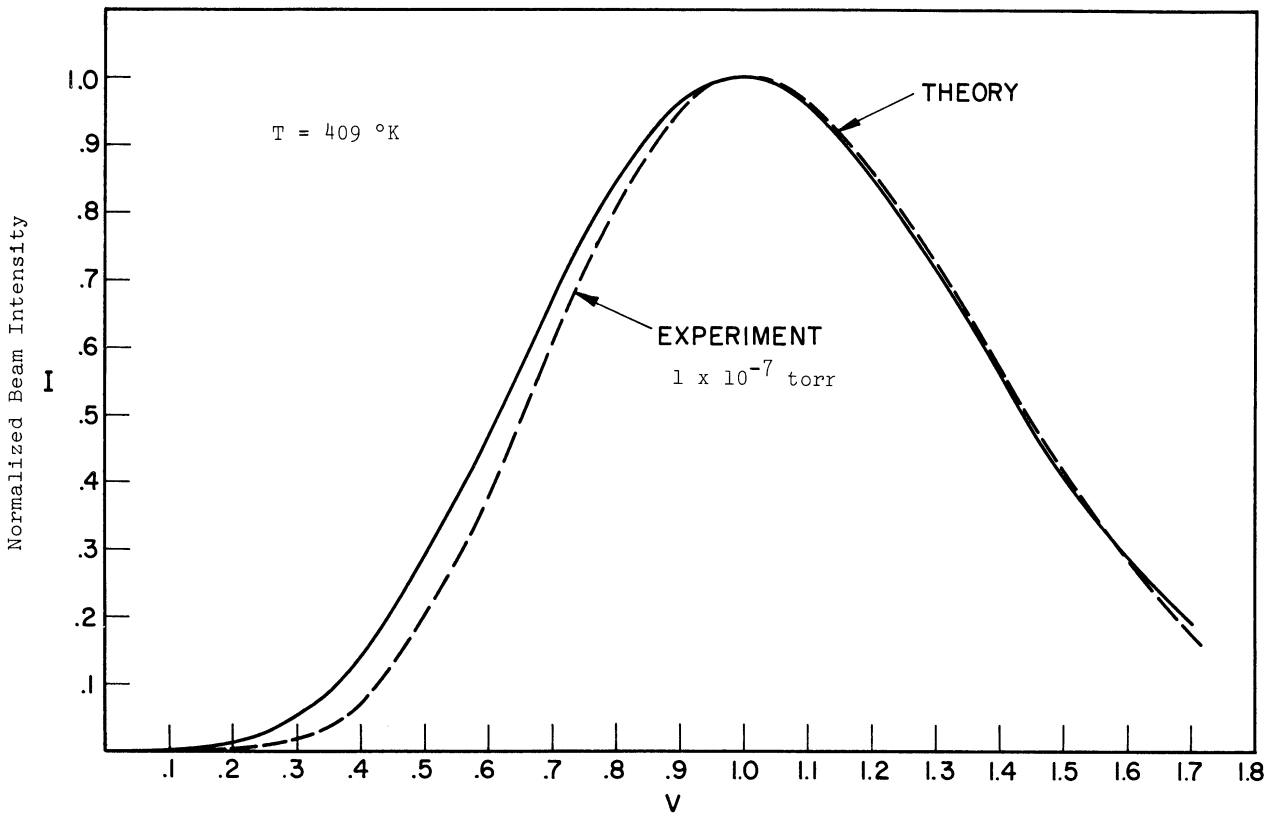

Figure 4.9 Cesium Velocity Profile with no Addition of Scattering Gas

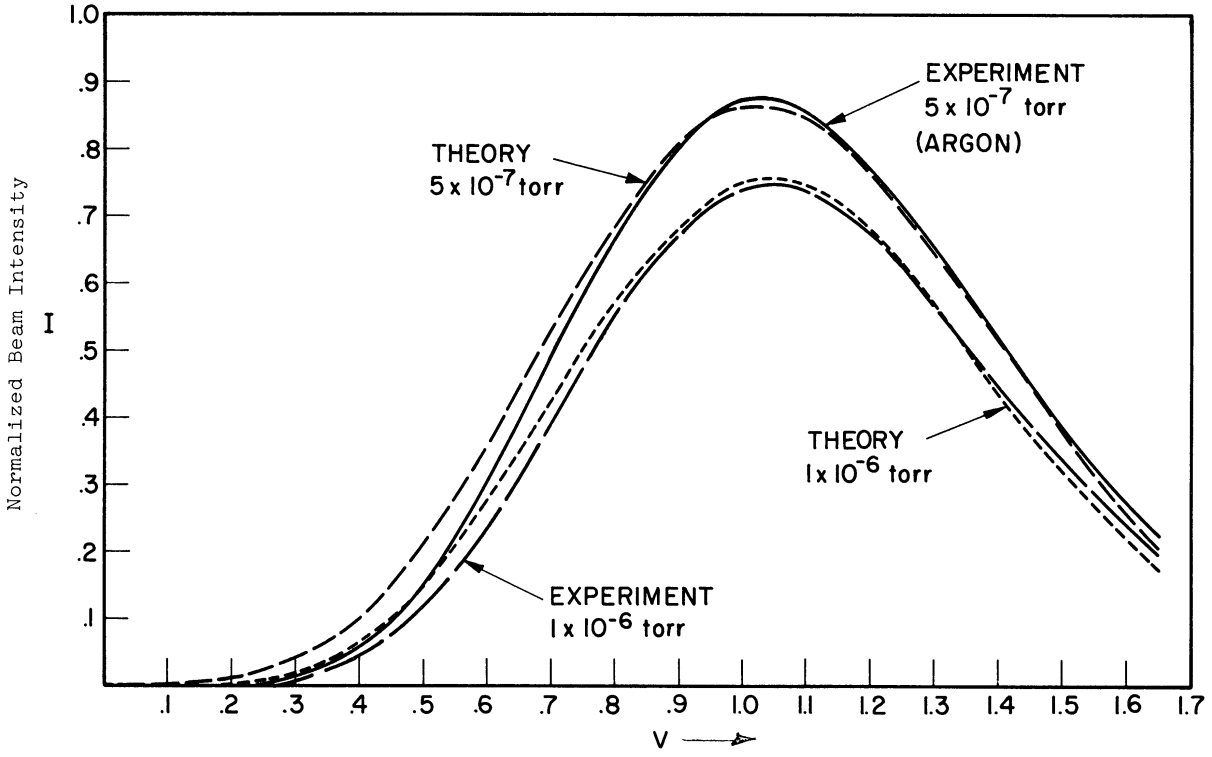

Figure 4.10 Cesium Velocity Profile in the Presence of Argon Scattering Gas

5. PROPERTIES OF N_2 IN RELATION TO TIME-OF-FLIGHT ANALYSIS

5.1 STRUCTURE OF N_2 MOLECULE

The main features of the energy levels in molecular nitrogen are shown in Figure 5.1 (Herzberg, 1950). The levels are divided into singlets (electrons paired off to form states with no electron spin angular momentum) and triplets (electrons with parallel spins). The excited states shown represent conditions of electronic excitation; the division of these states into sublevels from the other degrees of freedom within the molecule (rotation and vibration) is not shown.

Two of the excited states decay only very slowly to the $X^1\Sigma_g^+$ ground state:

The singlet $a^1\Pi_g$ state, at 8.7 ev above the ground state, has a lifetime of about 2×10^{-4} seconds. The $a^1\Pi_g \rightarrow X^1\Sigma_g^+$ transition is forbidden by the electric dipole selection rules which do not allow transitions between states of the same symmetry ($g \not\rightarrow g$) but can occur via a weaker, magnetic dipole interaction. This transition (actually a group of transitions when rotation and vibration are taken into account) is responsible for the Lyman-Birge-Hopfield bands in the molecular nitrogen spectrum.

The triplet $A^3\Sigma_u^+$ state, at 6.17 ev above the ground state, has a lifetime more than 10^{-2} seconds (Lichten, 1957; Carleton and Oldenberg, 1962). The $A^3\Sigma_u^+ \rightarrow X^1\Sigma_g^+$ transition is forbidden because electric dipole matrix elements do not exist between the singlet and triplet states; heuristically one can say that an external electric field will not serve to reorient electron spins with

respect to each other. This transition is responsible for the Vegard-Kaplan bands in the N_2 spectrum.

The properties of the metastable states of molecular nitrogen are compared to those of other atmospheric constituents in Table 5.I.

5.2 ELECTRON IMPACT EXCITATION OF METASTABLE N_2

The excitation of molecular nitrogen has been investigated in detail by Schulz (1959). His work (Figure 5.2) shows that the $A^3\Sigma_u^+$ state can be preferentially excited with an electron gun of modest resolution ($\sim$1 eV). Schulz's work yields only relative cross sections; the absolute cross section for electron impact excitation of metastable N_2 is expected to be on the order of 3×10^{-17} cm^2 at an electron energy of about 7.2 ev (Figure 5.3).

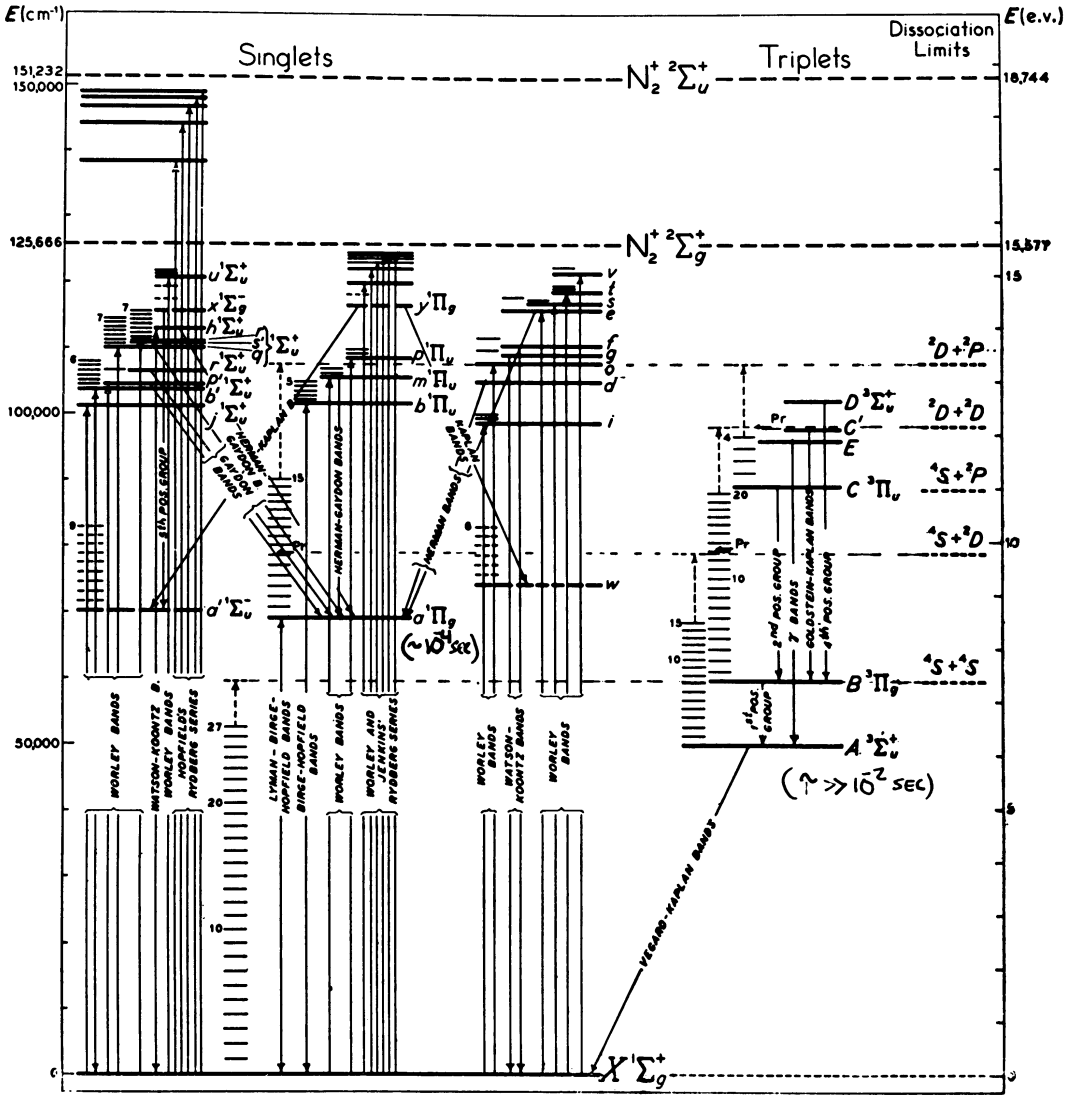

Figure 5.1 Energy Level Diagram of N_2 Molecule
[After Herzberg (1950)]

Table 5.I Properties of metastable states of some atmospheric gases.

Species	% of Total Number of Particles at 200km	% of Total Number of Particles at 350km	Dissociation/ Ionization Energy (ev)	Metastable State	Lifetime of Metastable State (Sec)	Energy of Metastable State Above Ground State (ev)	Electron Excitation Cross-Section (cm^2)	Number of Auger Electrons Ejected Per Incident Metastable on Given Surface
O	40.6	78.3	13.550 (2)	1_S (3)	.74 (4,5)	4 (6)		
				5_S (3)		9.2 (6)		
				1_D (3)	110 (7), 135 (5)	2 (6,7)		
N_2	53.0	19.2	9.78/15.58 (8)	$A^3\Sigma_u^+$ (9)	$>10^{-2}$ (9) .3 - 3 (10)	6.1688 (16)	$(1.4-35)\times10^{-17}$ @ 15ev (10)	~.06 W§
				$a^1\Pi_g$ (9)	$(1.7\pm.3)\times10^{-4}$ (9)	8.5486 (16)	$\sim3.5\times10^{-17}$ @ 17ev (11)	
O_2	6.3	1.3	3.64/12.1 (8)	$a^1\Delta_g$ (3)	<5000†	.9773 (16)		
				$b^1\Sigma_g^+$ (3)	<7†	1.6267 (16)		
				$c^3\Delta_u$ (3)		~4.2 (8,16)		
He	0.1	1.2	24.59 (12)	^3S (12)	$>10^5$ (12)	19.82 (12)	3×10^{-18} @ 21ev (12)	.29±.03 Au (12,13) .24 Pt (14) .306±.025 W (15)
				1_S (12)	> .14 (12)	20.61 (12)	1×10^{-18} @ 22ev (12)	.29±.03 Au (12, 13) .40 Pt (14) .306±.025 W (15)

(1) Jacchia, 1965; (2) Handbook of Chemistry and Physics, 1965-66; (3) Brink, 1966; (4) Paulson and Shepherd, 1965; (5) Wiese et al, 1966; (6) Herzberg, 1944; (7) Omholt, 1960; (8) Gilmore, 1966; (9) Lichten, 1957; (10) Carleton, 1966; (11) Green and Barth, 1965; (12) Holt and Krotkov, 1966; (13) Stebbings, 1957; (14) Dorrestein, 1942; (15) MacLennan, 1966; (16) Gilmore, 1967.

§See Section 6.4 of this report.

†Estimated from single Einstein A coefficient (Kummler and Bortner, 1967).

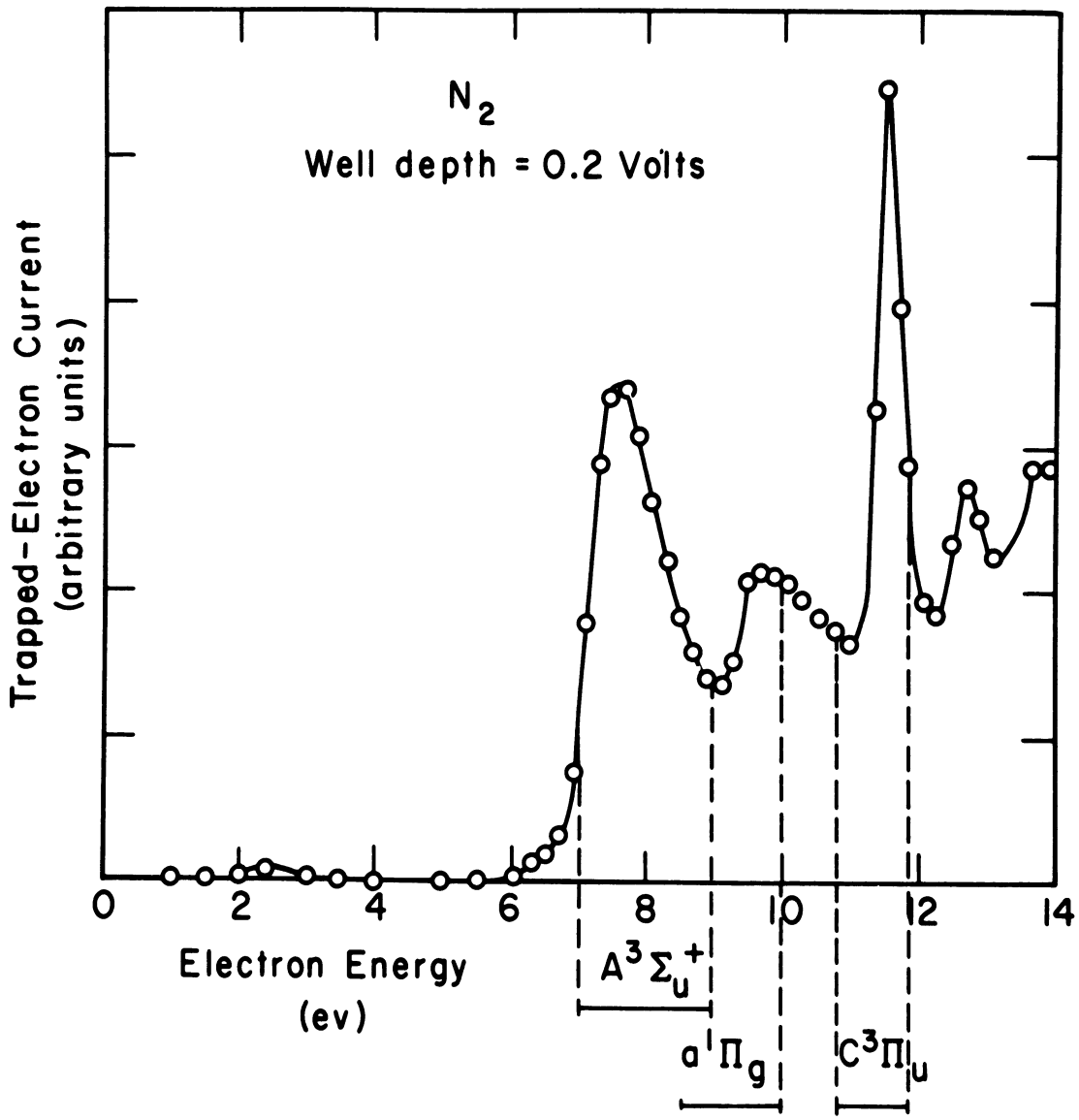

Figure 5.2 Electron-N_2 Collision Study Results
[After Schülz (1959)]

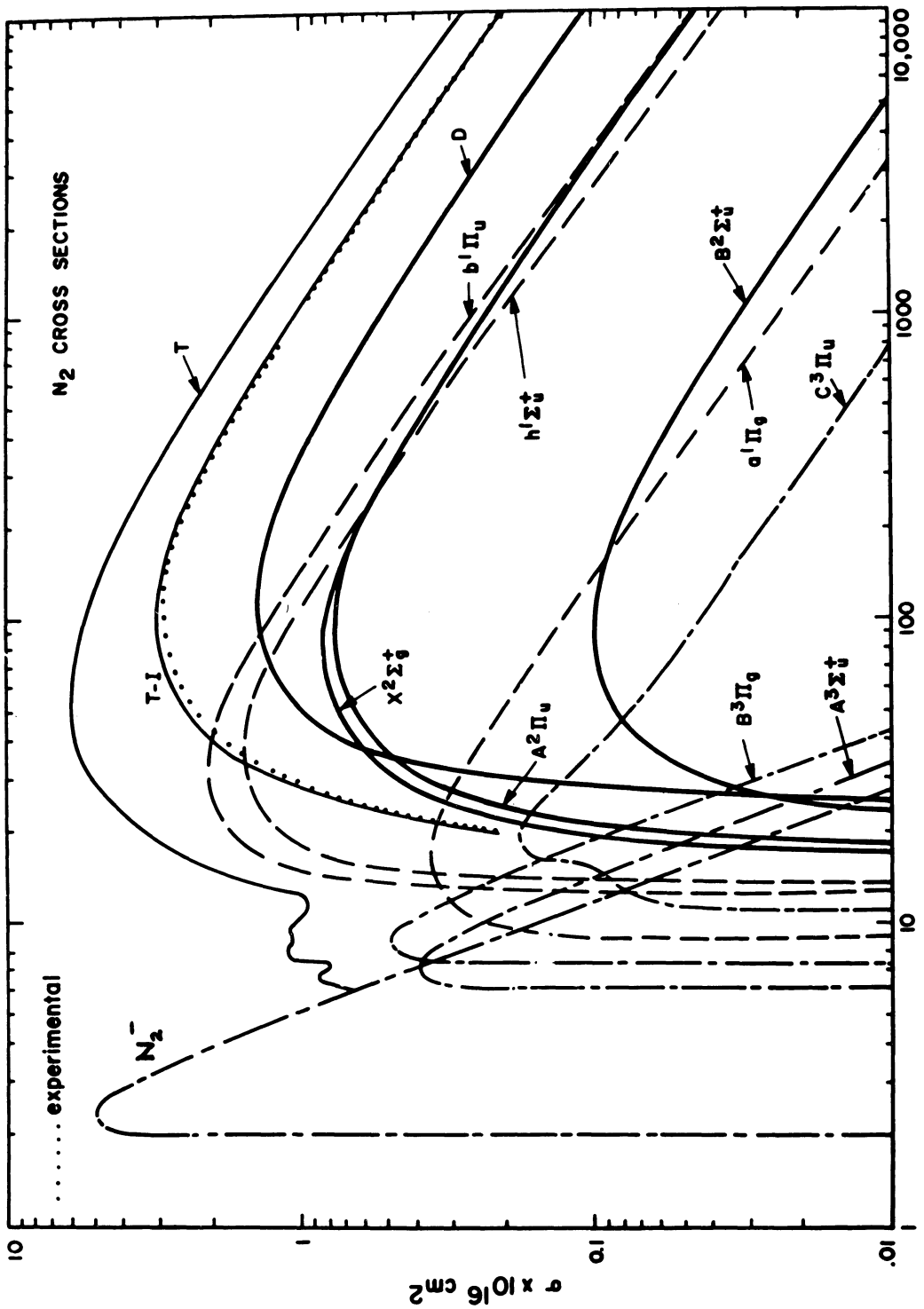

Figure 5.3 Excitation and Ionization Cross-sections of N_2 [After Green and Barth (1965)]

5.3 COLLISION QUENCHING OF METASTABLE MOLECULES

A metastable state in an atom or a molecule exists by virtue of the special symmetry of the excited state. Electric dipole transitions occur only between states of different parity (a symmetry property which characterizes the state wavefunction under inversion of the coordinate system), so that excited states with the same parity as the ground state may exhibit very long lifetimes.

The particular symmetry of an actual atomic or molecular wave function can be destroyed by external perturbations. The sensitivity of the lifetime to external disturbances depends on the proximity of states of opposite parity in the atom or molecule. For example the $2^2S_{1/2}$ state of atomic hydrogen is metastable with a lifetime of about 0.1 seconds, but an external electric field as weak as 5 v/cm will reduce the lifetime to less than 10^{-6} seconds; the presence of the nearby 2P level is responsible for the sensitivity of the 2S lifetime to external perturbations. The lifetimes of other metastable states (2^3S helium, $A^3\Sigma_u^+$ N_2, etc.) are not so sensitive to perturbations as is hydrogen, but collisions of any kind may act as effective quenching mechanisms.

The quenching of metastables in intermolecular collisions has been investigated (Hunten and McElroy, 1966; Hasted, 1964). From these investigations, it is known that the quenching cross sections depend strongly on the detailed properties of the metastable and its collision partner. It appears that quenching from intermolecular collisions will not be troublesome for MTOF studies on nitrogen, but more information on the absolute values of the

cross section for the quenching of N_2 by atmospheric molecules would be helpful.

The quenching of metastable states by wall collisions has not been studied extensively, but workers at the Smithsonian Astrophysical Laboratory (Carleton, 1966) state that metastable N_2 has a (40% $\pm$ 20%) chance of bouncing from a teflon surface without being de-excited. For the experiments under consideration in this report, however, it is important to have collimator materials which are very efficient for quenching; metal surfaces should serve well in this capacity.

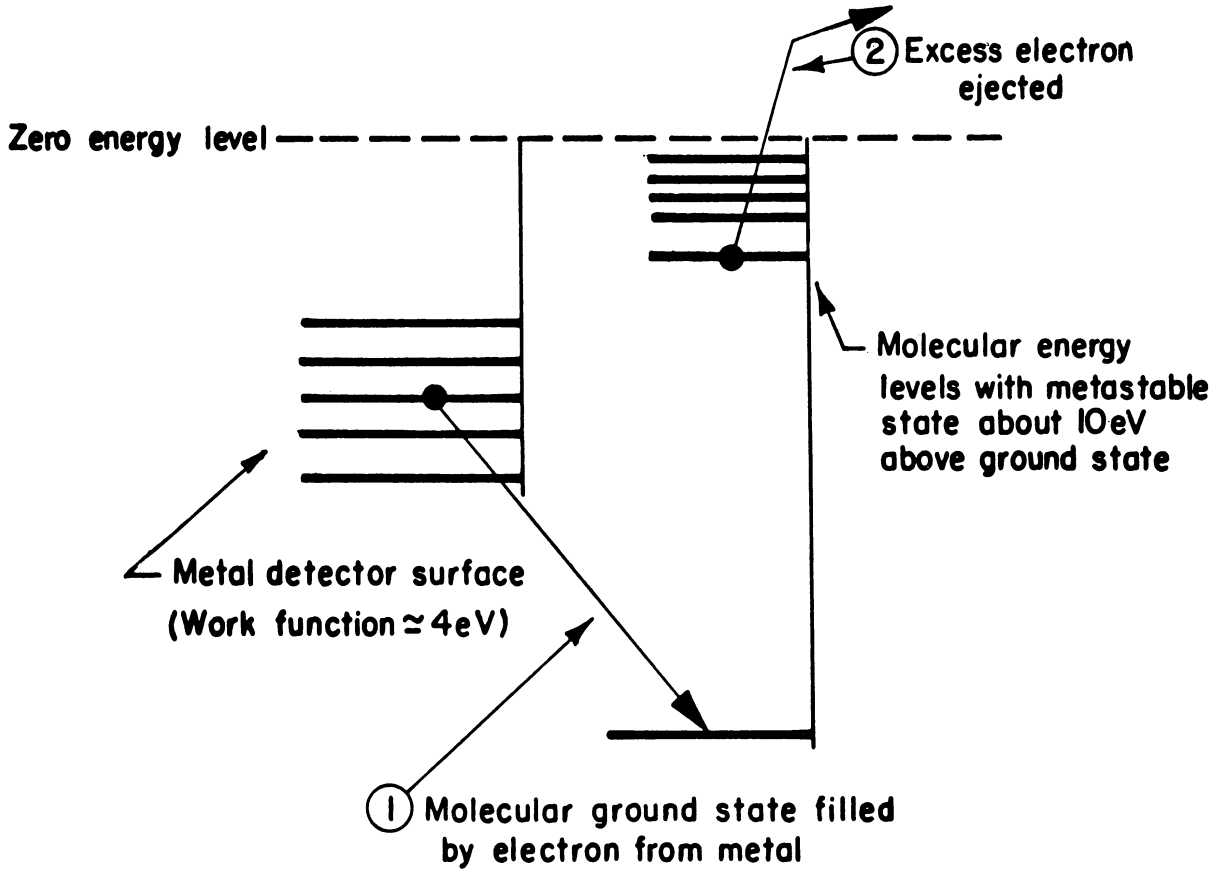

Figure 6.1 Auger Detection

As the neutral, metastable molecules comes near to the metal surface of the Auger detector, an electron from the conduction band in the metal occupies the vacant molecular ground state. The molecule then finds itself with an extra electron which is promptly ejected. The ejected "Auger" electron can then be counted with an electron multiplier.

6. EXPERIMENTS ON DETECTORS OF METASTABLE MOLECULES

6.1 AUGER DETECTORS

The essential feature of an efficient Auger detector is a surface through which electrons can tunnel easily (Figure 6.1). The material to be used depends upon the atom or molecule to be detected.

For measurements of metastable helium, argon, and other systems in which the metastable state is more than 10 ev above the ground state, the choice is not critical. There are definite advantages to selecting a material with a high electronic work function to minimize the undesired background from photons, excited molecules not of interest, and other sources of noise.

For systems with lower metastable energy (oxygen, magnesium, etc.), it is desirable to have a low work function metal for the detector surface. Lurio and his associates (Lurio, 1962) at the IBM Watson laboratories have employed a freshly deposited cesium surface for which the work function is about 1.8 ev. Metastable states with excitation energies as low as 2.2 ev ($Ca\ ^3P$) have been detected on the cesium surfaces, and 2.7 ev states are seen routinely. The cesium surfaces are continually deposited during the measurements of the metastable species. The measurements are made in oil-pumped systems with an ambient pressure of about 10^{-7} torr with a liquid nitrogen trap surrounding most of the detector. Without continual deposition, the efficiency of the detector falls rapidly with time.

The present discussion is concerned with the suitability of Auger detectors for satellite-borne experiments. Information

about the long-range stability and sensitivity to contamination of detectors for metastable nitrogen is of particular interest. To obtain information on these questions, an apparatus for the generation and detection of metastable gas beams has been set up. On the basis of the experiments performed with clean and contaminated detectors, it is concluded that the Auger detector is quite suitable for the proposed applications.

6.2 EXPERIMENTAL APPARATUS

The apparatus consists of a gas-handling system and a vacuum chamber which contains an electron gun and the detector itself. An overall view of the apparatus is shown in Figure 6.2. The interior of the vacuum chamber is shown in Figure 6.3.

The vacuum chamber is cylindrical with a diameter of 30 cm and height of 30 cm, and is pumped with a 400 ℓ/sec oil-diffusion pump. With no gas input the pressure in this chamber is easily reduced to less than 10^{-6} torr.

6.2.1 The Gas-handling System

A schematic diagram of the gas-handling system is shown in Figure 6.4. The storage volume of approximately 1.6 liters contains gas at a pressure of about 100 torr. The needle valve is used to regulate the gas flow into the delivery volume so that the pressure in it is several cm of oil. The manometer oil is Octoil-S, chosen for its low vapor pressure.

6.2.2 The Electron Gun

The electron gun, shown on the left in Figure 6.3 and in Figure

6.5, consists of a spiral filament of tungsten wire mounted parallel to and below the molecular beam, and of a hollow semi-cylindrical anode mounted above the beam. Electron confinement is enhanced by placing the whole assembly between the poles of a 1500 g magnet. The filament is 2 cm long, and the space between it and the anode is slightly less than 1 cm. The filament is heated by 6A ac and the anode current drawn ranges between 0.3 and 2.0 ma for applied potentials of 5 to 30 v. Support for the filament is provided by two nickel wires which also act as current leads.

6.2.3 The Detection System

The beam emerging from the collimator collides with a tungsten (or other metal) plate mounted on the end of a tube which can be moved back and forth to change the length of the beam path. A fraction ($\sim$10%) of the metastable molecules eject electrons from this Auger surface plate, and a fraction of these electrons are in turn received by a collector mounted on the same tube. The resulting current is measured with a Keithley 610 BR electrometer. Both the Auger surface and the collector are electrically isolated (the latter having a resistance to ground of the order of 10^{12} - 10^{13} Ω), and the Auger surface is biased at -22 1/2 v relative to ground. The collector remains essentially at ground potential.

The movable tube, of 1/2" diameter stainless steel, is inserted into the experimental chamber through a gland. Mechanical support is provided by teflon rings, and vacuum sealing is provided by an O-ring. The signal is fed from the collector to the electrometer by means of a coaxial cable.

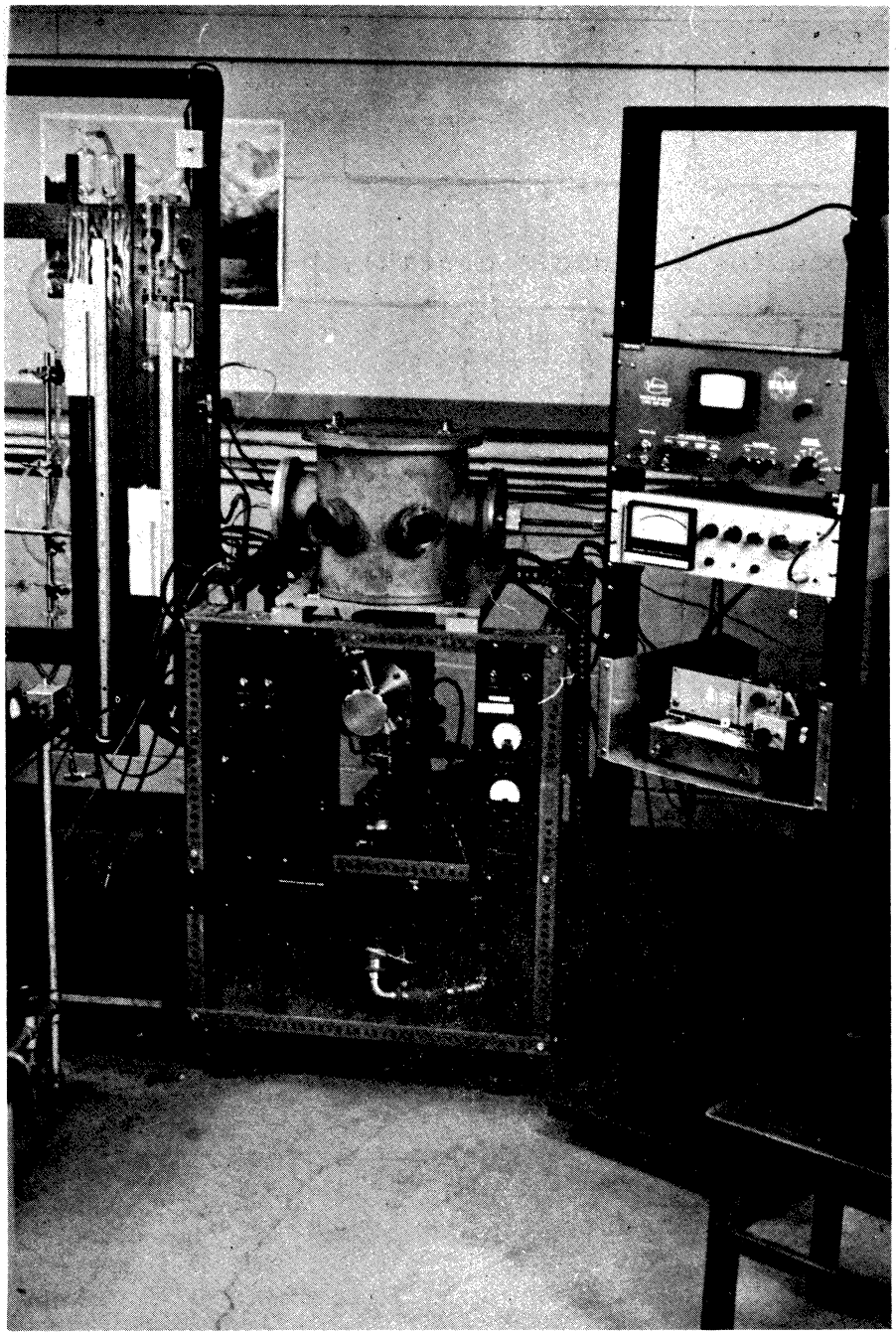

Figure 6.2 Apparatus for Experiments on Detectors of Metastable Molecules.

The manometers and other parts of the gas handling system are mounted on the rack shown at the left of the figure. The vacuum chamber and pumping system are in the center. The electrometer and other electronic equipment are mounted on the rack at the right.

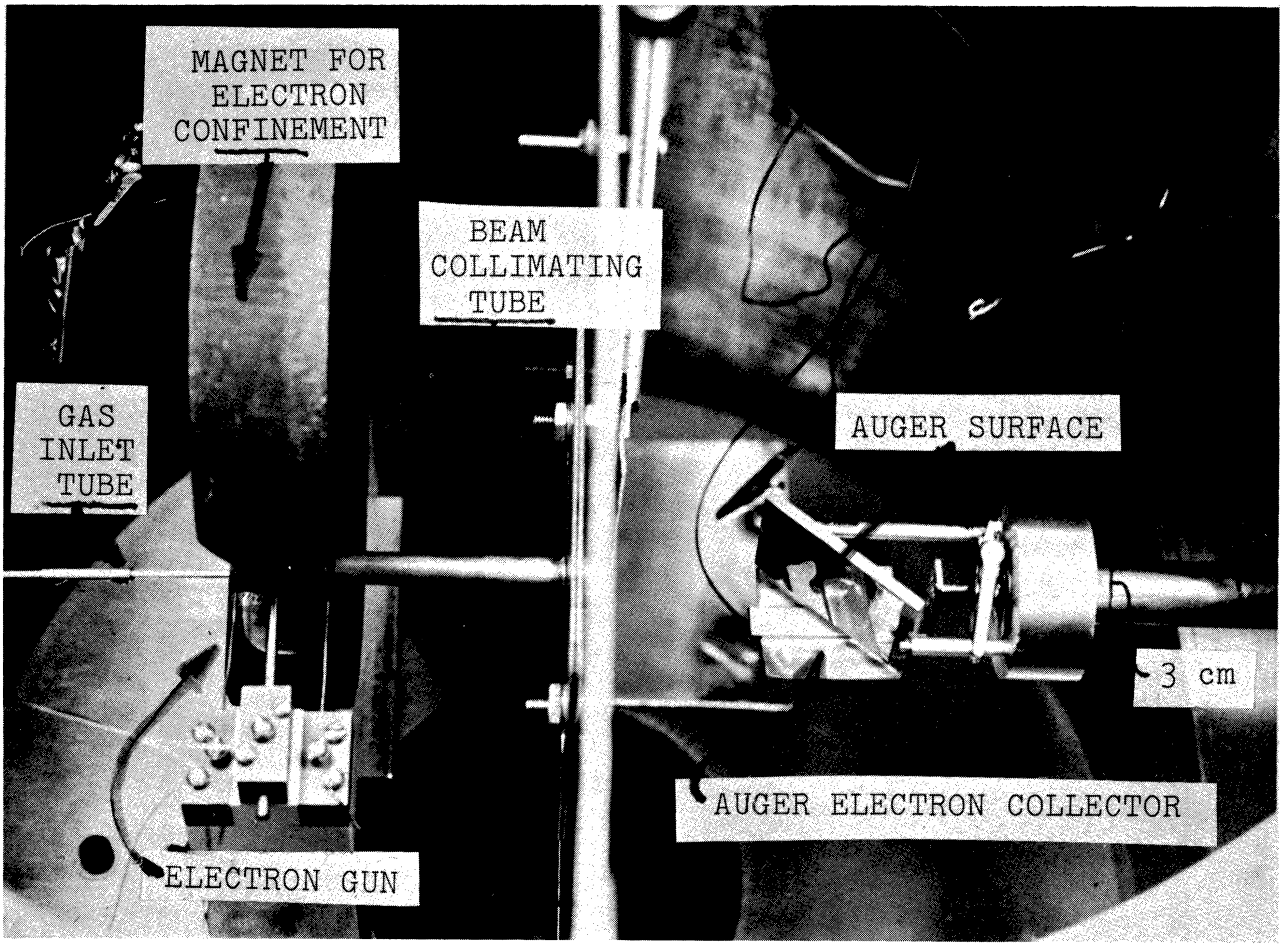

Figure 6.3 Interior of Vacuum Chamber.

A dividing wall (center) separates the electron gun assembly on the left from the detector unit at the right.

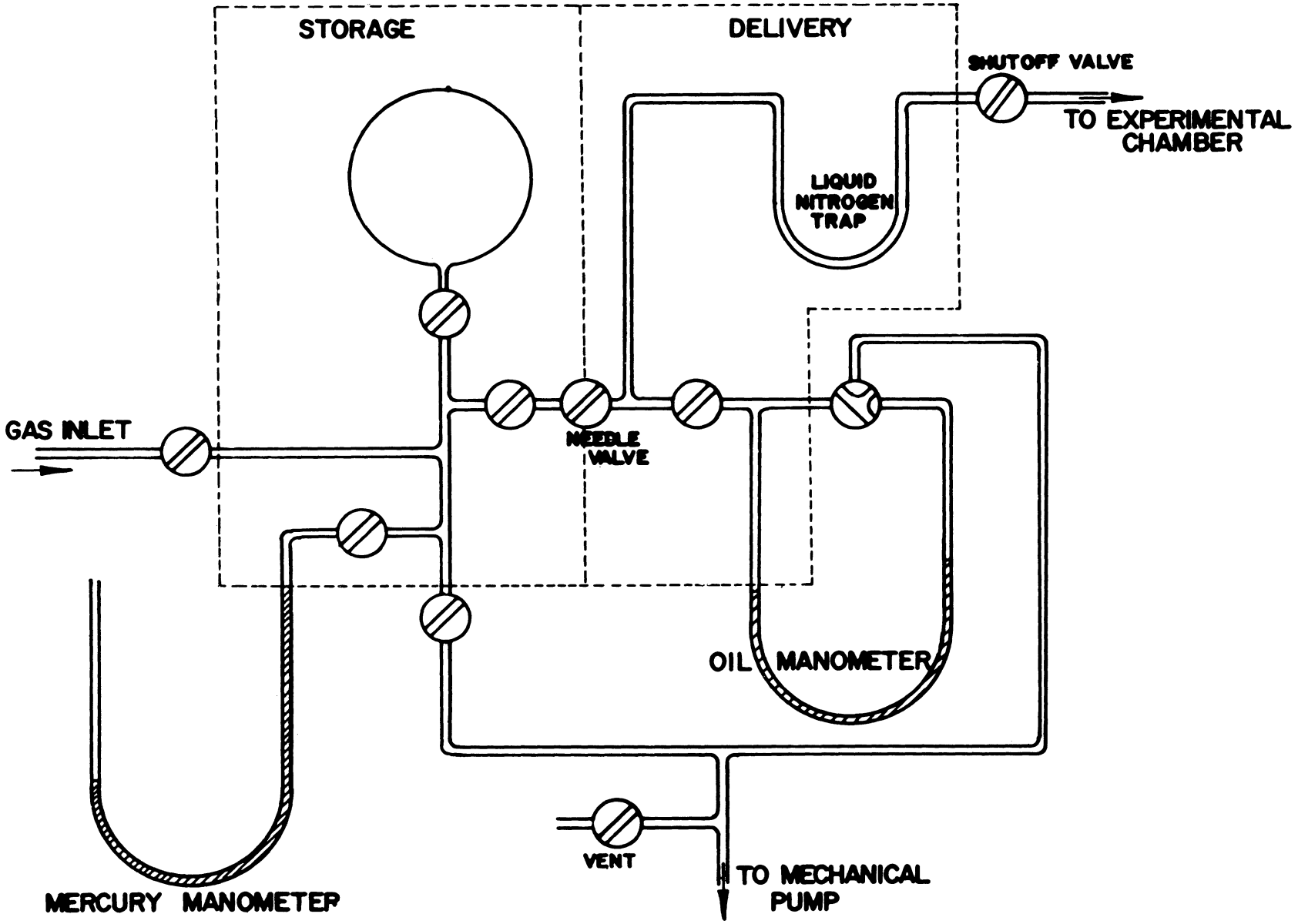

Figure 6.4 Schematic diagram of gas-handling system.

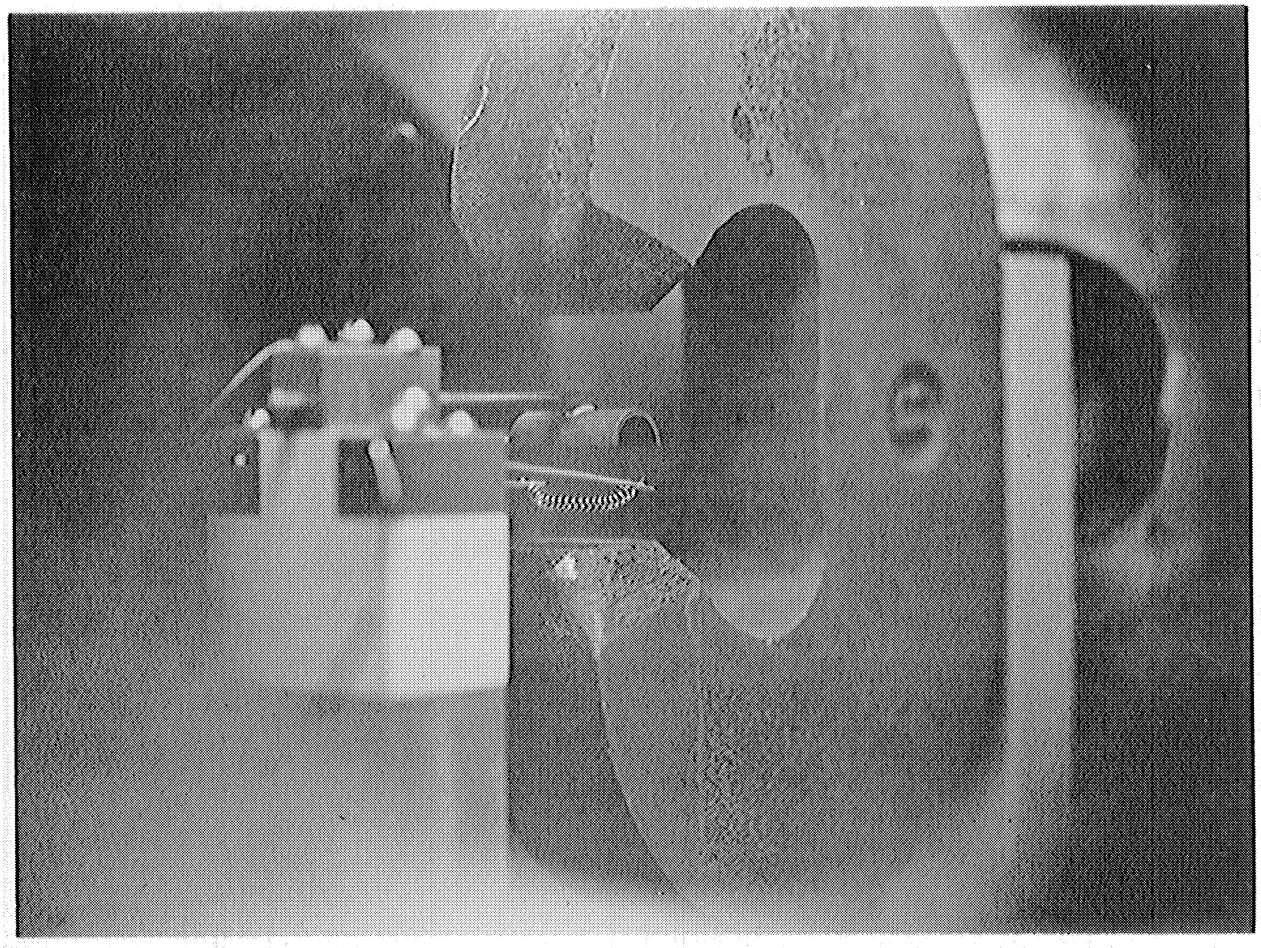

Figure 6.5 Electron gun, snowing filament, anode, and magnet.

6.3 EXPERIMENTAL PROCEDURE

A typical trial run consists of mounting the detector surface under examination, of pumping the system for about an hour to obtain a pressure of 1×10^{-6} torr or less, and then of measuring the beam signal and the detector background for a variety of gases as a function of gas flux, electron current, and electron energy. With large gas flux, the system pressure goes as high as 1×10^{-4} torr.

In experiments like the one described, the signal due to metastable atoms must be distinguished from that of stray ions and electrons, and that due to electrons ejected by ultraviolet photons. The 1500 gauss magnetic field in the electron bombardment region prevents the drift of stray charged particles to the detector, while a tube collimator serves to shield the Auger surface from the direct view of the bright filament. Ultraviolet photons from excited gas molecules are not a problem, as verified by running a beam of O_2 through the apparatus. Molecular oxygen does not have metastable states at high enough energies to eject electrons from unsensitized surfaces, but the bombarding electrons should excite roughly the same number of ultraviolet transitions in O_2 as in N_2. The very small signal seen with O_2 indicates that ultraviolet photons are not responsible for the signals seen with N_2, Ar, He and air.

The gases used for these tests are helium, argon, nitrogen, and oxygen; in addition, tests have been made with undried air from the laboratory. The gases, obtained from an industrial supplier, are not free of contaminants; the samples are of a purity such that no foreign gas emission lines are visible when a discharge

of the gas in question is examined with a hand spectroscope, but this test is not a sensitive one for impurities. Gases from industrial suppliers generally have purities better than 95%, however, and small amounts of impurities will not affect the interpretation of the experimental results given in this report.

No traps have been employed to keep water vapor out of the gas beams; in fact, some of the tests with air have been made with samples taken from the laboratory on days when the humidity has been very high. These samples have been chosen deliberately to test the sensitivity of the entire system to the presence of water vapor, since the ultimate flight experiments may well have a strong H_2O background. No deleterious effects have been noted, but it must be recalled that our electron gun cathode is of pure tungsten; if a treated or doped cathode is used, then troubles may be expected from H_2O.

6.4 PERFORMANCE OF METASTABLE DETECTOR

6.4.1 Clean Surfaces

The gas beam system described in the previous paragraphs has been used to test the operation of various metal surfaces for the detection of beams of metastable atoms. The detector operation has been examined as a function of beam species, of Auger surface material and its preparation, and of general system history.

Before being mounted, the detector is cleaned with abrasives and organic solvents; during the time of mounting and system pump-down, the detector is exposed to the laboratory air and the back-

streaming pump oils. In the present system, there is no provision for cleaning the detector after system evacuation. For subsequent work, it may be desirable to have a way of baking the detector surface when the vacuum is below 10^{-6} torr. By the usual surface physicist's standards, the "clean" detector condition in these experiments is rather dirty; however, the cleaned surface does provide a reference against which to compare the measurements in which the detector surface has been grossly contaminated.

The absolute efficiency of the Auger detectors used is difficult to determine from these experiments because of large uncertainties in electron beam density and in gas beam density, but our estimate of 6% efficiency for metastable N_2 on tungsten is in accord with the results of others (Freund, 1964).

6.4.2 Effect of Gross Contamination

Immediately after several of the runs with a clean detector, the system was opened briefly, and the detector surface was thoroughly covered with fingerprints; the system was immediately pumped down, and the gas flow rate and electron gun conditions were reestablished. The fingerprints had no apparent effect on the efficiency of the Auger detector for metastable argon or nitrogen. In one of the tests of Auger detectors, the cleaned tungsten surface was replaced with an uncleaned 25¢ piece direct from the experimenter's pocket (Figure 6.6). The detection efficiency of the coin was about the same as that of the tungsten.

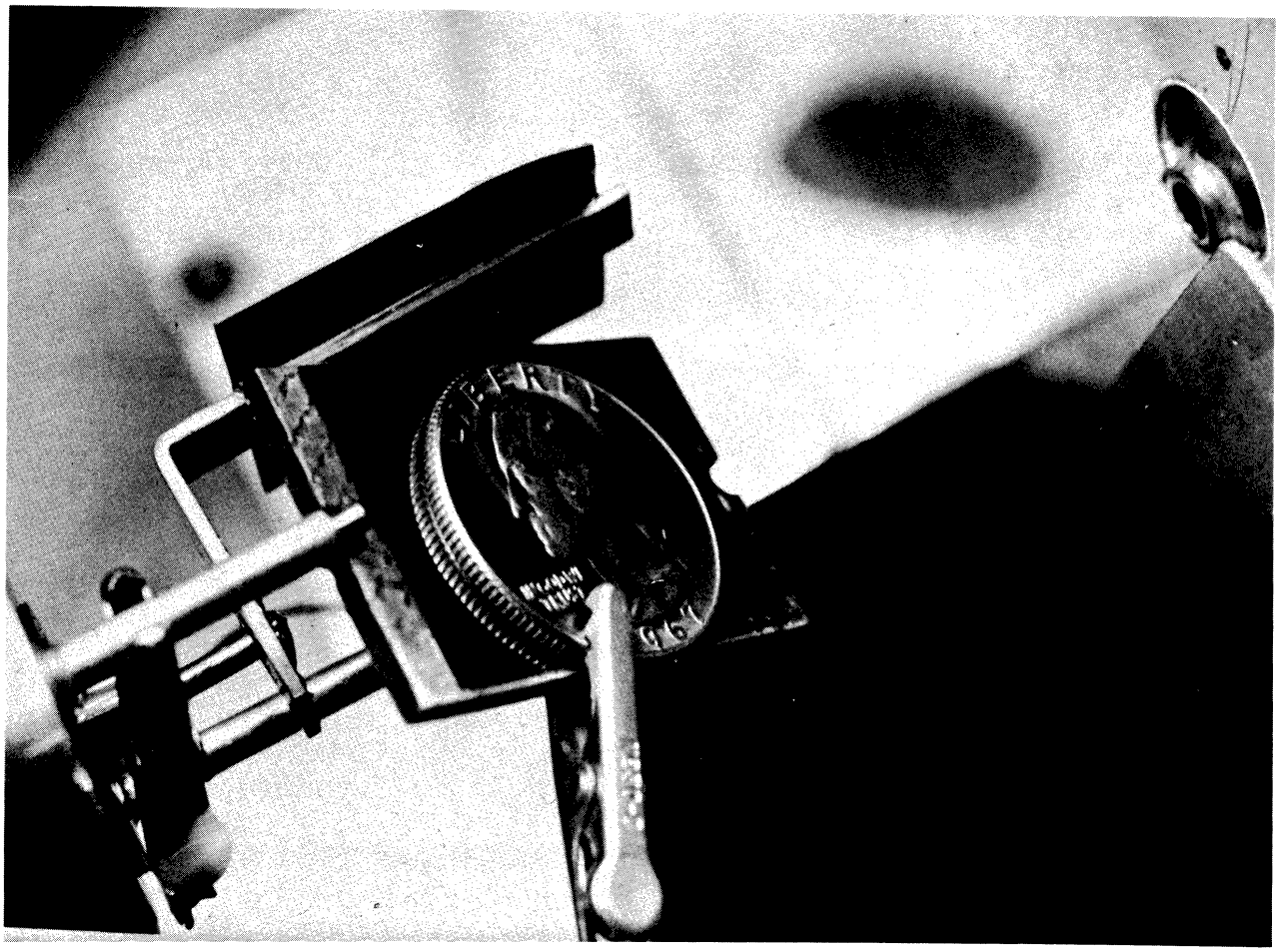

Figure 6.6 Contaminated surface for Auger detection.

An unclean coin gives about the same detection efficiency as the "clean" tungsten surface described in Section 6.4.1. The metastable beam emerges from the hole shown in the upper right of the figure.

6.4.3 Stability

A comparison of our results with those of others (Freund, 1964) leads us to believe that the stability of a given surface for Auger detection depends on the difference between the work function Φ of the surface and the energy E_M of the metastable state in question. If the difference $E_M - \Phi$ is small, then the surface must be prepared carefully and kept free of contamination. If the difference is relatively large (on the order of 5 ev), as is the case with the gases used in our experiments, then special surface preparation does not seem necessary. It should be noted that long-term changes smaller than 10% are difficult to interpret in the present experiments because of variations in gas flux and electron gun conditions. On the other hand, since measurements in the proposed satellite experiment will be made on a scale of minutes during perigee, long term changes in detector efficiency are relatively inconsequential.

6.5 FURTHER DISCUSSION

6.5.1 Source for Cesium Deposition of Auger Surface

If it is desired to employ a deposited cesium surface for detection of low-lying metastable states, the cesium beam is usually generated in a small metal oven heated to 80° C. Under laboratory conditions, the oven for the alkali is loaded under an inert gas atmosphere and then quickly pumped down to minimize the reaction of the alkali oven load with the air. For satellite experiments, however, the cesium may react with the atmosphere during the long

interval between the time of unit assembly and the time of launch; unless some provision is made to seal off the alkali oven load, the cesium may not be available to coat the Auger surface properly.

Beams of cesium from ovens containing cesium chloride together with chips of calcium have been produced. This combination is stable for long periods of time if temperatures are kept below 50° C and if storage is under a fairly dry atmosphere. When the oven is heated, the substitution reaction $2CsCl + Ca \rightarrow CaCl_2 + 2Cs$ provides a steady supply of cesium. With such an arrangement, no highly reactive, pure cesium metal need be exposed to the pre-launch conditions. A variety of cesium and rubidium halides have been tested in this laboratory and all seem to go equally well.

6.5.2 Lifetime of the $a^1\Pi_g$ Metastable State of N_2

In the present system the metastable detector can be translated along the axis of the beam. Consequently, a measurement of the lifetime of $N_2(a^1\Pi_g)$, believed to be on the order of 2×10^{-4} seconds (Lichten, 1957), was tried. The short lifetime implies that the signal from this component of metastable N_2 should be a strong function of the electron gun-detector distance. The measurement on $a^1\Pi_g$ is complicated by the fact that the $A^3\Sigma_u^+$ state of N_2 is also metastable with a lifetime in excess of 10^{-2} seconds (Carleton and Oldenberg, 1962), and the present electron gun does not have sufficient energy resolution to excite only one of these states. However, the results show a distinct decay in the N_2 metastable population at a rate consistent with the 2×10^{-4} sec lifetime of the shorter lived state. A new apparatus is being used to make a precision measurement of the lifetimes.

7. TEST SURFACES FOR GAS INTERACTION

7.1 SELECTION OF TEST SURFACES

With a fairly simple indexing mechanism, it will be possible to study the interaction of four to six different surfaces with the incoming molecular flux. The common spacecraft materials, such as stainless steel, aluminum, titanium, and solar cell units, will be examined. Since the actual selection of target surfaces will not influence the general design of the experiment, changes can be made at any time.

A calibration surface for one of the target indexer positions will be useful. The surface should be atomically clean and smooth during the time when the gas-surface interaction is being measured. Since surfaces are known to contaminate very rapidly in times on the order of minutes even if background gas is present at 10^{-7} torr, it will be necessary to prepare the calibration (or "scientific") surface while the experiment is in orbit, just before the measurements on that particular surface are made. Various ways for preparing the surface have been considered, and two methods have been used in preliminary laboratory work.

7.2 LABORATORY STUDY OF VAPOR-DEPOSITED SURFACES

7.2.1 Molecular Dissociation as Deposition Method

Satisfactory reproducible films of controlled thickness and surface character can be made from a variety of materials by heating a small quantity of the material of interest beyond its melting temperature and by allowing the resulting vapor to condense on a suitable substrate. For most metals a considerable amount of

electrical heating power is necessary to deposit a usable film over an area of 1 cm^2. Thus, this method does not seem suited for first orbital experiments.

An alternative method (Frazer, et al, 1959; Greene, 1961) in which a molecular vapor is made to dissociate thermally on a heated substrate offers a way to deposit a clean target surface without using an extraordinary amount of power from spacecraft batteries. Under the present study contract, experiments have been conducted in which ultra-pure tungsten surfaces have been formed by allowing tungsten hexacarbonyl $W(CO)_6$ to dissociate on a warm metal backing surface. Examination of the resulting tungsten deposits with an optical microscope, as well as measurements of the work function and ion emitting properties, strongly suggest that the surfaces are reproducibly pure and uniform.

7.2.2 Experimental Apparatus

The experiments on dissociation deposition of tungsten have been carried out in a small vacuum system which can be pumped to 10^{-6} torr by its 200 ℓ/sec oil diffusion pump and liquid nitrogen trap. Mounted in the center of the chamber is a small section of a conducting material on which the tungsten is to be deposited. Mechanical support for this target is provided by two conductors which lead to an external current supply via vacuum feed-throughs. The entire target assembly is maintained at +22 volts with respect to ground by a battery in order to make ion emission measurements after the deposition is completed. The insulation resistance of the target circuit need be only high enough to avoid draining the 22-volt battery.

A collector electrode is mounted about 5 mm from the target. This electrode is coupled to a Cary Model 31 vibrating reed electrometer through a carefully cleaned vacuum feed-through. The insulation resistance of the collector circuit must be kept higher than the 10^{11} ohm input impedance of the electrometer circuit.

A short metal side arm of the vacuum envelope contains a reservoir for the carbonyl sample. The side arm is provided with a simple external electric or gas heater to warm the sample.

7.2.3 Experimental Procedure

The target material on which the tungsten is to be deposited is chosen arbitrarily from rhenium, tantalum, tungsten, or platinum-tungsten alloy (92% Pt, 8% W). Experience with the above samples indicates that the characteristics of the deposited surface are independent of the substrate material. Wire or ribbon targets of 1 cm length are used; a typical target is a 0.025 mm diameter wire which is built up to 0.25 mm diameter (a tenfold increase) by vapor deposition.

After the target is mounted and the tungsten carbonyl ($\sim$1 gm) is loaded, the system is evacuated and the target is heated to 600-700°C by an appropriate current. The carbonyl reservoir is then gently heated to about 40°C (not critical), and deposition begins immediately. The vaporizing W-carbonyl presents a very large load for the present vacuum system, so that it is not possible to carry out the deposition with the diffusion pump on. During deposition the forepump (3 cfm) alone maintains the pressure at about 10^{-2} torr. Because the principal gas load is the carbon

monoxide which evolves from the decomposition of W-carbonyl, it is important that the forepump be vented outside the laboratory.

The rate of deposition and the ultimate thickness of a deposit can be satisfactorily controlled. For example, the 0.025 mm diameter wire can be built up to a diameter of 0.25 mm in about 10 minutes. In situations when the cross section of the target changes drastically, as in this instance, it is necessary to increase the heater current gradually in order to maintain the target temperature.

After the deposition has been completed, heat is removed from the W-carbonyl and the diffusion pump valve is opened in order to bring the pressure to 10^{-6} torr. The spontaneous positive ion emission from the target is then measured as a function of target temperature. Finally, the surface is inspected at 400X with a microscope.

7.2.4 Tests of Deposited Surface

From extensive experience with wires of rhenium, tungsten, and tungsten alloy, it is known (Datz, et al., 1960) that the positive ion emission from the heated surface can originate in the body of the metal as well as from surface contamination. The usual wire obtained from the supplier contains impurities from lack of care in manufacture, as well as additives, such as potassium, which improve the drawing qualities of the tungsten. The ion background from these wires is large and erratic and increases markedly with temperature. Wire obtained by drawing single crystals of tungsten generally has a lower background frequently punctuated by

large bursts of emitted positive ions. These bursts, which are known as the "anomalous flicker effect" in vacuum tube technology, occur when a large number ($\sim 10^6$) of impurity atoms clustered along a dislocation in the microcrystalline structure of the wire all come out at once.

In contrast to the behavior of the usual tungsten wire, the surfaces formed with W-carbonyl exhibit a very low positive ion background which is practically temperature independent and nearly devoid of large ion bursts. These tests indicate the much improved purity of the tungsten surface formed by vapor decomposition. Visual examination of the surfaces shows the deposits to be rough with a uniform, semicrystalline structure. The limited pumping speed available in the present apparatus has prevented the formation of the W-carbonyl surfaces under high vacuum conditions. According to Kaminsky (1965), a target temperature of $\sim 700^{\circ}C$ will prevent CO from staying with the surface during its formation, but cracked pump oils and other residuals doubtless contribute to surface impurities. It will be interesting to carry out the surface formation experiments with metal carbonyls under better vacuum conditions.

7.2.5 Discussion of the Deposition Experiment

The use of deposition via thermal dissociation for satellite experiments has a number of attractive features:

(1) The temperature necessary to vaporize the small reservoir of the metal carbonyl, typically $40^{\circ}C$ in a volume of 0.1 cm^3, is easily achieved.

(2) The power which is needed to warm the target substrate to 600°C serves to bake out the substrate as well as to dissociate the vapor that strikes it.

(3) The electrical power requirement is relatively very low (it is estimated that deposition of a film 10^{-3} cm thick on a 1 cm^2 target will require about 1% of the power needed to do the same thing using the usual vapor deposition method).

(4) The metallic surface will be deposited only on the heated surface in the apparatus. In the usual vapor deposition setup every exposed surface (insulators, etc.) is coated with the vaporized material.

Tungsten carbonyl has been used for the formation of surfaces in these measurements, but other metal carbonyls may exhibit similar properties.

The target substrate can be heated to the temperature required for molecular dissociation by focusing the rays of the sun on the target with a small converging lens. This procedure reduces the required power by a factor of at least 1000. Heating the target in this manner becomes particularly attractive if the experiments are to be conducted in a manned space station, because an astronaut can guide the lens for the short time needed to deposit the clean surface.

7.3 LABORATORY STUDY OF CRYSTAL CLEAVING FOR A CALIBRATION SURFACE

Certain crystals, notably the alkali halides, are easily cleaved along their crystal planes. The resultant surfaces are

known to be microscopically regular, so they provide useful calibrating surfaces, both for laboratory and flight experiments.

Experiments on semi-automatic ways to cleave lithium fluoride have been performed under the present contract. Several dozen trials have been made in which a prism of LiF is mounted in a small guillotine (Figure 7.1), the cutting edge of which is an ordinary single-edged razor blade. The blade is given a sharp impulse with a spring or with the tap of a hammer, and the crystal cleaves neatly. The method works well if the LiF prism is placed with care and a small starting groove is prepared in the prism for the blade. From many standpoints, the use of a cleaved crystal plane as a reference surface is attractive. Its structure is well understood, the effect of the regular array of atoms in the crystal on the molecular flux lends itself to theoretical calculations as done by Oman and his associates (Oman, et al, 1964), and it is possible to prepare the cleaved surface with a simple mechanism while the experiment is in orbit.

7.4 DISCUSSION OF OTHER METHODS OF SURFACE PREPARATION

R. Oman and the Grumman group (Grumman report on this study for the month of March, 1967, contract NAS 8-21096) have suggested that the surfaces be prepared in the laboratory and encapsulated under ultra-vacuum conditions before being sent into orbit. A noble gas backfill is to be used to minimize surface contamination between the time of preparation and the moment when the capsule is opened and the surface is exposed for the experiment. Since very pure helium will desorb very readily when the sample is

exposed to the vacuum of space, it appears to be the best gas for backfill. The efficacy of encapsulation as storage for a scientific surface for time on the order of days has not yet been demonstrated, but the method has the virtue of versatility: any stable material can be prepared and sent up for the measurements.

The conventional ways of preparing surfaces for scientific investigation have been discussed (Kaminsky, 1965, Chapter 3, pp. 28-33, and references there cited), but their complexity and demands on space craft power make them ill-suited for space experiments.

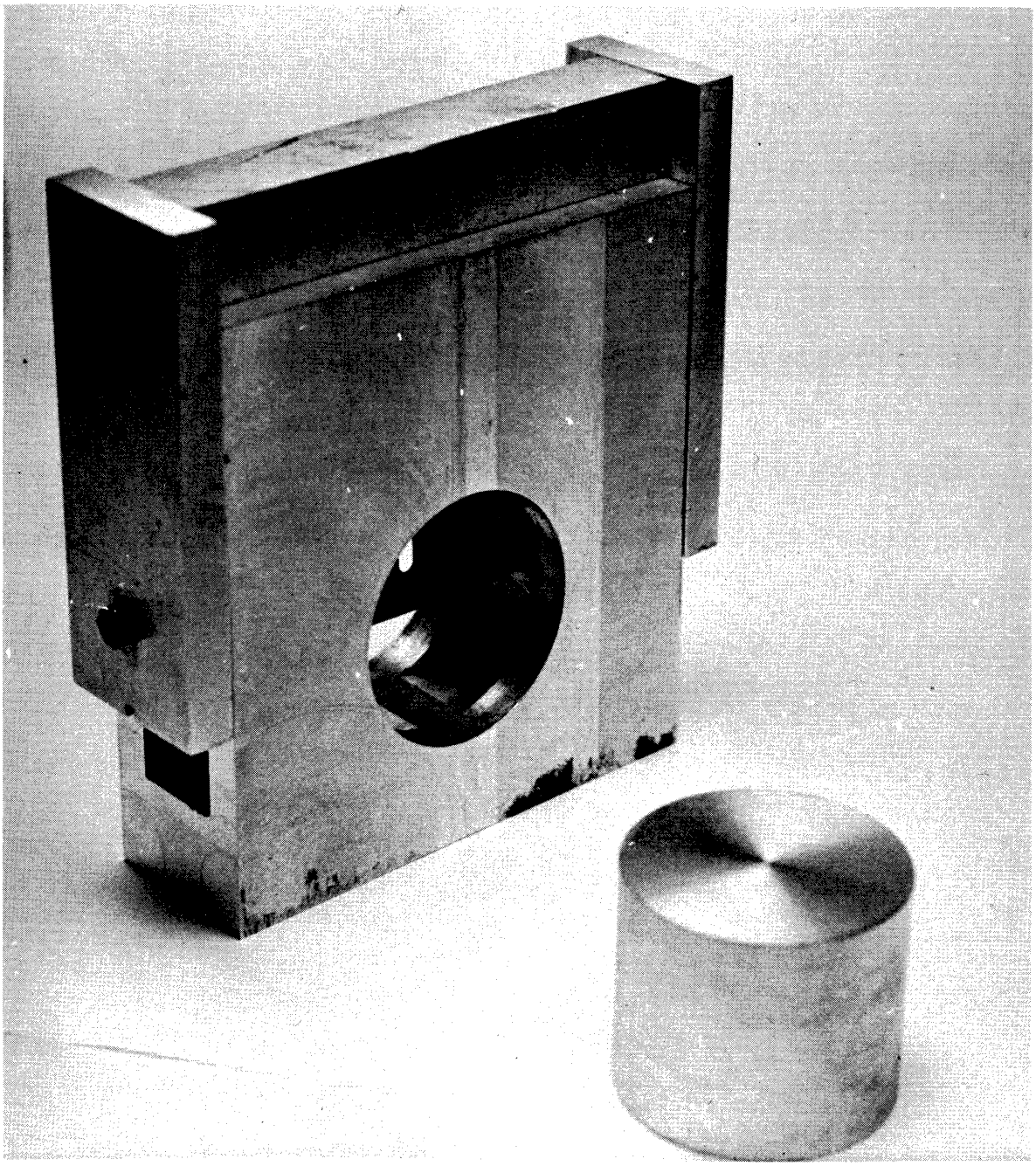

Figure 7.1 Guillotine for Crystal Cleaving

8. SUMMARY AND RECOMMENDATIONS

8.1 ACCOMPLISHMENTS OF THE STUDY

The work performed under the present contract is summarized below. Included with each effort described are its implications for a possible satellite experiment.

A variety of experiments relevant to the development of an orbital experiment utilizing a metastable time-of-flight analyzer has been performed:

1) Modifications in molecular velocity distributions which arise from collisions between the beam (reflected) molecules and the background gas have been studied (Section 4). It has been found that collimated molecular beams can be remarkably deficient in slow molecules even if background pressures are less than 10^{-5} torr, but that these results can be understood on the basis of kinetic theory and known collision cross sections. Thus, the effects of background gas scattering can be accounted for in data reduction by using calculations based on kinetic theory.

2) The use of the Auger electron ejection process for the detection of metastable nitrogen and argon beams has been investigated (Section 6). It has been found that a selective metastable detector which is astonishingly insensitive to mistreatment can easily be constructed. The ruggedness and reliability of such a detector make it admirably suited for space experiments.

3) A study has been made of some novel methods for preparing

clean target surfaces in an orbital environment (Section 7). It has been found that a pure tungsten (or other metal) surface can be produced easily by the thermal dissociation of a molecular vapor; the selective deposition and relatively low power required in this process make it superior to an evaporation coating method for satellite applications. It has also been shown that a simple spring-loaded knife can be used to cleave certain types of crystals semi-automatically; the triggering of such a device by remote control once the satellite is in orbit can provide an atomically clean, regular lattice for studying rates of surface contamination and for providing data of a quality suitable for theoretical interpretation.

A number of theoretical studies related to the MTOF method have also been carried out:

1) Calculations of molecular fluxes incident on an experiment in a possible orbit have been made (Section 2). The results provide information necessary for experimental design.

2) A general analysis has been made of the correlation between the velocity distribution of molecules reflected from a target surface and the output signals from an MTOF analyzer (Section 3). It has been found that, with proper instrument design, the velocity distribution of the reflected particles can be very simply related to the MTOF output, and that this output is relatively

insensitive to changes in electron gun parameters. Further, the modifications of the data due to molecular recoil during electron bombardment have been found to be small and easily accounted for in data reduction. Thus, the MTOF analyzer can be constructed without stringent tolerances and can easily provide velocity distribution data.

3) The properties of molecular nitrogen which are relevant to the MTOF analysis have been presented (Section 5). Like the flux calculations, these data provide information necessary for proper design of the instrument.

8.2 RECOMMENDATIONS

The objective of the study terminated by this report has been the definition of a satellite-borne experiment to investigate gas-surface interaction phenomena relevant to satellite drag. The results of this study, summarized in the previous paragraph, indicate that a meaningful experiment of this type can be constructed using relatively simple and rugged equipment. It is recommended that a cluster of metastable time-of-flight analyzers be built for the study of the fast component of N_2 flux reflected from a small number of target surfaces located outside the satellite (see Section 1.2). This experimental concept offers both good quality data and reliability through simplicity in design.

APPENDIX

THE SIMPLIFIED FLUX RELATION OBTAINED BY PHYSICAL ARGUMENTS

As indicated in Section 3.5, the zeroth order term for the normalized metastable flux density

$$f_o^*(t,\tau;L,W)=\frac{L}{t^2}g(\frac{L}{t})$$

can be interpreted as the flux arising from an instantaneous ($\tau=0$) excitation of particles in an infinitesmally thin ($W=0$) slice of the neutral beam. It is the purpose of this appendix to show more physically how the above result follows from these conditions.

At time $t=0$ a certain number N^* of metastables is produced by a spike pulse of electrons forming a current sheet (see Figure A.1).

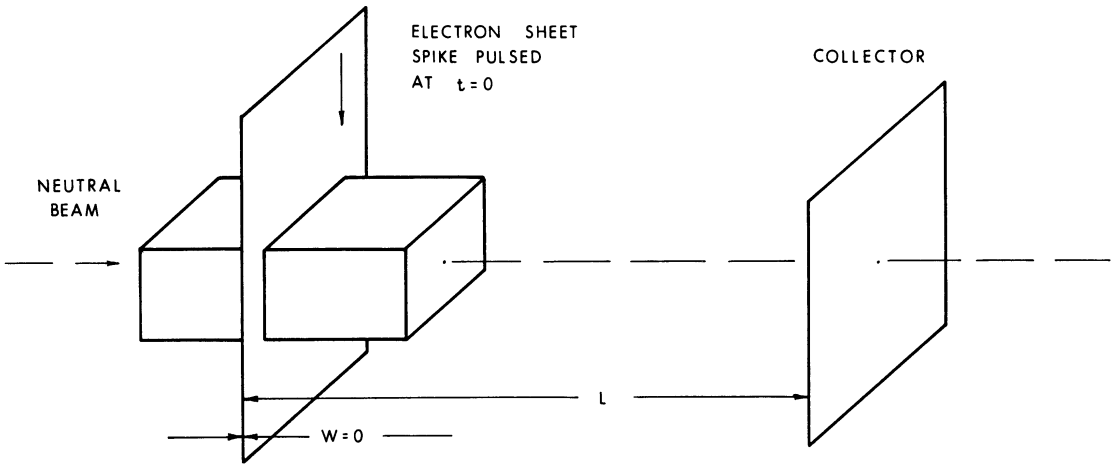

Figure A.1 Geometry of current sheet and neutral beam.

As the metastables leave the electron sheet, they gradually separate, the faster particles leaving the slower ones behind. Consequently, the initially thin slice spreads out, becoming a packet which continually expands along the direction of motion of its particles.

To obtain a measure of this expansion, consider a gas with the simple velocity distribution g(v) shown in Figure A.2, focusing attention on particles having speeds within Δv of some arbitrary speed v. These particles will arrive at the

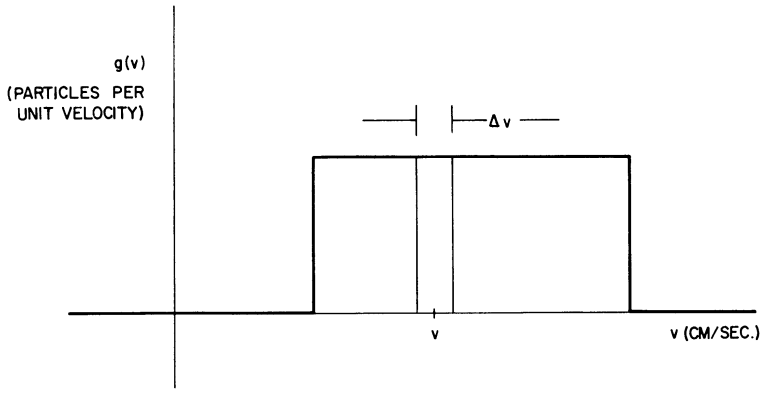

Figure A.2 Simple velocity distribution

collector after a time $t=\frac{L}{v}$. During this time, however, the higher speed particles will have been traveling an amount Δv faster than the slower ones. Consequently, at the collector the higher speed particles will be ahead of the slower ones by a distance Δl given by

$$\Delta l = t\ \Delta v$$
$$= \frac{L\ \Delta v}{v}$$

This quantity represents the thickness of the portion of the packet containing particles within Δv of v, and indicates that for the same Δv, an increment centered around a higher speed will have a smaller thickness, i.e., will be more concentrated.

To find the metastable flux, it is necessary first to determine the density n^*. If the number of metastables which have speeds within Δv of v is ΔN^*, then the density can be found through dividing this number by the volume ΔV occupied by the particles. By assuming the beam to have unit cross sectional area, the density of the particles occupying the increment Δl at the collector is therefore given by

$$n^* = \frac{\Delta N^*}{\Delta l} = \frac{\Delta N^* v}{L \Delta v}$$

For a general velocity distribution g(v), the number of metastables having speeds within v of v is given by

$$\Delta N^* = N^* g(v) \Delta v$$

so that

$$n^* = \frac{N^* v}{L} g(v)$$

Multiplying this expression by v yields the flux at the collector; dividing by N^* normalizes it. Thus

$$f^* = \frac{v^2}{L} g(v)$$

Since this quantity is the flux at the collector, the velocity v can be expressed in terms of the transit time to the collector

$$v = \frac{L}{t}$$

Consequently, the flux may finally be written in the form

$$f^* = \frac{L}{t^2} g \left(\frac{L}{t}\right)$$

as was intended to be shown.

REFERENCES

Bates, D. R., Editor, Atomic and Molecular Processes, Academic Press, New York, 1962.

Bechtel, J. H., Impurity Limits for Alkalis Used in Atomic Beam Experiments, Randall Laboratory Report, Department of Physics, The University of Michigan, 1967 (Unpublished).

Brink, G. O., Study of Excited States of Molecular Oxygen by Molecular Beam Magnetic Resonance Techniques, Cornell Aeronautical Laboratory, Inc., Buffalo, CAL REPORT No. RM-2156-P-1, Contract No. 49-146-XZ-483, November, 1966. AD 643 526.

Carleton, N. P. and Oldenberg, O., "Lifetime of the Lowest Excited Level of N_2," J. Chem. Phys., 36, 3460, 1962.

Carleton, N. P., Studies of Metastable Molecules of Atmospheric Interest, Smithsonian Astrophysical Observatory, Cambridge, Massachusetts, AFCRL-66-717, October, 1966, AD 642 851.

Datz, S., Minturn, R. E., and Taylor, E. H., "Thermal Positive Ion Emission and the Anomalous Flicker Effect," J. Appl. Phys., 31, No. 5, 880-883, May 1, 1960.

Dorrestein, R., "Excitation Functions of Metastable States in Helium and Neon Measured with the Help of the Electrons Ejected from Metal due to Metastable Atoms," Physica, 9 No. 5, 447-460, May, 1942.

Frazer, J. W., Burns, R. P., and Barton, G. W., "Low Background Tungsten Filaments for Surface Ionization Mass Spectroscopy," Rev. Sci. Instr., 30, 370, 1959.

French, J. B., "A Time of Flight Velocity Analyzer Using Metastable Molecules," Rarefied Gas Dynamics, Edited by C. L. Brundin, Academic Press, New York, 1967, pp. 1461-68.

Freund, R., "Radiofrequency Spectroscopy of Metastable CO," Ph.D. Dissertation, Harvard University, 1964 (Unpublished).

Gilmore, F. R., Potential Energy Curves for N_2, NO, O_2 and Corresponding Ions, RAND Memorandum, RM-4034-1-PR, April 1966.

Gilmore, F. R., Basic Energy-Level and Equilibrium Data For Atmospheric Atoms and Molecules, RAND Corporation Memorandum RM-5201-ARPA, March, 1967. AD 650 470.

Green, A. E. S., and Barth, C. A., "Calculations of Ultraviolet Molecular Nitrogen Emissions from the Aurora," J. Geophys. Res., 70, No. 5, 1083-1092, March 1, 1965.

Greene, E. F., "Reduction of Potassium Ion Background in Tungsten Surface Ionization Detectors for Molecular Beams," Rev. Sci. Instr., 32, 860, 1961.

Hasted, J. B., Physics of Atomic Collisions, Butterworths, Ltd., London, 1964.

Herzberg, G., Atomic Spectra and Atomic Structure, Dover, New York 1944.

Herzberg, G., Diatomic Molecules, 2nd edition, D. Van Nostrand, 1950.

Holt, H. K. and Krotkov, R., "Excitation of n=2 States in Helium by Electron Bombardment," Phys. Rev., 144, No.1, 82-93, April 8, 1966.

Hostettler, H. and Bernstein, R., "Improved Slotted Disk Type Velocity Selector for Molecular Beams." Rev. Sci. Instr., 31, 872, 1960.

Hunten, D. M. and McElroy, M. B., "Quenching of Metastable States of Atomic and Molecular Oxygen and Nitrogen," Reviews of Geophysics, 4, 303, 1966.

Jacchia, L. G., "Static Diffusion Models of the Upper Atmosphere with Empirical Temperature Profiles," Smithsonian Cont. to Astrophys., 8, No. 9, 1965.

Kaminsky, M., Atomic and Ionic Impact Phenomena on Metal Surfaces, Academic Press, New York, 1965.

Kusch, P. and Hughes, V., "Atomic and Molecular Beam Spectroscopy," Vol. 37/1, Handbuch der Physik, Springer, Berlin, 1959.

Kusch, P., "Notes on Resolution in Scattering Measurements," J. Chem. Phys., 40, 1964.

Kummler, R. H. and Bortner, M. H., The Role of Metastable, Neutral Electronically Excited Species in Atmospheric Deionization, Space Sciences Laboratory, General Electric Company, Missile and Space Division, Technical Information Series, R67SD20, May, 1967. AD 654516.

Lamb, W. E., Jr. and Retherford, R. C., "Fine Structure of the Hydrogen Atom. Part I," Phys. Rev., 79, No. 4, 549-572, August 15, 1950.

Leventhal, M., Robiscoe, R. T. and Lea, K. R., "Velocity Distribution of Metastable H Atoms Produced by Dissociative Excitation of H_2," Phys. Rev., 158, 49, 1967.

Lichten, W., "Lifetime Measurements of Metastable States in Molecular Nitrogen," J. Chem. Phys., 26, No. 2, 306-313, February, 1957.

Loeb, L., The Kinetic Theory of Gases, McGraw-Hill, New York, 1934, 99-103.

Lurio, A., "Hyperfine Structure of the 3p States of Zn^{67} and Mg^{25}," Phys. Rev., 126, No. 5, 1768-1773, June 1, 1962.

MacLennan, D. A., "Electron Ejection from an Atomically Clean Tungsten Surface by Helium and Neon Metastable Atoms," Phys. Rev., 148, No. 1, 218-223, August 5, 1966.

Oman, R. A., Bogan, A., Weiser, C.H., and Li, C. H., "Interactions of Gas Molecules with an Ideal Crystal Surface," AIAA Jour., 2, No. 10, 1722-1730, October, 1964.

Omholt, A., "The Time Delay of the Red (OI) Lines in the Aurora," Planet. Space Sci., 2, No. 4, 246-248, August, 1960.

Paulson, K. V. and Shepherd, G. G., "A Cross-Spectral Method for Determining the Mean Lifetime of Metastable Oxygen Atoms from Photometric Observations of Quiet Aurorae." J. Atmos. and Terr. Phys., 27, No. 7, 831-841, July, 1965.

Rothe, E. W. and Bernstein, R. B., "Total Collision Cross Sections for the Interaction of Atomic Beams of Alkali Metals with Gases," J. Chem. Phys., 31, 1619, 1959.

Rubin, K., Perel, J. and Bederson, B., "Measurement of the Total, Differential, and Exchange Cross Sections for the Scattering of Low-Energy Electrons by Potassium," Phys. Rev., 117, No.1, 151-158, January 1, 1960.

Schulz, G. J., "Measurement of Excitation of N_2, CO and He by Electron Impact, Phys. Rev., 116, 1141, 1959,

Stebbings, R. F., "Gaseous and Surface Reactions Involving Helium Metastable Atoms and Resonance Photons," Proc. Roy. Soc. Lond. A241, 270-282, August 2, 1957.

Stebbings, R. F., Fite, W. L., Hummer, D. G., and Brackmann, R. T., "Collisions of Electrons with Hydrogen Atoms. V. Excitation of Metastable 2 S Hydrogen Atoms," Phys. Rev., 119, No. 6, 1939-45, September 15, 1960.

Weast, S. M., Editor-in-Chief., "Ionization Potentials," Handbook of Chemistry and Physics, Chemical Rubber Company, 46th Edition, 1965-66, P. E41.

Wiese, W. L., Smith, M. W., and Glennon, B. M., Atomic Transition Probabilities. Hydrogen through Neon., NSRDS-NBS 4, Vol. 1, May 20, 1966.

BIBLIOGRAPHY

Alcalay, J., Experimental Study of Scattering in Atom-Surface Collisions with Atom Energies of the Order of 1 ev, University of California, Department of Engineering, Los Angeles, Report No. 67-20, June, 1967. N67-31556.

Boring, J. W., Momentum Transfer to Solid Surfaces by N_2 Molecules at Satellite Velocities, Research Laboratories for the Engineering Sciences, University of Virginia, Technical Report Contract NAS1-2538, Report No. EP-4018-139-67U, February, 1967.

Cobas, A. and Lamb, W. E., Jr., "On the Extraction of Electrons from a Metal Surface by Ions and Metastable Atoms," Phys. Rev., 65 Nos. 11 & 12, 327-337, June 1 and 15, 1944.

Crews, J. C., Scattering of Helium from the Cleavage Plane of Lithium Fluoride, Union Carbide Corporation, Nuclear Division, Physics Department, Technical Division, Oak Ridge, Tennessee, Contract W-7405--ENG-26, N67-25917, December, 1966.

Dugan, C. H., "Energetic Metastable O_2 Molecule," J. Chem. Phys. 46, 1534, 1967.

Freund, R. and Klemperer, W., "Radiofrequency Spectrum of the $a^3\Pi$ State of Carbon Monoxide," J. Chem. Phys. 43, 2422, 1965.

Hagena, O. F., "Velocity Distribution Measurements of Molecular Beams Scattered from Solid Surfaces," Applied Physics Letters, 9, No. 10, 385-387, November 15, 1966.

Hagstrum, H. D., "Auger Ejection of Electrons from Tungsten by Noble Gas Ions," Phys. Rev., 96, No. 2, 325-335, October 15, 1954.

Hagstrum, H. D., Theory of Auger Ejection of Electrons from Metals by Ions," Phys. Rev., 96, No. 2, 336-365, October 15, 1954.

Hagstrum, H. D., "Auger Ejection of Electrons from Tungsten by Noble Gas Ions," Phys. Rev., 104, No. 2, 317-318, October 15, 1956.

Hagstrum, H. D., "Auger Electron Ejection from Germanium and Silicon by Noble Gas Ions," Phys. Rev., 119, No. 3, 940-952, August 1, 1960.

Hagstrum, H. D., "Detection of Metastable Atoms and Ions," J. Appl. Phys., 31, 897, 1960.

Hinchen, J. J., Malloy, E. S., and Carroll, J. B., Scattering of Thermal Energy Gas Beams by Metallic Surfaces II, United Aircraft Research Laboratories, United Aircraft Corporation, East Hartford, Connecticut, Report F910439-7, June, 1967. AD654720.

Hurlbut, F. C. Energy Transfer in Particle-Surface Interactions in Hypervelocity Flight: Commentary and Bibliography, RAND Corporation, Memorandum, RM-4884-PR, July, 1967.

Lichten, W., "Some New Metastable States of Molecules," J. Chem. Phys., 37, 2152, 1962.

Miller, R. and Kusch, P., "Velocity Distribution in Potassium and Thallium Atomic Beams," Phys. Rev., 99, 1314, 1955.

Muschlitz, E. E. and Goodman, L., "Lifetime of the $^3\Sigma_u$ State of Nitrogen," J. Chem. Phys., 21, 2213, 1953.

Oman, R. A., Bogan, A., and Li, C. H., "Theoretical Prediction of Momentum Energy Accommodation for Hypervelocity Gas Particles on an Ideal Crystal Surface," Rarefied Gas Dynamics, Vol. 2, Academic Press, New York, 1966, 396-416.

Schaetzle, W. J., An Experimental Study of Molecular Surface Interactions at Velocities up to and exceeding Space Probe Escape Velocities, Bureau of Engineering Research, University of Alabama, Final Report, Contract NAS8-5326, June 15, 1966. N67-18518.

Wilkinson, P. G., and Mulliken, R. S., "Forbidden Band Systems in Nitrogen. II. The a' $^1\Sigma_u^-$ ← X $^1\Sigma_g^+$ System in Absorption," J. Chem. Phys., 31, No. 3, 674, September, 1959.